Faculty of Science and Engineering

School of Earth and Planetary Sciences

Discipline of Geophysics

Continuous borehole seismic monitoring of a carbon dioxide storage

Roman Isaenkov

This thesis is presented for the Degree of Doctor of Philosophy of Curtin University

April 2023

DECLARATION

To the best of my knowledge and belief this thesis contains no material previously published by any other person except where due acknowledgement has been made.

This thesis contains no material which has been accepted for the award of any other degree or diploma in any university.

Signature:

Date: 06 April 2023

ABSTRACT

Active time-lapse seismic monitoring technology is essential for carbon storage projects due to its ability to track the CO_2 plume evolution in space and time. The standard industry monitoring approach (known as 4D seismic) is to acquire one 3D seismic survey before injection (baseline) and a series of monitor surveys during and after injection. Assuming that nothing in the subsurface has changed except CO_2 reservoir properties, a comparison of baseline and monitor surveys is supposed to highlight the presence of CO_2. However, such surveys can interfere with other land users and require crew and equipment on site, which becomes expensive over years or decades of monitoring. These factors limit the frequency of repeat surveys to one or a maximum two per year – and this may miss critical processes such as CO_2 leakages or fault re-activations.

These limitations may be addressed by a permanent seismic reservoir monitoring (PRM) system with permanent sources and receivers, which can track subsurface changes in near real-time over decades. Permanent sources can be installed on the surface or in shallow boreholes. Permanent receivers can be buried in trenches or also installed inside wells. Borehole installations are often preferred as this approach minimises the influence of weather and variable near-surface on sources and receivers. Permanent installation minimises land access requirements, allows automatisation of the system (crew is not required), and as such can be frequent (in some cases – daily). However, main PRM limitation is high installation cost as a lot of equipment is required to run the project in the first place.

Permanent monitoring is still in its infancy and as such, no standard PRM design exists. This is mainly due to the different tasks and different available equipment each project has. As such, there is no standard way to automate the acquisition, storage and processing of the data - each project can have some unique new features. The work of this thesis aimed to develop automated data acquisition, storage, processing and interpretation of PRM data acquired at the CO2CRC Otway Stage 3 project with the main focus on data processing. The work is published in five publications.

The first paper describes the acquisition setup, on-site data storage solution, processing and assessment of PRM's initial repeatability. The initial data processing compresses the data from 1.3 TB/day to 500 MB/day and provides good repeatability over the half-year period. The second publication describes the improvement of the initial workflow, and presents

monitoring results and their comparison with a high-lateral-resolution 4D VSP data. We detected the CO_2 plume on the second day of injection and monitored its evolution over more than a year of monitoring. As the data were recorded by a rather new tool – distributed acoustic sensing (DAS) – it was important to compare its sensitivity versus a standard geophone tool. The results of the third publication shows that DAS is more sensitive to rock stiffness changes than geophones which needs to be taken into account.

The forth paper studies the effect of mispositioning on 4D VSP repeatability. We found, that for surface 4D VSP data even a few meter mispositioning can lead to strong non-repeatability due to highly-varying near-surface. The last publication explores a tube wave excited by a permanent seismic source in a horizontal pipeline transpherring CO_2 to the injector well. The tube wave velocity and amplitudes vary over a period of injection and we assume it could be used as a flow monitoring tool.

ACKNOWLEDGMENTS

I would like to take this opportunity to express my gratitude to all those who have contributed to the completion of my PhD thesis.

Firstly, I would like to acknowledge my supervisory panel. I want to thank my main supervisor Dr Konstantin Tertyshnikov and co-supervisor Prof. Roman Pevzner for many fruitful discussions, guidance through my research, brilliant ideas, and a gentle push when I need to keep going and support during hard times. I thank Dr Sinem Yavuz and Dr Alexey Yurikov for their support, guidance, and fruitful discussions.

I thank Prof. Boris Gurevich for constructive discussions, reading and editing my texts and greatly improving my writing skills. I thank Dr Stanislav Glubokovskikh for their scientific enlightenment and the suggestion of starting this PhD study.

I wish to thank other Curtin University staff members, students and friends who helped me during my PhD on different occasions: Prof. Maxim Lebedev, Prof. Andrej Bona, Robert Verstandig, Dominic Howman, Murray Hehir, Nichole Sik, Aimee Calkin, Sofya Popik, Evgenii Sidenko, Dr Roman Beloborodov.

I am sincerely thankful to my examiners for dedicating their time to reading and improving my thesis.

I would like to acknowledge CO2CRC for providing a scholarship for this research. Funding for CO2CRC Otway Project is provided through its industry members and research partners, the Australian Government under the CCS Flagships Programme, the Victorian State Government, and the Global CCS Institute. CO2CRC received financial assistance provided through Australian National Low Emissions Coal Research and Development. ANLEC R&D is supported by Low Emission Technology Australia (LETA) and the Australian Government through the Department of Industry, Science, Energy and Resources. Stage 3 of the Project was additionally funded by BHP. Landowners and the Moyne Shire community (Victoria, Australia) are also acknowledged for their support of the Project.

LIST OF PUBLICATIONS INCLUDED IN THE THESIS

1. Isaenkov, R., Pevzner, R., Glubokovskikh, S., Yavuz, S., Yurikov, A., Tertyshnikov, K., Gurevich, B., Correa, J., Wood, T., Freifeld, B., Mondanos, M., Nikolov, S., Barraclough, P., 2021. An automated system for continuous monitoring of CO2 geosequestration using multi-well offset VSP with permanent seismic sources and receivers: Stage 3 of the CO2CRC Otway Project. International Journal of Greenhouse Gas Control 108, 103317, https://doi.org/10.1016/j.ijggc.2021.103317.

2. Isaenkov, R., Pevzner, R., Glubokovskikh, S., Yavuz, S., Shashkin, P., Yurikov, A., Tertyshnikov, K., Gurevich, B., Correa, J., Wood, T., 2022. Advanced time-lapse processing of continuous DAS VSP data for plume evolution monitoring: Stage 3 of the CO2CRC Otway project case study. International Journal of Greenhouse Gas Control 119, 103716, https://doi.org/10.1016/j.ijggc.2022.103716.

3. Isaenkov, R., Glubokovskikh, S., Tertyshnikov, K., Pevzner, R., Bona, A., 2020. Effect of Rocks Stiffness on Observed DAS VSP Amplitudes, EAGE Workshop on Fiber Optic Sensing for Energy Applications in Asia Pacific. European Association of Geoscientists & Engineers, pp. 1-5, https://doi.org/10.3997/2214-4609.20224011.

4. Isaenkov, R.; Tertyshnikov, K.; Yurikov, A.; Shashkin, P.; Pevzner, R, 2022. Effect of Source Mispositioning on the Repeatability of 4D Vertical Seismic Profiling Acquired with Distributed Acoustic Sensors. Sensors (Basel, Switzerland), 22 (24), https://doi.org/10.3390/s22249742

5. Isaenkov, R., Yurikov, A., Tertyshnikov, K., Gurevich, B., Pevzner, R., 2022. Continuous DAS Recording with Permanent Seismic Sources Reveals Peculiar Tube Waves Associated with the Fluid Flow, EAGE GeoTech 2022 Third EAGE Workshop on Distributed Fibre Optic Sensing. European Association of Geoscientists & Engineers, pp. 1-4. https://doi.org/10.3997/2214-4609.20224011.

STATEMENT OF CANDIDATE ABOUT THE CONTRIBUTION OF CO-AUTHORS

I am the first author of all the publications included in this thesis. Each of these publications is based primarily on my own work, which was done in cooperation with my co-authors. I wrote the papers myself and they were later reviewed and edited by my co-authors. The contribution of each co-author is listed in the Appendix A.

INTRODUCTION AND OVERVIEW

1.1 BACKGROUND AND MOTIVATION

Carbon capture and storage (CCS) is a technology that involves capturing carbon dioxide (CO_2) emissions from industrial processes or power plants, transporting the CO_2 to a storage site, and injecting it deep underground for long-term storage. CCS technology is a key component of energy transition designed to mitigate climate change caused by anthropogenic carbon emissions. CCS technology allows capturing carbon dioxide from a refinery, iron, steel, petrochemical and concrete industries, and only CCS can reduce emissions generated by fossil fuels (IEA 2015). CCS is predicted to account for 13% of the total CO_2 emission reduction by 2050, storing 6 billion tonnes of CO_2 per year (IEA 2015). “Many models could not limit likely warming to below 2°C if bioenergy, CCS, and their combination (BECCS) are limited” (Pachauri and Meyer 2014).

1.1.1 Carbon Capture and storage projects

CCS projects have been successfully applied to capture CO_2 all around the world. As of 2022, 196 CCS projects are in operation and 61 new CCS facilities are announced, which capture 244 million tonnes of carbon dioxide per annum. While most of these projects capture carbon dioxide from industry, some capture CO_2 from power plants (Mattos 2018).

A typical CCS project includes CO_2 capture, transportation, injection and monitoring. CO_2 is captured from stationary CO_2 emitting facilities (power plants, industrial facilities or natural gas fields with high CO_2 concentration), cooled down and compressed to a liquid state, and transported via pipelines or vessels to the storage facility. CO_2 is then injected into the reservoir through a borehole. There are several possible types of storage reservoirs: saline aquifers, depleted oil and gas reservoirs, producing oil/gas reservoirs that use injected CO_2 for enhanced oil recovery.

Monitoring and verification are necessary for CO_2 geosequestration to manage storage performance and risks (Jenkins 2020). Active seismic monitoring has successfully been applied in several industrial-scale geosequestration projects (Ajayi, Gomes, and Bera 2019). Compared

to other remote sensing methods, active seismic monitoring has better spatial coverage and spatial resolution (Johnston 2013).

Examples of CCS projects with monitoring and verification program are numerous (Jenkins, Chadwick, and Hovorka 2015). The projects are distributed widely around the globe: Otway, Australia (Cook 2014); US projects: Decatur (Finley, 2014b), Aquistore (Worth et al. 2014); Nagaoka (Kikuta et al. 2005) from Japan; Ketzin, Germany (Martens et al. 2013), Lacq, France (Prinet et al. 2013) and Snøhvit, Norway (Hansen et al. 2013), In Salah, Algeria (Eiken et al. 2011).

1.1.2 Time-lapse monitoring of CCS

Time-lapse seismic can detect a relatively small amount of gas (Isaenkov et al. 2022), track gas propagation within geological media and identify leakages. Time-lapse seismic monitoring consists of 2D/3D surface seismic or 3D vertical seismic profiling (VSP) surveys repeated periodically (e.g. each year). Subsurface changes are then tracked by comparing surveys prior and after injection. Such an approach is common for oil and gas projects (Johnston and Laugier 2012; Onuwaje et al. 2009; Amoyedo, Slatt, and Marfurt 2011); however this approach can be too expensive for CCS projects, especially because these projects may require very frequent monitoring to detect unforeseen events such as CO_2 leakages from the primary reservoir or fault reactivation. Hence, reducing operational costs is essential for effectively implementing seismic monitoring on CCS projects (Correa et al. 2018).

Moreover, onshore time-lapse seismic monitoring survey operations can be time-consuming (several weeks or months) and land-invasive (installation of receivers and operating seismic sources), and may be disruptive to other land uses. Permanent seismic reservoir monitoring (PRM) can address some of these issues. Permanent installations can reduce the time of a single survey to a few days, enable automation of acquisition and processing, and allow for more frequent surveys (Zwartjes et al. 2015; Isaenkov et al. 2021). In the PRM approach, receivers and sources are often installed in trenches and/or shallow wells, which minimises the land disturbance.

Repeatability is a crucial parameter for a time-lapse seismic method. It defines how small time-lapse signal can be detected. For a given PRM system, repeatability would be defined by the chosen sources and receivers types, installations and near-surface conditions. Schisselé et al. (2009) compared surface, mixed, and buried permanent installations of sources and receivers, and showed that a buried installation has the best possible repeatability. Also, different near-surface conditions can result in different levels of repeatability. For example,

varying groundwater levels or migrating dunes can affect permanent source or receiver performance, resulting in seasonal variations of repeatability (Kashubin et al. 2011; Jervis et al. 2012).

Permanent sources can be installed on the surface or in wells for better repeatability, however, the latter is more expensive. Orbital vibrators (Nakatsukasa et al. 2017; Wang et al. 2020; Dou et al. 2017) can be installed on the surface or in shallow wells (Lopez et al. 2015). Permanent receivers can be buried in the trenches below the surface (Pevzner et al. 2015) or installed in wells (geophone strings or fibre optics sensors) (Pevzner et al. 2021; Bakulin et al. 2012).

Distributed acoustic sensing technology (DAS) enables to convert a well equipped with fibre optics into a distributed array of dynamic strain sensors (Parker, Shatalin, and Farhadiroushan 2014) with up to 25 cm channel spacing. The main limitation of using DAS is its directivity pattern. The sensitivity of straight DAS cables decreases as cosine squared of an angle of incidence for P-waves (Kuvshinov 2016). Straight fibres are not practical for surface seismic implementations as reflected P-waves will arrive predominantly at near-normal incidence to the fibre. On the other hand, for borehole deployments, DAS is a competent tool for near-offset VSP methods where target P-waves generally travel along the bore/fibre. For example, the 4D DAS VSP approach provides sufficient data quality in deep-water conditions (Mateeva et al. 2017).

1.1.3 CO2CRC Otway Project

CO2CRC Otway International Test Centre (OITC) is an extremely well-characterised CCS site with over 16 history years of research (CO2CRC 2023). My research is a part of CO2CRC Stage 3. The OITC is located in the Australian state of Victoria, 150 km west-southwest of the city of Melbourne. The Otway project intends to develop new techniques and advance existing methods in CCS. The development of an automated PRM technique to monitor a small-scale CO_2 injection is one of the main objectives of the Stage 3 Otway project.

CO2CRC Otway Project is the first Australian demonstration project of carbon dioxide geological storage. The Otway project is divided into three stages: Stage 1 (2004-2009) was focused on safe CO_2 transportation, injection and storage into the depleted gas reservoir; Stage 2 (2009 – 2019) was focused on risk reduction during safe injection into a saline aquifer and monitoring of its evolution, and Stage 3 (2017 – 2022) on development of cost-effective subsurface monitoring.

The monitoring program for Stage 3 is based on the results of Stage 2C experiments and field trials conducted from 2015 to 2018 to study the sensitivity in detecting a small leakage by a time-lapse surface seismic (Pevzner et al. 2017; Pevzner et al. 2020; Cook 2014). During Stage 2C, 15 kilotons of CO_2/CH_4 supercritical mixture had been injected into Lower Paaratte formation at approximately 1500 m depth via the CRC2 injection well.

The main component of Stage 2C 4D seismic monitoring was a permanently deployed geophone array buried 4 m below the surface (Pevzner et al. 2020). One baseline and five monitor 3D seismic surveys were acquired during this stage (Popik et al. 2020). Also, 3D VSP was acquired in the CRC1 well with a ten-level geophone tool deployed at about 900 m depth. Additional five offset VSP surveys were acquired after each monitoring 3D seismic survey. The main finding during this stage, which contributed to Stage 3 design, were:

1. Seismic properties of the Lower Paaratte formation are sensitive to the presence of supercritical CO_2/CH_4 mixture
2. Time-lapse seismic detected the signal at every stage of monitoring starting from as minimum as five kt (Glubokovskikh et al. 2016; Pevzner et al. 2017; Popik et al. 2020)
3. 4D VSP plume image agrees with surface time-lapse seismic results
4. SOVs were proven to be a reliable seismic source with a repeatable signature and sufficient bandwidth
5. Weather effects on the near-surface conditions are the primary source of the time-lapse noise in the data (Yavuz et al. 2019)

The first dataset with an SOV was acquired in March 2016 and showed a frequency content of up to 80 Hz and good repeatability (below 20% NRMS and below 0.1 ms time discrepancy) (Dou et al. 2017). This confirmed the feasibility of SOV as a permanent source for monitoring applications. However, there are two limitations related to such sources. The lack of phase control reduces the repeatability of the rotating eccentric masses. The produced signal amplitude is proportional to the square of frequency due to the rotational nature of the motion (centrifugal force is proportional to the angular velocity squared). This results in lower energy content at low frequencies. However, the source phase can be compensated during processing using a signal recorded by a pilot 3-component geophone buried 3 m below the SOV. Stacking several sweeps increases the signal-to-noise ratio, including low frequencies. Thus, these SOV limitations can be minimised with tailored survey design and processing.

After the completion of the injector CRC3 well and its instrumentation with DAS fibre cable cemented behind the casing, several experiments were performed before Stage 3:

1. Correa et al. (2017) analysed geophones and engineered DAS fibre data and showed that DAS and geophone data are comparable for up to 1 km offset for the reservoir interval
2. Egorov et al. (2018) successfully calculated and interpreted the results of FWI data for time-lapse DAS data
3. Correa et al. (2018) showed a successful application of DAS VSP with an SOV for the detection of CO_2

Based on the successful trials of DAS VSP with an SOV, the *Stage 3* PRM design is based on installing several permanent SOVs and wells equipped with DAS fibre to monitor injection of 15 kt of supercritical gas was injected into the same Lower Paaratte formation via the CRC3 well located 650 m downdip westwards from the CRC2 well. Five wells about 1600 m deep were equipped with enhanced back-scattering fibre-optic cables, and nine SOVs were installed on the surface over an area of about 1 km^2. The SOVs operated every second day with DAS in the wells recording continuously, allowing the acquisition of a monitor vintage every second day.

The main limitation of the proposed PRM system is a limited coverage. The one well-SOV pair images an area along one 2D transect. To verify the results of the permanent monitoring, additional 4D VSP monitoring was acquired. One baseline survey was acquired before the injection, the first monitor after five kilotons of CO_2 injected and the second after the end of the injection (15 kilotons CO_2).

Unlike 4D seismic with a mobile source such as vibroseis, the PRM design has a small number of permanent sources, resulting in lower fold, coverage and repeatability. On the other hand, PRM can operate almost continuously, producing vintages every day. The processing successive vintages simultaneously can improve repeatability (Mateeva et al. 2020). However, the number of PRM projects with frequent acquisition is relatively small, and standardised processing tools for such data are yet to be developed.

The thesis addresses seven different problems related to permanent borehole seismic monitoring using DAS:

- Store enormous amounts of data daily recorded by DAS system; a sophisticated network and storage capabilities are required to operate such a system

- Automate the processing of such a large volume of data was one of the main objectives
- Utilise data features (VSP, orbital vibrators, densely spaced vintages) for tailored processing to improve repeatability
- Trace CO_2 plume migration and cross-check with 4D DAS VSP data
- Analyse the effect of source mispositioning on 4D VSP repeatability
- Analyse the effect of rock stiffness on DAS amplitudes in a well
- Detect and study a tube wave in a gathering line transporting CO_2 to the injection well

1.2 THE OBJECTIVES AND OUTLINES

The overall objective of this thesis is to explore the methodology and processing of continuous borehole seismic to monitor carbon dioxide geosequestration with the help of DAS technology. Five publications explore PRM survey design and results, rock stiffness's effect on DAS, source mispositioning's effect on repeatability, and study tube waves in a CO_2 gathering line. Below I outline more details about each objective:

Objective 1. Develop the PRM monitoring system, automate acquisition and processing, develop a data storage and processing facility, study initial data repeatability.

As discussed in the Background section, the number of PRM projects worldwide is relatively small. Currently, there is no common standard in the design of such projects, and every project has unique features. For a PRM project to run successfully, it requires reliable equipment and communication network, sufficient data storage, fast remote access (the Otway site is located in Victoria, while the operating team was in Perth, Western Australia).

The outlined problems are addressed in Paper 1 - **An automated system for continuous monitoring of CO_2 geosequestration using multi-well offset VSP with permanent seismic sources and receivers: Stage 3 of the CO2CRC Otway Project.** In this paper, we explain the monitoring system design, present the equipment connection diagrams and descriptions, and the data handling procedures. Initial 1.3 TB of daily data are converted to about 500 MB during the automated processing workflow and sent to the cloud storage to be downloaded in the Perth office for further processing. Images of the data at different processing steps are provided. The initial repeatability study shows that different SOVs have a different levels of repeatability, while all the wells have a relatively similar level of repeatability. Repeatability

decreases over time with a different rate for different SOVs and is linked to seasonal variations.

Objective 2. Improve processing algorithm utilising data features (VSP, orbital vibrators, densely spaced vintages), detect and trace CO_2 plume migration. Confirm monitoring results with 4D VSP.

DAS-VSP monitoring produces 45 2D transects every 2 days and can be processed independently as standard offset-VSP data. However, the acquired data have several unique features that can be utilised to improve processing results. In Paper 2, **Advanced time-lapse processing of continuous DAS VSP data for plume evolution monitoring: Stage 3 of the CO2CRC Otway project case study,** we use some of these features to advance processing. VSP data allow the deterministic wavelet estimation using the direct wave. Knowing the wavelet for every vintage improves repeatability by correcting the wavelet for the effects of seasonal variations. Orbital vibrators can rotate in different directions, clockwise and counterclockwise, producing the P-wave wavefields with similar polarisations and oppositely polarised S-wave wavefields. We found that stacking these rotations together improves the P-wave signal and attenuates S-wave wavefield.

The most important advantage of prolonged acquisition is having multiple baseline vintages, so that different baselines can be chosen for different monitor vintages to minimise the effect of near-surface variations and enhance repeatability.

At the end of the paper, we confirm the results of the PRM by comparing them with 4D VSP data. Moreover, the greater level of repeatability in PRM data compared to the 4D VSP approach allowed the detection of previous Stage 2C plume remobilisation. This previous plume was injected into the same formation five years before the current Stage 3 commenced into the CRC2 well, which is 650 m up-dip to the east.

Objective 3. Study and correct the effect of rock stiffness on DAS amplitudes.

As noted in the Background, DAS is a relatively new sensor technology and differs from its predecessors (geophones). Most DAS interrogators measure strain rate along the fibre while the geophones measure the particle velocity. These differences are explored in the peer-reviewed extended conference abstract (Paper 3) - **Effect of rocks stiffness on observed DAS VSP amplitudes.** We showed that the difference in amplitudes between the geophones and DAS is quite significant and can reach up to 2.2 times over a 1300 m interval. This needs to be

accounted for before any amplitude analysis. For this purpose, we developed a formula to calculate the correction coefficient based on the rock density and P-wave velocity.

Objective 4. Study the effect of mispositioning on 4D VSP repeatability.

In Paper 2, we compared the PRM approach against the 4D VSP seismic. During the 4D VSP monitoring survey, several shot points were shifted from the original baseline shot point locations, resulting in poorer repeatability. The number of studies of onshore mispositioning effect on 4D VSP repeatability is very limited. Paper 4, **Effect of Source Mispositioning on the Repeatability of 4D Vertical Seismic Profiling Acquired with Distributed Acoustic Sensors,** outlines such a study. It utilises data acquired during the Otway Stage 3 4D VSP experiment and another experiment conducted at the Curtin/National Geosequestration Laboratory (NGL) research facility, specifically designed to study the effects of mispositioning on the repeatability of 4D VSP data. We found out that spatial near-surface variations can be a strong source of non-repeatability when source mispositioning exceed 1-2 meters.

Objective 5. Study a tube wave induced by a permanent seismic source in the gathering line during CO_2 injection.

While monitoring the carbon dioxide geosequestration at the Otway site during Stage 3, we detected a pellicular tube wave generated by an SOV and recorded by a surface fibre optical cable installed in the same trench as the gathering line. The tube wave appeared when the injection started and disappeared several months after the injection stopped. The properties of this tube wave (apparent velocity and amplitude) vary over the monitoring period and can probably be used for CO_2 flow monitoring purposes. The design of the experiment and some results are described in the peer-reviewed extended conference abstract (Paper 5) **Continuous DAS recording with permanent seismic sources reveals peculiar tube waves associated with the fluid flow**.

1.3 THESIS PUBLICATIONS AND THEIR RELATION TO THE THESIS TOPIC

1. ***Isaenkov, R., Pevzner, R., Glubokovskikh, S., Yavuz, S., Yurikov, A., Tertyshnikov, K., Gurevich, B., Correa, J., Wood, T., Freifeld, B., Mondanos, M., Nikolov, S., Barraclough, P., 2021. An automated system for continuous monitoring of CO2 geosequestration using multi-well offset VSP with permanent seismic sources and receivers: Stage 3 of the CO2CRC Otway Project. International Journal of Greenhouse Gas Control 108, 103317.***

Paper 1 describes the permanent seismic monitoring system based on a combination of permanent seismic sources and borehole fibre optic sensors. A permanent automated

continuous seismic CO_2 geosequestration monitoring system was installed at the CO2CRC Otway Project site (Victoria, Australia) in early 2020. The system comprises five deviated ~1600 m deep wells equipped with distributed acoustic sensing (DAS) acting as seismic receivers and nine seismic orbital vibrators (SOV) as permanent seismic sources. DAS recording is performed continuously by three iDASv3 units. Each SOV operates for 2.5 h at a time; all SOVs operate sequentially (during daytime only), producing a single vintage every two days. Each vintage consists of 45 offset VSP transects covering predicted CO_2 plume migration paths over ~0.7 km^2. An automated data processing implemented on-site reduces data volume from ~1.3 TB/day to ~500 MB/day, with the results automatically transmitted to the office daily. The repeatability analysis based on pre-injection data (acquired from May to October 2020 before the injection started in December 2020) shows that variability of SOV performance is the primary source of non-repeatability, while borehole measurements are pretty stable. An SOV waveform could reach NRMS value from 20 to 100 % within a few days. However, deconvolution of the seismograms with the waveform estimated from the direct wave reduces the repeatability to NRMS values within 10–15 %.

2. ***Isaenkov, R., Pevzner, R., Glubokovskikh, S., Yavuz, S., Shashkin, P., Yurikov, A., Tertyshnikov, K., Gurevich, B., Correa, J., Wood, T., 2022. Advanced time-lapse processing of continuous DAS VSP data for plume evolution monitoring: Stage 3 of the CO2CRC Otway project case study. International Journal of Greenhouse Gas Control 119, 103716.***

Paper 2 explores the advantages of the PRM dataset acquired with permanent borehole DAS receivers and SOVs at the Otway site to monitor the injection of 15 kt of CO_2 into a saline aquifer. The data reveal seasonal repeatability variations, mainly created by seasonal variations in precipitation levels. We showed that for each monitor dataset, the optimal baseline is the one acquired during the same season. The wavefield decomposition of P and S waves further improves the signal-to-noise ratio. The consistency of the source signature is improved using Wiener filtering. These algorithms improve the data repeatability from about 15–20% to 10–15% of NRMS values. With such a high level of repeatability, the CO_2 plume signal is detected on the second day of the injection. Moreover, the system detected remobilisation of the CO_2 plume injected into the same formation 650 m up-dip five years earlier during Stage 2C of Otway project. The remobilisation is the result of interaction with CO_2 injected during Stage 3.

Furthermore, the subsequent time-lapse changes of a stable CO_2 plume injected in the same reservoir 650 m up-dip five years earlier as a part of the previous Stage 2C were detected.

3. ***Isaenkov, R., Glubokovskikh, S., Tertyshnikov, K., Pevzner, R., Bona, A., 2020. Effect of Rocks Stiffness on Observed DAS VSP Amplitudes, EAGE Workshop on Fiber Optic Sensing for Energy Applications in Asia Pacific. European Association of Geoscientists & Engineers, pp. 1-5.***

Paper 3 examined a factor affecting amplitudes in downhole seismograms - dependence on rock stiffness and density at the receiver location. Unlike surface seismic scenarios, in VSP, there is usually a systematic change of receiver conditions as rocks naturally become stiffer with depth due to compaction. Thus, we expect a trend in the intensity of the seismic signals on both geophones and DAS, which will be more pronounced on the latter. Thus, amplitudes should be corrected for that effect before any quantitative amplitude analysis or migration of VSP data. We outline an analytical model relating the DAS measurements to rock stiffness and validate it using full-waveform elastic simulations. We illustrate the theory using zero-offset VSP data.

4. ***Isaenkov, R.; Tertyshnikov, K.; Yurikov, A.; Shashkin, P.; Pevzner, R, 2022. Effect of Source Mispositioning on the Repeatability of 4D Vertical Seismic Profiling Acquired with Distributed Acoustic Sensors. 24.***

Paper 4 explored the mapping of the CO_2 plume using 4D VSP data. Due to local activity, some of the monitor surveys' shot points were shifted, resulting in strong mispositioning and a decrease in repeatability. Here, we study the effect of mispositioning on the repeatability of borehole time-lapse seismic. While the mispositioning effect has been extensively studied for surface 4D seismic, the number of such studies for VSP is limited. To study the impact of source mispositioning on data repeatability, we performed two VSP experiments at two onshore sites with a vibroseis source. The first study was carried out at the Otway site and showed that the effect of source mispositioning on repeatability is negligible in comparison with the effect of temporal variations of the near-surface conditions. To avoid these limitations, we conducted a same-day controlled experiment at the Curtin University site. This second experiment showed that the effect of source mispositioning on repeatability is controlled by the degree of lateral variations of the near-surface conditions. Unlike in marine seismic measurements, lateral variations of near-surface properties can be strong and rapid and degrade the repeatability noticeably for a few meter shifts of the source. The greater the mispositioning, the higher the chance of such significant variations. When the near-surface conditions are laterally homogeneous, the effect of typical source mispositioning is small, and in all practical monitoring applications, its contribution to non-repeatability is negligible.

5. ***Isaenkov, R., Yurikov, A., Tertyshnikov, K., Gurevich, B., Pevzner, R., 2022. Continuous Das Recording with Permanent Seismic Sources Reveals Peculiar Tube Waves***

Associated with the Fluid Flow, EAGE GeoTech 2022 Third EAGE Workshop on Distributed Fibre Optic Sensing. European Association of Geoscientists & Engineers, pp. 1-4.

While monitoring the CO_2 injection at the Otway site, we observed a peculiar tube wave generated in a horizontal pipeline that transferring CO_2 to the injector well. We explored several seismic parameters that could potentially benefit fluid flow monitoring. If further studies are successful, gathering pipe monitoring can be a valuable part of future PRM projects.

1.4 CONCLUSIONS AND OUTLOOK

1.4.1 An automated system for continuous monitoring of CO_2 injection

The monitoring system designed to monitor a small-scale CO_2 injection at Otway acquires a seismic vintage every two days and requires almost no human effort on site. Such a system can coexist with industrial or farm areas as it produces a tolerable level of noise and operates within the allowed schedule. Moreover, the borehole design minimises land use and thus minimises disruption with landowners.

The repeatability analysis shows that the receivers are not affected by varying near-surface conditions, which improves repeatability. The wavelets emitted by the permanent sources can be reconstructed from the data recorded by borehole receivers. These wavelets are then used to correct for non-repeatability of the sources caused by varying near-surface conditions mainly due to seasonal weather variations. Initial wavelet repeatability after deconvolution achieved 10-15 % of NRMS.

The short turnaround time (2 days) allows acquiring 180 vintages per year. This amount of vintages allows representing data in 3D (receiver depth - recording time (seconds) - recording date (days)). This new dimension (slow time) opens new possibilities for processing. Potentially, we could develop a machine learning algorithm to use such datasets to predict a more stable time-lapse signal and reduce amount of time-lapse noise.

Krull, Buchholz, and Jug (2019) proposed Noise2Void self-supervised machine learning algorithm to suppress random noise on images. It utilises the ability to predict a pixel signal based on neighbour pixels but not the noise (if noise is random and cannot be predicted). Birnie et al. (2021) expanded Noise2Void application to process seismic data. Its applications seems promising for Otway SOV data, as neighbour vintages contain similar time-lapse signal

but time-lapse noise at least partially random. This could improve the detection of smaller scale signals.

The system is designed for each SOV to operate for 2.5 hours one after another and thus it takes two days to run all SOVs to acquire a full vintage. Potentially, several SOVs can run simultaneously if operated at different frequencies. The recorded data will contain signal from several SOVs but the data can be deblended in frequency domain. For example, if two SOVs could be run simultaneously, we could acquire a full vintage a day or use this data to improve signal-to-noise ratio by about 1.4 times.

Seismic monitoring program for Stage 3 was designed to monitor a small-scale injection, much smaller than any commercial size CCS projects. However, all of the components used in Stage 3 are ready to be deployed to monitor larger-scale injections.

4D VSP with DAS has already been successful in reservoir monitoring in oil & gas industry (Mateeva et al. 2017). The Otway site was the first site instrumented with engineered fibres for DAS sensing, but this can be directly translated to any other projects. Furthermore, 4D VSP on land can potentially be replaced with a near surface array comprised of buried omnidirectional DAS cables or a series of shallow instrumented wells. This is an important subject of future research.

SOVs are powerful enough to be used as permanent seismic sources for large offsets. The downside of the SOVs is relatively poor repeatability. Stage 3 explicitly benefited from VSP geometry, which allows compensation of the recorded signal for seasonal variations of the SOV signature (similar problems are likely to arise with conventional seismic sources). As such, we believe that even if SOVs can be paired with a surface receiver array, there has to be a downhole array in the vicinity of SOV to control the far-field signature.

The range of problems and the type of monitoring appropriate for a large-scale injection that can be solved using DAS/SOV pair is somewhat different compared to Stage 3. Most likely, the role of this type of surveys will be in conformance monitoring or a “perimeter” monitoring where a ‘fence’ of wells and SOVs can be monitoring critical transects.

1.4.2 Advanced time-lapse processing of continuous PRM data

Analysis of a year-long dataset with two days of sampling in slow time shows that seasonal changes in the near-surface are the primary source of non-repeatability. The difference can be as much as 40 % NRMS. These variations are mainly created by weather changes in different seasons, affecting soil physical properties. We created several techniques to minimise the

effect of these variations on time-lapse data. We stack clockwise and counterclockwise rotations of the orbital vibrator to reduce the non-repeatable shear-wave wavefield. This works by decomposing circular polarisation of the source into vertical and horizontal components. The vertical component contains mainly P-wave energy while the horizontal component produces mainly S-waves. Thus, the vertical component has significantly less S- and SP- wave energy compared to original data. This procedure involves stacking which, also improves the signal-to-noise ratio by about 40%.

To minimise the effect of seasonal variations, we developed a 'smart' baseline selection processing workflow. We select the best matching vintage from the extended 90 vintage baselines for each monitor vintage to account for the seasonal variations in the data. This reduces NRMS from 15% to about 12 % NRMS on average. For future applications, I would recommend to have a longer baseline – a year in our case – to record most of the possible weather variations. The length of the baseline is likely to be dependent on the climate of the area and near-surface conditions. Also, it is possible to employ a neural network to select a linear combination of all base vintages to create the best-matching baseline. It would improve the current implementation of a single-vintage baseline or several-vintages baseline, whose selection is based on a single attribute.

1.4.3 Despite the low fold of the data in the continuous offset VSP setup, due to high level of repeatability the CO_2 plume was detected as early as two days after the start of the injection. Furthermore, the data reveal possible re-mobilisation of a pre-existing plume created by a previous injection in the same reservoir. Potentially, such a system can be employed for CO_2 dissolution monitoring. Gradual dissolution of CO_2 in the brine will result in changes of P wave velocity and density, however these changes are likely to be quite small. However, the monitoring system with high enough repeatability can potentially detect it. Effect of rock stiffness on observed DAS VSP amplitudes

Receiver sensitivity depends on local stiffness and density of rocks at the receiver location, leading to systematic spatial variations changes of the measured strains. It is thus crucial to consider this variation when analysing seismic imaging or amplitude. The effect of rock stiffness on DAS sensitivity is higher than that of geophones, with field experiment data indicating a maximum difference of almost 7 dB (2.2x times) over a 1300 m interval. To avoid significant errors, this effect must be taken into account during DAS amplitude processing and interpretation.

The conversion filter from particle velocity to DAS reveals that DAS is not precisely a strain rate. It behaves like a strain rate at low wavenumbers and small gauge and pulse lengths but differs under other circumstances. Despite various perspectives in the literature, it is still unclear what DAS measures due to internal interrogator processing. To create an appropriate filter for rock stiffness effect compensation, understanding the output units of DAS is necessary. Thus, further research on the recorded units of DAS is required.

1.4.4 Effect of source mispositioning on 4D VSP repeatability

We studied the effect of mispositioning on repeatability based on two experiments. The experiment at Otway shows domination of seasonal repeatability variation effect on mispositioning. The second same-day experiment was designed to avoid seasonal variations and simulated mispositioning from tens of centimiters to tens of meters.

We observed zonal distribution of repeatability, which is related to spatial variations of near-surface conditions. The effect of near surface on repeatability is significantly larger than the one from mispositioning. However, in presence of strong lateral variations in near surface conditions, source mispositioning as small as several meters can lead to a significant decrease in repeatability. Thus, we suggest keeping mispositioning as small as possible, preferably within the 1-2 meters to avoid strong non-repeatability.

We studied only the effect of mispositioning on repeatability, not the processing techniques to improve repeatability in such a case. In our study, all the shot point were correlated with the same synthetic sweep signal. Possibly, correlation with the on-plate sweep recording or signature deconvolution could partially recover repeatability. Such a study would be of a great interest.

1.4.5 Continuous DAS recording with permanent seismic sources reveals peculiar tube waves associated with the fluid flow

The transportation of CO_2 through pipelines is an important component of CCS technology, which involves capturing CO_2 from industrial processes and storing it underground. During the injection of CO_2 into an underground reservoir, seismic sources are commonly used to monitor the propagation of the CO_2 plume. However, these seismic sources can also excite tube waves in the horizontal pipeline, which can affect the properties of the CO_2 flow.

Our results show that the tube wave parameters, such as the wave velocity, vary over time during the injection of CO2 into the pipeline. We assume that these variations are linked to the properties of the CO_2 flow, such as the flow rate, pressure, and temperature. However, theoretical and physical modelling are required to prove this hypothesis. If successful, a combination of DAS and permanent seismic source can be used for continuous monitoring of the CO_2 flow.

2 REFERENCES

Ajayi, Temitope, Jorge Salgado Gomes, and Achinta Bera. 2019. 'A review of CO 2 storage in geological formations emphasizing modeling, monitoring and capacity estimation approaches', *Petroleum Science*, 16: 1028-63 https://doi.org/10.1007/s12182-019-0340-8.

Amoyedo, Sunday, Roger M Slatt, and Kurt J Marfurt. 2011. 'Time-lapse (4D) effect and reservoir sand production pattern in a mature North Sea field', *The Leading Edge*, 30: 1020-25

Bakulin, AV, RM Burnstad, MA Jervis, and PG Kelamis. 2012. "The feasibility of permanent land seismic monitoring with buried geophones and hydrophones." In *74th EAGE Conference and Exhibition incorporating EUROPEC 2012*, cp-293-00789. European Association of Geoscientists & Engineers

Birnie, Claire, Matteo Ravasi, Sixiu Liu, and Tariq Alkhalifah. 2021. 'The potential of self-supervised networks for random noise suppression in seismic data', *Artificial Intelligence in Geosciences*, 2: 47-59

CO2CRC. 2023. 'CO2CRC'. http://co2crc.com.au/co2crcs-otway-stage-3-project-recognised-cslf/

Cook, P. 2014. *Geologically Storing Carbon: Learning from the Otway Project Experience* (CSIRO PUBLISHING)

Correa, Julia, Anton Egorov, Konstantin Tertyshnikov, Andrej Bona, Roman Pevzner, Tim Dean, Barry Freifeld, and Steve Marshall. 2017. 'Analysis of signal to noise and directivity characteristics of DAS VSP at near and far offsets — A CO2CRC Otway Project data example', *The Leading Edge*, 36: 994a1-94a7 https://doi.org/10.1190/tle36120994a1.1.

Correa, Julia, Konstantin Tertyshnikov, Todd Wood, Sinem Yavuz, Barry Freifeld, and Roman Pevzner. 2018. "Time-lapse VSP with permanent seismic sources and distributed acoustic sensors: CO2CRC Stage 3 equipment trials." In *14th Greenhouse Gas Control Technologies Conference Melbourne*, 21-26. http://dx.doi.org/10.2139/ssrn.3365561

Dou, Shan, Todd Wood, Jonathan Ajo-Franklin, Michelle Robertson, Thomas Daley, Barry Freifeld, Roman Pevzner, and Boris Gurevich. 2017. "Surface orbital vibrator for permanent seismic monitoring: A signal contents and repeatability appraisal." In *2017 SEG International Exposition and Annual Meeting*, 5. Houston, Texas: Society of Exploration Geophysicists https://doi.org/10.1190/segam2017-17797822.1.

Egorov, Anton, Julia Correa, Andrej Bóna, Roman Pevzner, Konstantin Tertyshnikov, Stanislav Glubokovskikh, Vladimir Puzyrev, and Boris Gurevich. 2018. 'Elastic full-waveform inversion of vertical seismic profile data acquired with distributed acoustic sensors', *Geophysics*, 83: R273-R81 https://doi.org/10.1190/geo2017-0718.1.

Eiken, Ola, Philip Ringrose, Christian Hermanrud, Bamshad Nazarian, Tore A Torp, and Lars Høier. 2011. 'Lessons learned from 14 years of CCS operations: Sleipner, In Salah and Snøhvit', *Energy Procedia*, 4: 5541-48 https://doi.org/10.1016/j.egypro.2011.02.541.

Glubokovskikh, Stas, Roman Pevzner, Tess Dance, Eva Caspari, Dmitry Popik, Valeriya Shulakova, and Boris Gurevich. 2016. 'Seismic monitoring of CO2 geosequestration: CO2CRC Otway case study using full 4D FDTD approach', *International Journal of Greenhouse Gas Control*, 49: 201-16 http://dx.doi.org/10.1016/j.ijggc.2016.02.022.

Hansen, Olav, Douglas Gilding, Bamshad Nazarian, Bård Osdal, Philip Ringrose, Jan-Boye Kristoffersen, Ola Eiken, and Hilde Hansen. 2013. 'Snøhvit: The history of injecting and storing 1 Mt CO2 in the fluvial Tubåen Fm', *Energy Procedia*, 37: 3565-73 https://doi.org/10.1016/j.egypro.2013.06.249.

IEA. 2015. "Carbon Capture and Storage: The solution for deep emissions reductions." In.: IEA

Isaenkov, Roman, Roman Pevzner, Stanislav Glubokovskikh, Sinem Yavuz, Pavel Shashkin, Alexey Yurikov, Konstantin Tertyshnikov, Boris Gurevich, Julia Correa, and Todd Wood. 2022. 'Advanced time-lapse processing of continuous DAS VSP data for plume evolution monitoring: Stage 3 of the CO2CRC Otway project case study', *International Journal of Greenhouse Gas Control*, 119: 103716 https://doi.org/10.1016/j.ijggc.2022.103716.

Isaenkov, Roman, Roman Pevzner, Stanislav Glubokovskikh, Sinem Yavuz, Alexey Yurikov, Konstantin Tertyshnikov, Boris Gurevich, Julia Correa, Todd Wood, Barry Freifeld, Michael Mondanos, Stoyan Nikolov, and Paul Barraclough. 2021. 'An automated system for continuous monitoring of CO2 geosequestration using multi-well offset VSP with permanent seismic sources and receivers: Stage 3 of the CO2CRC Otway Project', *International Journal of Greenhouse Gas Control*, 108: 103317 https://doi.org/10.1016/j.ijggc.2021.103317.

Jenkins, Charles. 2020. 'The State of the Art in Monitoring and Verification: an update five years on', *International Journal of Greenhouse Gas Control*, 100: 103118 https://doi.org/10.1016/j.ijggc.2020.103118.

Jenkins, Charles, Andy Chadwick, and Susan D. Hovorka. 2015. 'The state of the art in monitoring and verification—Ten years on', *International Journal of Greenhouse Gas Control*, 40: 312-49 http://dx.doi.org/10.1016/j.ijggc.2015.05.009.

Jervis, M, A V. Bakulin, R M. Burnstad, Cecile Beron, and Eric Forgues. 2012. "Observations of surface vibrator repeatability in a desert environment." In *74th EAGE Conference and Exhibition incorporating EUROPEC 2012*, cp-293-00790. EAGE Publications BV https://doi.org/10.3997/2214-4609.20148786.

Johnston, David H, and Bernard P Laugier. 2012. 'Resource assessment based on 4D seismic and inversion at Ringhorne Field, Norwegian North Sea', *The Leading Edge*, 31: 1042-48 https://doi.org/10.1190/tle31091042.1.

Johnston, David H. 2013. *Practical Applications of Time-lapse Seismic Data* (Society of Exploration Geophysicists) https://doi.org/10.1190/1.9781560803126.

Kashubin, Artem, Christopher Juhlin, Alireza Malehmir, Stefan Lüth, Alexandra Ivanova, and Niklas Juhojuntti. 2011. "A footprint of rainfall on land seismic data repeatability at the CO2 storage pilot site, Ketzin, Germany." In *2011 SEG Annual Meeting*. OnePetro https://doi.org/10.1190/1.3628076.

Kikuta, Katsuhiko, Seiji Hongo, Daiji Tanase, and Takashi Ohsumi. 2005. "Field test of CO2 injection in Nagaoka, Japan." In *Proceedings of seventh international conference on greenhouse gas control technologies*, 1367-72.

Krull, Alexander, Tim-Oliver Buchholz, and Florian Jug. 2019. "Noise2void-learning denoising from single noisy images." In *Proceedings of the IEEE/CVF conference on computer vision and pattern recognition*, 2129-37.

Kuvshinov, B. N. 2016. 'Interaction of helically wound fibre-optic cables with plane seismic waves: Interaction of fibre-optic cables', *Geophysical Prospecting*, 64: 671-88 https://doi.org/10.1111/1365-2478.12303.

Lopez, JL, PB Wills, JR La Follett, JC Hornman, JHHM Potters, M van Lokven, C Perkins, and C Trefanenko. 2015. "Permanent seismic reservoir monitoring for real-time surveillance of thermal EOR at Peace River." In *Third EAGE Workshop on Permanent Reservoir Monitoring 2015*, 1-5. European Association of Geoscientists & Engineers https://doi.org/10.3997/2214-4609.201411961.

Martens, Sonja, Axel Liebscher, Fabian Möller, Jan Henninges, Thomas Kempka, Stefan Lüth, Ben Norden, Bernhard Prevedel, Alexandra Szizybalski, and Martin Zimmer. 2013. 'CO2 storage at the Ketzin pilot site, Germany: fourth year of injection, monitoring, modelling and verification', *Energy Procedia*, 37: 6434-43 https://doi.org/10.1016/j.egypro.2013.06.573.

Mateeva, A., J. Lopez, D. Chalenski, M. Tatanova, P. Zwartjes, Z. Yang, S. Bakku, K. de Vos, and H. Potters. 2017. '4D DAS VSP as a tool for frequent seismic monitoring in deep water', *The Leading Edge*, 36: 995-1000 https://doi.org/10.1190/tle36120995.1.

Mateeva, Albena, Denis Kiyashchenko, Yuting Duan, Tianrun Chen, and Kanglin Wang. 2020. 'Considerations in planning, acquisition, processing and interpretation of 4D DAS VSP.' in, *SEG Technical Program Expanded Abstracts 2020* (Society of Exploration Geophysicists) https://doi.org/10.1190/segam2020-3428312.1.

Mattos, A., Durusut, E. 2018. 'Industrial Carbon Capture Business Models' https://assets.publishing.service.gov.uk/government/uploads/system/uploads/attachment_data/file/759286/BEIS_CCS_business_models.pdf.

Nakatsukasa, Masashi, Hideaki Ban, Mamoru Takanashi, Ayato Kato, Kyle Worth, and Donald White. 2017. 'Repeatability of a rotary seismic source at the Aquistore CCS site.' in, *SEG Technical Program Expanded Abstracts 2017* (Society of Exploration Geophysicists) https://doi.org/10.1190/segam2017-17780266.1.

Onuwaje, A, A Adejonwo, I Al-Mandhary, R Detomo Jr, O Effiom, W Gouveia, N Kremers, E Legius, A MacLellan, and R Mcclenaghan. 2009. "The Bonga 4D–Shell Nigeria's First Deepwater Time Lapse Monitor." In *71st EAGE Conference and Exhibition incorporating SPE EUROPEC 2009*, cp-127-00581. EAGE Publications BV https://doi.org/10.3997/2214-4609.201400588.

Pachauri, RK, and LA Meyer. 2014. 'Climate Change 2014: Synthesis Report. Contribution of Working Groups I, II and III to the Fifth Assessment Report of the Intergovernmental Panel on Climate Change'

Parker, Tom, Sergey Shatalin, and Mahmoud Farhadiroushan. 2014. 'Distributed Acoustic Sensing-A New Tool for Seismic Applications', *First Break*, 32: 61-69 https://doi.org/10.3997/1365-2397.2013034.

Pevzner, R., K. Tertyshnikov, V. Shulakova, M. Urosevic, A. Kepic, B. Gurevich, and R. Singh. 2015. "Design and deployment of a buried geophone array for CO2 geosequestration monitoring: CO2CRC Otway Project, Stage 2C." In *SEG Technical Program Expanded Abstracts 2015*, 266-70. Society of Exploration Geophysicists https://doi.org/10.1190/segam2015-5902309.1.

Pevzner, Roman, Roman Isaenkov, Sinem Yavuz, Alexey Yurikov, Konstantin Tertyshnikov, Pavel Shashkin, Boris Gurevich, Julia Correa, Stanislav Glubokovskikh, and Todd Wood. 2021. 'Seismic monitoring of a small CO2 injection using a multi-well DAS array: Operations and initial results of Stage 3 of the CO2CRC Otway project', *International Journal of Greenhouse Gas Control*, 110: 103437 https://doi.org/10.1016/j.ijggc.2021.103437.

Pevzner, Roman, Milovan Urosevic, Dmitry Popik, Valeriya Shulakova, Konstantin Tertyshnikov, Eva Caspari, Julia Correa, Tess Dance, Anton Kepic, Stanislav Glubokovskikh, Sasha Ziramov, Boris Gurevich, Rajindar Singh, Matthias Raab, Max Watson, Tom Daley, Michelle Robertson, and Barry Freifeld. 2017. '4D surface seismic tracks small supercritical CO2 injection into the subsurface: CO2CRC Otway Project', *International Journal of Greenhouse Gas Control*, 63: 150-57 https://doi.org/10.1016/j.ijggc.2017.05.008.

Pevzner, Roman, Milovan Urosevic, Konstantin Tertyshnikov, Hussain AlNasser, Eva Caspari, Julia Correa, Tom Daley, Tess Dance, Barry Freifeld, Stanislav Glubokovskikh, Andrew Greenwood, Anton Kepic, Dmitry Popik, Sofya Popik, Matthias Raab, Michelle Robertson, Valeriya Shulakova, Rajindar Singh, Max Watson, Sinem Yavuz, Sasha Ziramov, and Boris Gurevich. 2020. 'Chapter 6.1 - Active surface and borehole seismic monitoring of a small supercritical CO2 injection into the subsurface: experience from the CO2CRC Otway Project.' in Junzo Kasahara, Michael S. Zhdanov and Hitoshi Mikada

(eds.), *Active Geophysical Monitoring (Second Edition)* (Elsevier) https://doi.org/10.1016/B978-0-08-102684-7.00024-8.

Popik, Sofya, Roman Pevzner, Konstantin Tertyshnikov, Dmitry Popik, Milovan Urosevic, Valeriya Shulakova, Stanislav Glubokovskikh, and Boris Gurevich. 2020. '4D surface seismic monitoring the evolution of a small CO2 plume during and after injection: CO2CRC Otway Project study', *Exploration Geophysics*: 1-11 https://doi.org/10.1080/08123985.2020.1735934.

Prinet, Catherine, Sylvain Thibeau, Marc Lescanne, and Jacques Monne. 2013. 'Lacq-Rousse CO2 capture and storage demonstration pilot: Lessons learnt from two and a half years monitoring', *Energy Procedia*, 37: 3610-20 https://doi.org/10.1016/j.egypro.2013.06.254.

Schisselé, E, E Forgues, J Echappé, J Meunier, O De Pellegars, and C Hubans. 2009. "Seismic repeatability–Is there a Limit?" In *71st EAGE Conference and Exhibition incorporating SPE EUROPEC 2009*, cp-127-00414. European Association of Geoscientists & Engineers https://doi.org/10.3997/2214-4609.201400421.

Wang, Xiaolei, Bing Xue, Rensheng Cui, Guoliang Gu, Chaoyong Peng, Yu Zheng, and Jiansi Yang. 2020. 'A method of phase identification for seismic data acquired with the controlled accurate seismic source (CASS)', *Geophysical Journal International*, 222: 54-68 https://doi.org/10.1093/gji/ggaa108.

Worth, Kyle, Don White, Rick Chalaturnyk, Jim Sorensen, Chris Hawkes, Ben Rostron, Jim Johnson, and Aleana Young. 2014. 'Aquistore project measurement, monitoring, and verification: from concept to CO2 injection', *Energy Procedia*, 63: 3202-08 https://doi.org/10.1016/j.egypro.2014.11.345.

Yavuz, Sinem, Julia Correa, Roman Pevzner, Barry Freifeld, Todd Wood, Konstantin Tertyshnikov, Sofya Popik, and Michael Robertson. 2019. 'Assessment of the permanent seismic sources for borehole seismic monitoring applications: CO2CRC Otway Project', *ASEG Extended Abstracts*, 2019: 1-5 https://doi.org/10.1080/22020586.2019.12073157.

Zwartjes, PM, TB Barker, JC Hornman, and J Przybysz-Jarnut. 2015. "Quantitative interpretation of nine months of daily SeisMovie™ data to monitor steam injection at Schoonebeek." In *77th EAGE Conference and Exhibition 2015*, 1-5. European Association of Geoscientists & Engineers https://doi.org/10.3997/2214-4609.201412548.

3 PUBLISHED PAPERS

An automated system for continuous monitoring of CO_2 geosequestration using multi-well offset VSP with permanent seismic sources and receivers: Stage 3 of the CO2CRC Otway Project

https://doi.org/10.1016/j.ijggc.2021.103317

Roman Isaenkov[1,2], Roman Pevzner[1,2], Stanislav Glubokovskikh[1,2], Sinem Yavuz[1,2], Alexey Yurikov[1,2], Konstantin Tertyshnikov[1,2], Boris Gurevich[1,2], Julia Correa [3], Todd Wood[3], Barry Freifeld[4], Michael Mondanos[5], Stoyan Nikolov[5], Paul Barraclough[2]

[1] Curtin University, Department of exploration geophysics, 26 Dick Perry Avenue, 6151 Kensington, Australia

[2] CO2CRC, 11 – 15 Argyle Place South, Carlton, VIC, 3053, Australia

[3] Lawrence Berkeley National Laboratory, 1 Cyclotron Road, MS 74R-316C, Berkeley, CA, USA, 94720

[4] Class VI Solutions, Inc., 711 Jean St., Oakland, CA, USA, 94610

[5] Silixa Ltd., Silixa House, 230 Centennial Park, Centennial Avenue, Elstree WD6 3SN, UK

Corresponding author:

Roman Isaenkov

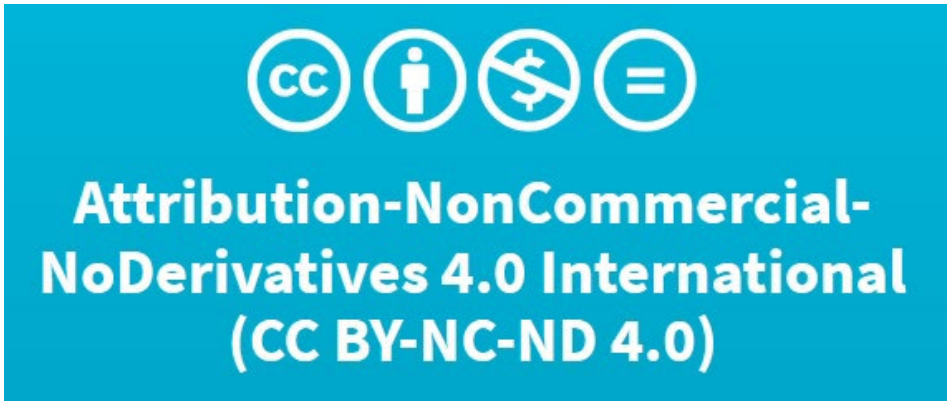

Abstract

A permanent automated continuous seismic CO_2 geosequestration monitoring system for was installed at CO2CRC Otway Project site (Victoria, Australia) in early 2020. The system is composed of five deviated ~1600 m deep wells equipped with distributed acoustic sensing (DAS) acting as seismic receivers and nine seismic orbital vibrators (SOV) as seismic sources. DAS recording is performed continuously by three iDASv3 units. Each SOV operates for 2.5 hours at a time, and hence all SOVs operating sequentially (during daytime only) produce in a single vintage every two days. Each vintage consists of 45 offset VSP transects covering predicted CO_2 plume migration paths over ~0.7 km^2 area. An automated data processing implemented on-site reduces data size from ~1.3 TB/day to ~500 MB/day with the results transmitted to the office daily.

The repeatability analysis based on pre-injection data (acquired from May to October 2020 before the injection start in December 2020) shows that variability of SOV performance is the main source of non-repeatability while borehole measurements are stable. An SOV waveform could reach NRMS value from 20 to 100% within a few days. However, deconvolution of the seismograms with the waveform of the direct wave reduces the repeatability to within 10-15% NRMS.

Keywords:

- Distributed acoustic sensors
- Permanent reservoir monitoring
- Time-lapse seismic
- Repeatability
- Seismic orbital vibrators

1 INTRODUCTION

Seismic methods are very useful for monitoring and verification programs for carbon capture and storage (CCS) projects in saline aquifers because the seismic properties of these reservoirs are often sensitive to the presence of supercritical CO_2 (Davis et al., 2019). In particular, time-lapse (TL) surface seismic – a series of repeated 3D seismic surveys has become a standard tool for delineation of a CO_2 plume (part of the subsurface occupied by the injected gas). A number of CO_2 projects around the world have reported clear TL anomalies associated with the injection of CO_2 Sleipner

(Norway) (Chadwick et al., 2009), Aquistore (Canada) (Roach and White, 2018), Ketzin (Germany) (Lüth et al., 2017), Otway (Australia) (Pevzner et al., 2017a) and Decatur (USA) (Bauer et al., 2019). Analysis of these TL anomalies pursues two main objectives (Wildenborg et al., 2014):

Verify CO_2 plume containment: the absence of any leakages from the allocated part of the reservoir (Jenkins, 2020);

Prove CO_2 plume conformance: predictions of existing reservoir models agree with the observe migration of the injected gas (Oldenburg, 2018).

Fulfilment of both monitoring objectives may require frequent snapshots of the subsurface, which is often unfeasible for conventional TL seismic - an expensive technology in terms of both financial costs and the time lag between data acquisition and processing. Another complication may arise due to limited land access to storage sites because many CCS projects are likely to be located close to an industrial source of the captured gas. Hence, time intervals between the TL surveys are typically on the order of years, which may be inadequate for containment monitoring. Between surveys, a site operator must rely on production data and a limited set of downhole measurements, such as pore pressure and temperature (Benson et al., 2004; Hannis, 2013). These non-seismic monitoring methods lack spatial coverage and resolution to detect a CO_2 leakage that may occur hundreds of meters away from a borehole. In addition, calibration of the reservoir models to sparse snapshots of plume evolution is poorly constrained, which may compromise the conformance fluid flow simulations (Arts et al., 2003).

One way to address these challenges is by continuous seismic monitoring using permanently installed seismic equipment (sources and receivers). Despite high upfront costs of the installation, continuous monitoring is economic, because the data acquisition and processing can be fully automated and performed remotely with minimal labour costs. In addition, permanent systems have low environmental and/or societal impact, which allows them to operate at almost any time. Pioneering technology in this field, SeisMovie® by CGGVeritas (CGG, 2002), can provide automated daily updates of a reservoir image using 49 permanent borehole source points and 1500 hydrophone points over an area of 1.5 km^2 (Lopez et al., 2015). More recent advancements in continuous seismic monitoring are associated with distributed acoustic sensing (DAS), a relatively new technology that allows

measuring dynamic strain along a fibre-optic cable, thus transforming the cable into a dense array of seismic sensors (Hartog, 2017; Parker et al., 2014).

DAS uses optical fibre to measure axial strain or strain rate along with the fibre (Bakku, 2015). In essence, the optical fibre becomes a several kilometres line of seismic receivers with channel spacing up to first tens of centimetres. Compared to conventional geophones, DAS with a standard single-mode fibre (SMF) lack directional sensitivity and SNR ratio. However, development of engineered fibres (Shatalin S.V., In press 2020) improves DAS sensitivity substantially making DAS data quality comparable to that of geophones (Correa et al., 2017).

In recent years DAS technology was utilised for monitoring of CO_2 storage using Vertical seismic profiling (VSP) (Otway (Pevzner et al., 2020b), Decatur (Couëslan et al., 2013), Aquistore (White, 2019)). These studies show the high potential of TL 2D and 3D VSP for storage monitoring. Compared to surface seismic setup, borehole-based receivers have much better coupling with the formation and are more stable, resulting in lower TL noise. On the other hand, the number of monitoring wells is limited by high drilling cost thus reducing possible image coverage.

Seismic orbital vibrator (SOV) is a permanent seismic source which excites seismic waves by rotation of eccentric weights by an AC induction motor. SOV is a source of P and S waves as rotations produce both vertically and horizontally polarized force (Correa et al., 2018; Daley and Cox, 2001). The emitted seismic energy increases as angular frequency squared due to spinning origin of the source; this results in unbalanced frequency content. Unlike a similar permanent source ACROSS (Nakatsukasa et al., 2017), SOV lacks phase control and thus requires synchronisation using a recording of the source signature by a nearby geophone (Freifeld et al., 2016).

This paper presents a DAS VSP based permanent seismic monitoring system with SOVs deployed for Stage 3 of the CO2CRC Otway Project (Victoria, Australia). Stage 3 focuses on testing and development of cost-effective approaches to containment monitoring for CO_2 storage projects (Jenkins et al., 2017), and hence continuous multi-well offset VSP has naturally become a key component of this project. To simulate a leakage, 15,000 tonnes of supercritical CO_2/CH_4 (80/20 by molar volume) mixture (referred to as CO_2 below) will be injected into a saline clastic aquifer at 1550 m. Then CO_2 is expected to quickly move up-dip and form a relatively narrow plume elongated along an impermeable fault (Bagheri et al., 2020). Such a rapidly evolving plume

provides a good test for the capabilities of the multi-well offset VSP. Some of the key uncertainties for the monitoring were resolved at a previous phase of the Otway Project, Stage 2C, which featured a very similar injection into the same reservoir (Pevzner et al., 2020b). In particular, we know that CO_2 saturation will likely cause a significant reduction of the rock stiffness, which allows for a confident detection of a small amount of CO_2 at seismic resolution (Caspari et al., 2015; Glubokovskikh et al., 2020; Pevzner et al., 2017a). Furthermore, the seismic sources and DAS receivers deployed at the Otway site provided an excellent signal-to-noise ratio (SNR) in the field tests, thus enabling robust interpretation of the TL response in the offset VSP data (Correa et al., 2018; Egorov et al., 2018; Egorov et al., 2017). Therefore, design of the seismic monitoring system for Stage 3 focused on three main objectives:

1. Maximising the value of information in the data, such as increased spatial coverage, reduced probability of false detection of CO_2 plume arrival, accurate seismic estimates of the plume parameters;
2. Automation of the data processing and acquisition;
3. Stability of the instrumentation and hardware, including computing facilities and data transfer infrastructure.

Installation of the monitoring system was completed in February 2019 (Bagheri et al., 2020), and includes nine sources permanently deployed on the surface and five ~1600 m deep wells instrumented with advanced DAS systems (Figure 1).

The paper is organized as follows. We begin with a summary of the pre-Stage 3 field tests at the Otway site, which determined the monitoring system design. We then give a detailed description of the system and an automated data processing workflow along with the processing/storage hardware. This is followed by the analysis of the data quality, system stability and performance over the first ~130 days of pre-injection monitoring.

2 SUMMARY OF THE SEISMIC MONITORING AT THE OTWAY SITE

As indicated in the introduction, the seismic monitoring program for Stage 3 (active phase from 2019) of the CO2CRC Otway Project is based on field trials conducted at the Otway site during Stage 2C injection experiment (2015 – 2018) designed to test the sensitivity limits for the detection of a small leakage by conventional surface TL

seismic (Cook, 2014). To this end, 15,000 tonnes of supercritical CO_2/CH4 (80/20) mixture were injected at very low pressure (~200 kPa) through a dedicated CRC2 well into the Lower Paaratte formation, a sandstone brine-saturated reservoir located at a depth of 1500 m (Dance, 2013). Stage 3 involves a similar injection of 15,000 tonnes of supercritical CO_2 into the same formation through the CRC3 well, which is 700m east from CRC2.

Pevzner et al. (2020b) give a detailed summary of the seismic monitoring program for Stage 2C; here we just summarise the main monitoring techniques. The key component of the TL seismic was a permanently deployed geophone array, which was buried at 4 m depth below the surface. The surface seismic program consisted of six repeat 3D seismic surveys acquired with a 15 klbs vibroseis truck: a baseline and five monitors acquired during and after injection (Popik et al., 2020). Concurrently with the surface seismic, 3D VSP was acquired in CRC1 well with a ten-level geophone tool positioned ~900 m deep. At the completion of each surface seismic vintage, a set of five offset VSPs were acquired in CRC-1 well. The main findings of the Stage 2C that contributed to the design of the Stage 3 monitoring program are:

1. TL seismic was able to detect as little as 5,000 tons of supercritical CO_2 fluid and image subsequent plume changes (Glubokovskikh et al., 2016; Pevzner et al., 2017a; Popik et al., 2020). This means that the seismic properties of the Lower Paaratte formation reservoir are very sensitive to the presence of CO_2 in the pore space;
2. 3D VSP shows a clear plume image that agrees with the surface TL seismic;
3. Offset VSP in CRC1 using a 3C geophone tool has a clear TL response. Egorov et al. (2017) obtained quantitative estimates of the plume properties (thickness, reduction of the compressional velocity) using full-waveform inversion (FWI);
4. Surface orbital vibrators (SOVs) were proven to be a reliable source of seismic signal with a repeatable signature and sufficient bandwidth. Weather effects on the near-surface conditions are the main source of the TL noise in the data (Yavuz et al., 2019).

In addition to the four field experiments listed above, a few tests were conducted after completion of CRC3 well, an injector for Stage 3, which focused on the performance of DAS receivers cemented behind the casing:

1. Correa et al. (2017) showed that for offset up to 1 km at the target interval, SNR of the DAS data are at least comparable to that of geophones;
2. Egorov et al. (2018) showed the feasibility of FWI for TL DAS data;
3. Offset VSP with the combination of SOV and DAS detected the injected CO_2 plume (Correa et al., 2018);

Besides the learnings related to the performance of seismic techniques, Stage 2C provided a refined reservoir model of the Lower Paaratte formation. History-matching of the TL images of the injection highlighted several geological features that control the CO_2 flow, such as sub-seismic faults and sandstone/mudstone transitions (Dance et al., 2019; Glubokovskikh et al., 2020). Also, the observed plume dynamics in Stage 2C constrained the range of dynamic parameters, such as relative permeability and CO_2 saturation threshold on the gas mobility.

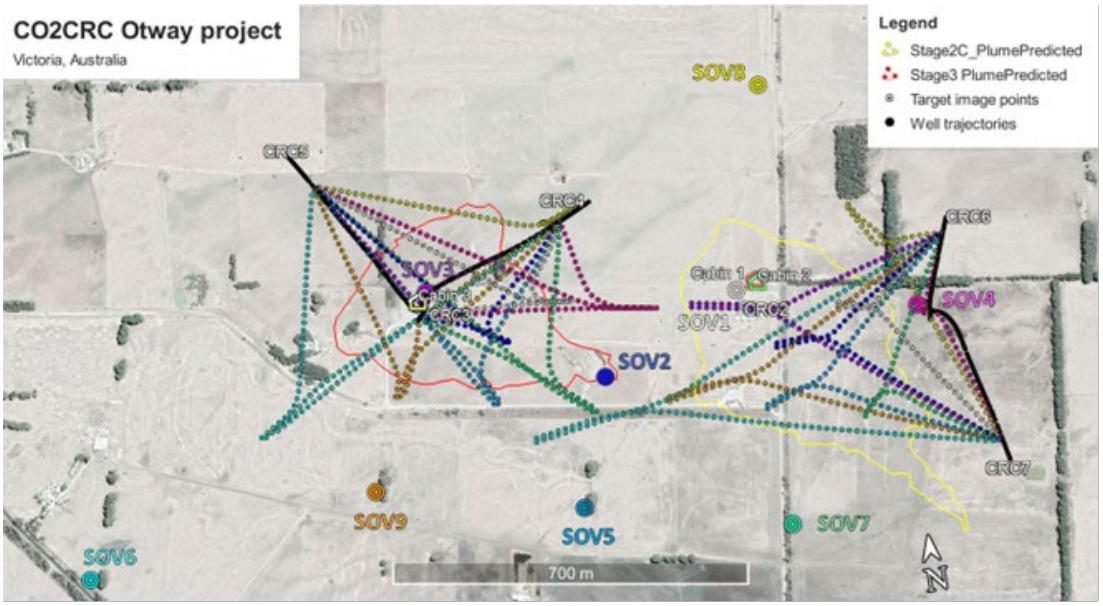

Figure 1 Location of monitoring wells (CRC3-CRC7), SOVs and cabins on Otway site. Small circles are imaging location at the reservoir level (1500 m depth) where colour corresponds to the SOV number. Simulated plume contours for Stage 2C (yellow) and Stage 3 (red) plumes at the end of Stage 3 injection are given for minimum CO_2 saturation of 1% and minimum plume thickness of 4 m (Jenkins et al., 2018).

3 SEISMIC MONITORING SYSTEM FOR STAGE 3

The improved understanding of the Lower Paaratte formation and capabilities of the SOVs and DAS-based offset VSP underpinned the design of Stage 3 seismic monitoring system. The system aims to provide optimal coverage (number of seismic rays reflecting from a given area of the subsurface) over the CO_2 plume predicted by the pre-injection reservoir simulations (Bagheri et al., 2020).

3.1 WELLS

Four deviated monitoring wells (CRC4-CRC7) were drilled and seven SOVs were installed on the site in January-February 2020 (Figure 1) (Bagheri et al., 2020; Pevzner et al., 2020a). Well locations were chosen to optimise pressure and seismic monitoring and based on the predicted plume location. Five deviated wells are drilled from two pads to reduce the drilling cost and environmental footprint. All wells are drilled to a depth 100 m below the reservoir. CRC4 and CRC5 wellheads are located next to CRC3 in the north-western part of the site. CRC4 deviates to the north-east direction, CRC5 – to the north-west. CRC6 and CRC7 are located 1 km to the east from CRC3. CRC6 deviates to the north and CRC7 deviates to the south. To facilitate future quantitative interpretation of the DAS measurement, all new wells have sonic logs starting from the depth of 900 m to the bottom hole and zero-offset VSP.

Boreholes extend beyond the depth of the storage reservoir with a total true vertical depth of about 1600-1700 m. The well paths start deviating after 500-800 m depth and then reach maximum inclination angle of 20°. DAS directivity, which may be approximated as $\cos^2\Theta$, where Θ is the angle between the fibre and particle displacement in the incident wave (Bona et al., 2017; Correa et al., 2017; Kuvshinov, 2016). In the following, we detail the installation of the instrumentation and electronics.

3.2 DAS UNITS AND FIBRE INSTALLATION

The fibre-optic sensors are interrogated by three recording units iDASv3 Carina (Silixa Ltd) (Shatalin S.V., In press 2020):

- iDASv3 #1 → CRC4 and CRC-3 wells;
- iDASv3 #2 → CRC7 and CRC-6 wells;

- iDASv3 #3 → CRC5 well and a Helically Wound Cable (HWC) buried in a shallow trench about 1000 m long between SOV3 and SOV4(HWC data are not analysed in this study).

Compared to most DAS systems, iDASv3 Carina™ system uses a specially engineered fibre (called Constellation™) with regularly spaced high optical reflectivity markers (Shatalin S.V., In press 2020), which increases the sensitivity of the receiver and reduces system noise substantially.

Such a design, one DAS unit per two receiver lines, is a compromise between a relatively high cost of a DAS unit, and the maximum length of the connected fibre to provide sufficient SNR. The longer the fibre the fewer laser pulses may be sent per second and the higher attenuation losses are within the fibre (Pevzner et al., 2018). DAS units use 10 m gauge length, 1 ms sampling rate, 16 kHz pulse repetition frequency and 4 m pulse length. One DAS unit is connected to about 5-6 km of fibre in total. In iDASv3 Carina system, the reflectivity markers are 5 m apart in the fibre, hence the minimum interference between the backscattered signals is achieved for 10 m gauge length and 4 m pulse width. Along with the sampling interval of 1 ms and 16 kHz pulse repetition frequency, these parameters of the DAS systems provide excellent SNR as was shown in the field tests by (Pevzner et al., 2018).

Figure 2 outlines the recording system for iDASv3 #2. First, a piece of single-mode fibre (SMF) buried in a trench connects to the DAS unit and the SMF cemented behind the casing of CRC7. Then SMF goes from CRC7 wellhead to the bottom of the hole (BH) where it is spliced to the constellation fibre (CF) (SMF and CF are physically in the same cable). Then CF reaches the wellhead of CRC7 where it is linked through the piece of trenched SMF to the CF at the wellhead of CRC6. The CF goes to BH, where it is spliced to the SMF and goes from BH to the wellhead of CRC6. The end of the fibre is connected to the attenuator to reduce the fibre's edge effects. The surface SMF is deployed in a trench to reduce the noise level and secure the fibre from potential damage.

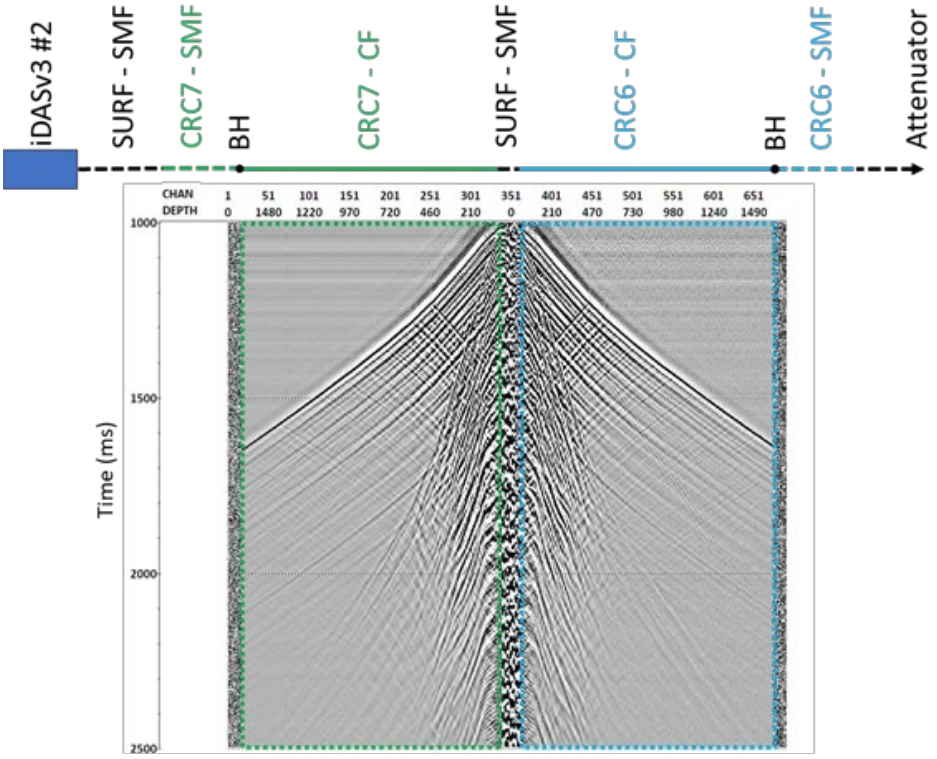

Figure 2 DAS fibre connectivity in CRC7 and CRC6 wells (Top) and corresponding shot gather acquired by SOV4 (bottom). iDASv3 is designed to operate an engineered fibre and produces lower data quality in SMF. Start of recording time is 1000 ms after the start of SOV rotation.

3.3 SOVs

Seismic orbital vibrator (SOV) is deployed on a concrete plate. A pilot SOV dataset at Otway was acquired in March 2016 and showed good repeatability and frequency content of up to 80 Hz (Dou et al., 2017). These results showed the feasibility of using SOV as a permanent source for monitoring purpose. Yet this source has two shortcomings. The SOV lacks phase control of the rotating eccentric mass, which results in decreased repeatability of the source signature. Moreover, the magnitude of the signal is proportional to centrifugal acceleration and thus increases as frequency squared resulting in lack of energy at low frequencies. However, source phase may be compensated during processing using sweep recorded by 3-component geophone buried 3 m below the SOV. Stacking of sweeps improves SNR in general which is most important at low frequencies.

To ensure a broad frequency band of the source signal, each SOV source consists of two motors of different sizes: a small motor (5 ton-force at 120 Hz; 70-105 Hz bandwidth) and a large motor (10 ton-force at 80 Hz, 8 Hz to 80 Hz bandwidth). SOV3-SOV9 can operate both motors simultaneously while SOV1 and SOV2 have only one motor each. The SOVs are set to run 22 clockwise (CW) and 22 counterclockwise (CCW) sweeps of 150 s duration, which are recorded during a 2.5 hours operation time for each SOV. To minimise the acoustic noise impact on the local community, the sources operate only in the daytime. It requires two days in total to run all SOVs.

CW and CCW rotations generate P waves of the same polarity and S waves of opposite polarities. Thus, the summation of CW and CCW is expected to enhance P waves and attenuate S waves while the subtraction of CW and CCW has an opposite effect (Dou et al., 2016). The CW and CCW summation is useful because we are primarily interested in reflected P waves. However, preliminary tests show that CW and CCW sweeps have different waveforms and thus a simple summation/difference provides a little gain in the data quality and more sophisticated processing procedures are required.

Given the trajectories of the wells, SOV locations are chosen to increase the seismic coverage over the predicted CO_2 plume. To ensure sufficient coverage and plume detectability, TL seismic response for given SOV locations (shown in Figure 1) was simulated using finite-difference modelling. For simplicity, one may assume that reflection points illuminate the first half of the transect formed by a well-SOV pair, 45 transects in total. Furthermore, each of the deviated wells is aligned with an SOV to form a vertical 2D section: NE-SW (CRC3, CRC4 and SOV8, SOV3, SOV6), NW-SE (CRC5, CRC4 and SOV3, SOV5), S-N (CRC7 and SOV4, SOV8) and N-S (CRC6 and SOV3, SOV7) (Figure 1). A 2D offset VSP geometry enables the application of 2D FWI (Egorov et al., 2018), which would be much more challenging in 3D with a sparse source coverage.

Note that in the offset VSP geometry, each reflection point is created by one source and one receiver, and thus fold is one for nearly all image points. An exception could be areas in the vicinity of vertical wells. Thus, the coverage is essentially represented by the density of image points at the reservoir level (rather than fold) given in Figure 1.

3.4 HARDWARE INFRASTRUCTURE

Continuous monitoring using DAS generates an enormous amount of data that could not be transferred to a remote processing centre. To enable real-time processing, extensive computing infrastructure is deployed at the site. The hardware for the continuous monitoring system is installed in three seismic cabins (Figure 1, Figure 4). The data collection/processing system includes one main processing server (50 terabytes storage), five pre-processing servers, two backup/archive servers, two storage servers (80 terabytes storage each), and two 40-slots tape libraries (480 terabytes each). Each cabin has a 25 Gb network switch to accommodate fast data transmission between the hardware components.

Cabin 1 is the only cabin that has Internet access, including LTE (Long-Term Evolution standard for wireless connection) and NBN (Australian National Broadband Network) links. These internet links are used to connect to one of the two gateway machines (Gate1 and Gate2) for remote access to all servers and enable data transfer from and to the facility. Cabin 1 houses a stratum-1 NTP (Network Time Protocol) time server, which guarantees the time synchronisation. In addition to these, Cabin 1 has a weather station and distributed temperature sensing (DTS) unit.

Cabin 2 has the main processing server, two pre-processing servers, one archive server, one tape library and a storage server. It communicates with Cabin 1 via a 1 Gb fibreoptic link. SOV sweeps recorded by 3C geophones are transferred to the storage server in Cabin 2. The iDASv3 #2 unit is located in Cabin 2 and continuously acquires data from CRC6 and CRC7 wells (Figure 4). Data form the unit are pre-processed by a dedicated server and the raw records are archived on tapes by two storage libraries in Cabins 2 and 3.

Cabin 3 has two DAS units, iDASv3 #1 and iDASv3 #3, three pre-processing servers, one archive server, one tape library and a storage server. Cabin 3 communicates with Cabin 2 via 50 Gb link (see Figure 3 diagram for fibre types). Data from each unit are pre-processed by a dedicated server and raw records from iDASv3 #1 and iDASv3 #3 are archived on tapes by two storage libraries in Cabins 2 and 3.

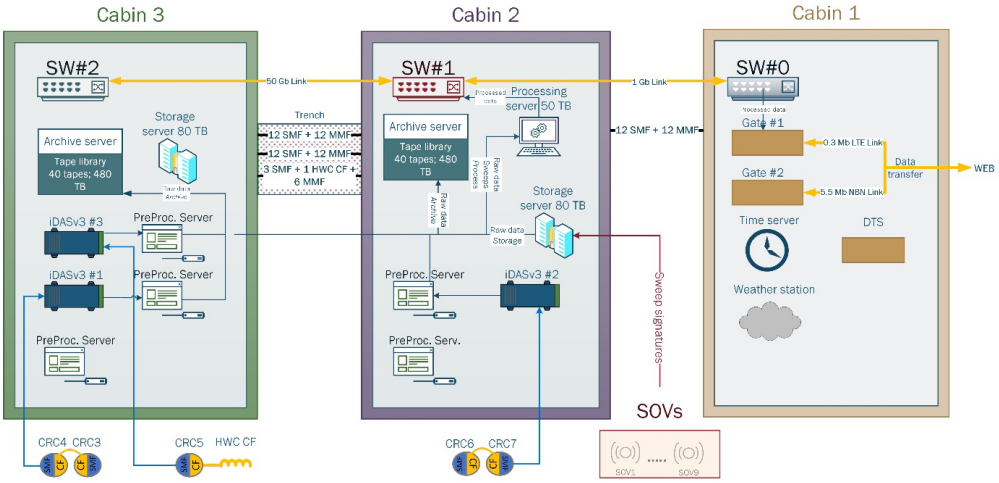

Figure 3 Hardware setup of the automated continuous monitoring system at the Otway research site. SMF – single-mode fibre, CF – Constellation fibre, HWC – helically wound cable.

4 AUTOMATED DATA PROCESSING

The DAS data is recorded continuously for passive monitoring. Then, the SOV records are selected from the continuous recording based on precise GPS time. The processing implements a set of standard offset VSP procedures. Optimal processing parameters are based on the first vintage acquired in May 2020. The parameters are hand-tuned for each SOV-well pair. Then the optimal parameters are applied repeatedly in the automated real-time data analysis (Yavuz et al., 2020).

4.1 PROCESSING FLOW

Table 1 outlines the main processing steps. First, we decimate the data by resampling it from 1 to 2 ms and stacking channels into 5 m bins. That decimation is valid as iDASv3 is designed to sample wavefield at 5 m intervals and we expect no frequencies above 250 Hz. Thus, neither decimation nor binning affects the information content but reduces data size by an order of magnitude.

The decimation and binning are followed by deconvolution of the record with the SOV source sweep recorded by 3C geophones. As discussed earlier, the power spectrum is strongly biased towards high frequencies. Thus correlation, commonly used in Vibroseis seismic, will make SOV spectrum even more unbalanced. Instead, we use deconvolution with the recorded sweep, which makes the energy more

evenly distributed across the frequency bandwidth (Daley and Cox, 2001). Next, all repeated CW and CCW sweep seismograms are stacked separately. At this point, the amount of data drops to 500 MB/day compared to the initial 100 TB/day.

Unlike the position of geophones, the exact location of each DAS receiver is not known precisely. Indeed, DAS measurement is spatially distributed (average strain rate over given gauge length) and its location along the fibre is measured by the laser pulse travel time and speed of light in the fibre. The latter is not known precisely. A 1% error in the speed of light results in the 10 m error in distance estimation at 1000 m. 6000 m of fibre can result in an error of about 60 m at the end of the fibre.

Fortunately, there are at least two known locations on the DAS cable which are known exactly: BH and the wellhead. The fibre changes from Constellation to single-mode fibres at BH, resulting in a significant SNR change (Figure 2). We locate the wellhead as the beginning of the region where upgoing waves reflect from the free surface and create downgoing waves. When both of these locations are identified on DAS data, we interpolate the geometry in-between based on the well deviation survey. Then, we remove all channels which are outside the well or contaminated by noise.

Signature deconvolution is an essential step that compensates for the variations of the source signature over time. We call it ‘designature’ to distinguish it from sweep deconvolution. Designature is done in two steps. First, we estimate the `source’ wavelet for each well-SOV pair and rotation by stacking the direct wave signal in ~700-1500 m depth interval (specified for each pair). The designature is followed by a bandpass filter to shape the resulting wavelet and remove the noise outside the useful bandwidth.

At the next step, a set of FK filters separates the wavefield to isolate and retain only primary PP reflections (which are later used for imaging). For far offsets (e.g. SOV6 and any well) the separation is challenging because P and S travel-times are almost flat and the FK filter is ineffective. Moreover, at large offsets (e.g., target reflections in CRC5-SOV7 and -SOV5), the very detection of PP waves becomes challenging as these waves arrive nearly normal to the fibre and hence DAS receivers are almost insensitive to them. However, PS waves are still clearly visible for such offsets and may be very useful for imaging.

The final step is 2D time migration. The migration 1D velocity model is built based on the zero-offset VSP first break travel times. Then, we use the anisotropic NMO equation (Alkhalifah and Tsvankin, 1995) to approximate the travel time field and straight rays for estimation of the offsets and angles. Then, the seismic image is formed by stacking the seismic amplitudes along the isochrones for each image point in a narrow 3° aperture. Amplitude scaling prior to stacking is based on Dillon (1990) VSP Kirchhoff migration algorithm. Since most of the wells are deviated, imaging points form a curved surface for most of the VSP-pairs (Figure 5d). As an example, Figure 4 shows the results of the key processing steps for the SOV4 - CRC7 pair.

Table 1 2D DAS-SOV VSP data processing flow

PROCEDURE	***DETAILS***
DATA INPUT	Not correlated data for each well-SOV pair
DATA DECIMATION	Resampling the DAS data from 1 ms to 2 ms and binning channels from 1 m to 5 m
SWEEP DECONVOLUTION	Deconvolution with the sweep recorded by the SOV geophone
VERTICAL STACKING	Stacking the seismograms for the sequential SOV sweeps
GEOMETRY	Assigning receiver (DAS) and source (SOV) geometry
WAVELET ESTIMATION	Wavelet estimation from the direct wave
DESIGNATURE	Deconvolution with the estimated wavelet
BANDPASS FILTER	Application of a bandpass filter (specific for each SOV-well pair)
WAVEFIELD SEPARATION	Application of FK filters to remove downgoing S- and upgoing S- and PS-waves (specific for each SOV-well pair)

AMPLITUDE CORRECTION	Compensation for the spherical divergence
MIGRATION	Kirchhoff migration in time domain, central dip = 0, image grid step dx = 5 m, dz = 1 m. 1D isotropic velocity model from zero-offset VSP.

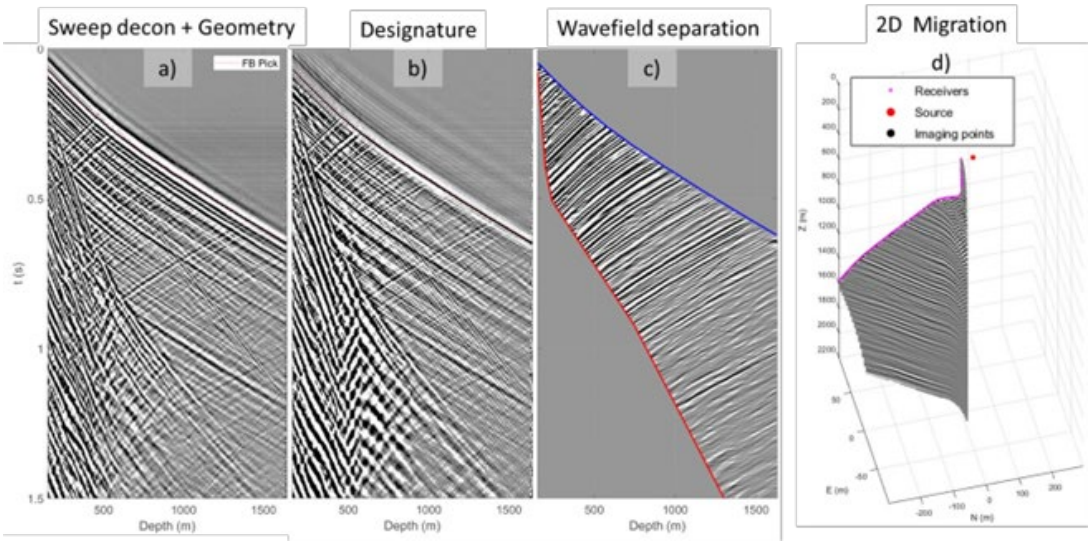

Figure 4 Seismograms after key processing steps for CRC7-SOV4 pair with the optimal parameters: sweep deconvolution and geometry assignment (a), designature (b), wavefield separation and muting (c) and 2D Migration (d). Refer to Table 1 for more details.

4.2 DATA FLOW

As discussed above, there are many steps between initial DAS records and the final migrated images. After 1.5 days from the first commencement of rotation of the first SOV, the system produces a QC report with the images. At this point, the original data size is reduced from about 100 TB to 500 MB. During these steps, data is sent from the DAS units to the processing and storage servers with the final results being sent daily to the office at Curtin University (Perth, Australia). In this section, we describe the flow of the data on the site and the time it takes to acquire, process and archive the data.

Figure 5 details the data flow from the DAS units to the office along with the corresponding data size and processing time at each step. Running four or five

SOVs takes about 10-12.5 hours each day. The first SOV starts rotating at about 10 pm UTC and the last SOV finishes at about 11 am UTC the next day. The passive data is recorded for another 13 hours until midnight UTC.

The raw DAS data is backed up on two tape libraries for another 8 hours. The data decimation begins when the back-up finishes at one of the tape libraries: one preprocessing server per DAS unit resamples the data for 1.5 hours. Then, the decimated seismic data is moved to the storage server and processing begins. Sweep deconvolution – the longest step - takes about 3 hours. During the next 20 minutes, the data is processed from the initial gathers to migrated images. All controlling scripts are implemented in MATLAB and are executing sequentially all the processing and archiving the recorded data.

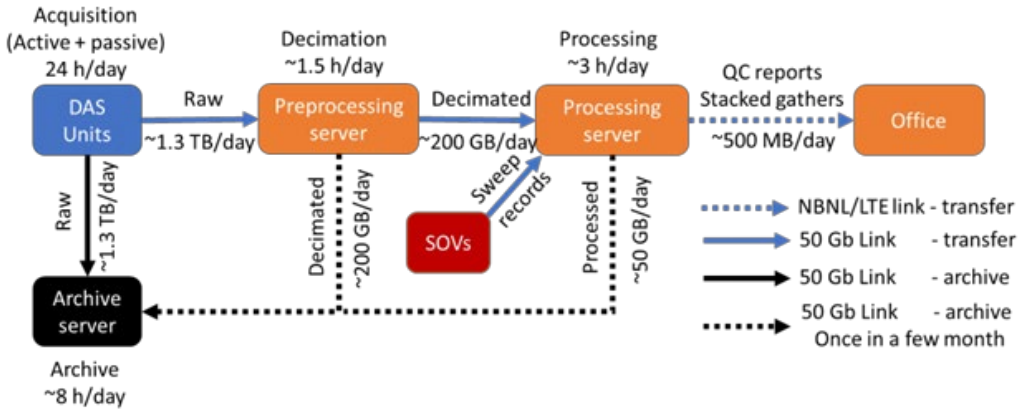

Figure 5 Simplified data flow diagram. Data is recorded by DAS Units continuously. Once per 24 hours it is backed up on two archive servers. When archiving is finished, data is decimated on the preprocessing server and processed on the processing server. Once a day QC reports and stacked gathers are sent to the office. Arrow labels indicate data flow direction and approximate data size. Approximate timing for each procedure is also given.

Continuous recording of three DAS units produces around 200 TB of data per vintage in an internal SIlixa ltd format. Figure 6 illustrates the data size reduction in the automatic processing flow. Over the entire course of the flow, data volumes are reduced by a factor of around $3 \cdot 10^6$. First, data is down-sampled at the interrogation unit (IU) from 16 to 1 kHz sampling frequency and from 0.25 to 1 m spatial sampling. Then, during software decimation, data is resampled further to 5 m channel spacing and 2 ms in time, reducing the data size by one more order of magnitude. Next, the sweep deconvolution converts the effective seismic record length from 150 s (duration

of a sweep plus listening time) to 4 s, which results in a reduction of the size to 20 Gb per vintage. Then, stacking of all the CW and CCW sweeps within the same vintage and SOV-well pair reduces the vintage size further to about 1 GB, which may be transmitted through the Internet. At this point, the stacked datasets are uploaded to the cloud storage and sent to the Perth office for time-lapse analysis and additional archiving. Then, the data size is reduced by a factor of two after geometry assignment, as some auxiliary and noisy channels are removed. Other processing steps such as designature (signature deconvolution) and wave fields separation do not reduce data size. Finally, 2D Kirchhoff provides an image of only 67 MB per vintage.

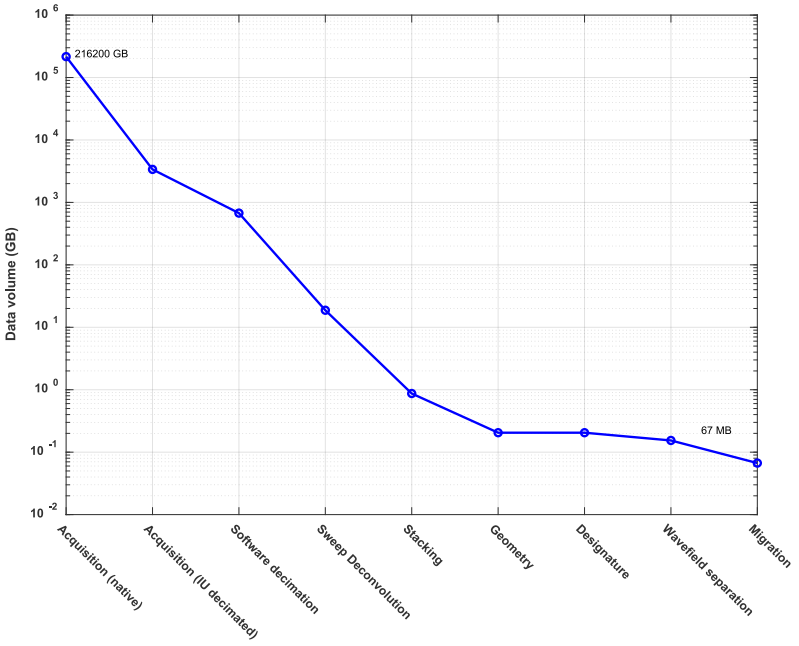

Figure 6 Data volume reduction after each processing step (given in Table 1) in the automatic processing flow of continuously acquired data at the Otway research site. At the end of processing, the data volume is reduced from 216 TB to 67 MB. This illustrates the importance of on-site processing as transferring even 20 GB per 2 days (after sweep deconvolution) may be challenging.

5 DISCUSSION OF PRE-INJECTION MONITORING RESULTS

From the first vintage acquired at the end of May 2020 to the end of October 2020, the deployed monitoring system accumulated more than 130 days of data. During this period, the seismic properties of the injection interval could be affected only by a

slow evolution of the Stage 2C CO_2 plume. This is expected to have a negligible effect on the seismic properties of the target interval as it is 700 m west from the previous injector while the plume is expected to migrate in the SE direction. Hence, we consider any time-lapse discrepancy between the pre-injection monitoring vintages as a time-lapse noise. Analysis of this noise provides a means to estimate three main factors that control the repeatability of the seismic signal and the detectability of the TL signal from the future Stage 3 injection: stability of the instrumentation, weather impact on the near-surface conditions and ambient noise.

5.1 PROBLEMS DURING ACQUISITION

Permanent deployment puts extremely high weight on the stability of the instrumentation because a system break-down during rapid time-lapse changes would compromise continuous monitoring. During the trial period (May-October 2020) the Stage 3 monitoring system had seven incidents that resulted in a complete or partial loss of the monitoring vintages. Three categories of problems arose during the acquisition of 66 vintages (132 days): power outages, DAS Unit failures and SOV failures (Table 2). Corresponding intervals of missing data are clearly visible a TL SNR map (Figure 7).

There were two full stoppages due to power outages. The first one was associated with construction works at the site and resulted in a loss of three vintages. The second power outage was due to a limited power supply at the site. While these incidents caused significant disruption to the Stage 3 system, electrical security may be less of an issue in a commercial project, where power supply for the boreholes/pumps is likely to be autonomous.

Not all SOV s are equally critical for leakage monitoring, as some of the sources contribute to the plume image accuracy rather than its detection. SOV1 and SOV2 improve coverage (Figure 1). Conversely, SOV6 illuminates the south-western part of the injection. That is why SOV6 failure over a period of ten vintages due to an infestation of the electronics by ants was of major concern.

Reliability of the DAS units is also of critical importance. Failure of one DAS unit leads to the loss of 20-40% of the data. iDASv3 #3 (CRC5) covers the north-western part of the injection, iDASv3 #1 (CRC3, CRC4) – the central area of injection zone and iDASv3 #2 (CRC6, CRC7) the eastern area of the site. During and immediately after injection, the central area covered by CRC3, CRC4 and CRC5 is most critical.

Event #	Vintages lost	Affected well(s)	Affected SOV(s)	Description
1	2.5	All	All	Power outage
2	17	CRC5	-	DAS Unit #3 failure
3	1	CRC3, CRC4	-	DAS Unit #1 failure
4	10	-	SOV6	SOV electronics damaged by ants
5	2	-	SOV5	Not operational
6	1	-	SOV1, SOV8	Electronics damaged by ants
7	1	-	SOV2	SOV radio connection is lost

Table 2 Summary of technical incidents during 132 days of acquisition

Apart from these incidents, all SOV-well pairs show stable SNR with a maximum confidence interval of about ±6 dB around the median value (Figure 7, top graph) of about 30 dB. However, not all Well-SOV pairs have similar data quality. Generally, the SNR depends on the source-receiver offset: the closer the source the stronger is the signal, while the noise level remains almost constant. This explains why the most distant SOV (SOV6) has the lowest SNR (Figure 7) resulting in low repeatability (Figure 9).

The SNR map is a useful tool to examine the data quality. A change in SNR may indicate a deterioration of a piece of equipment or some irregular condition at the site. For example, failure of iDASv3 #3 was preceded by a gradual decrease of SNR by 10 dB in CRC5.

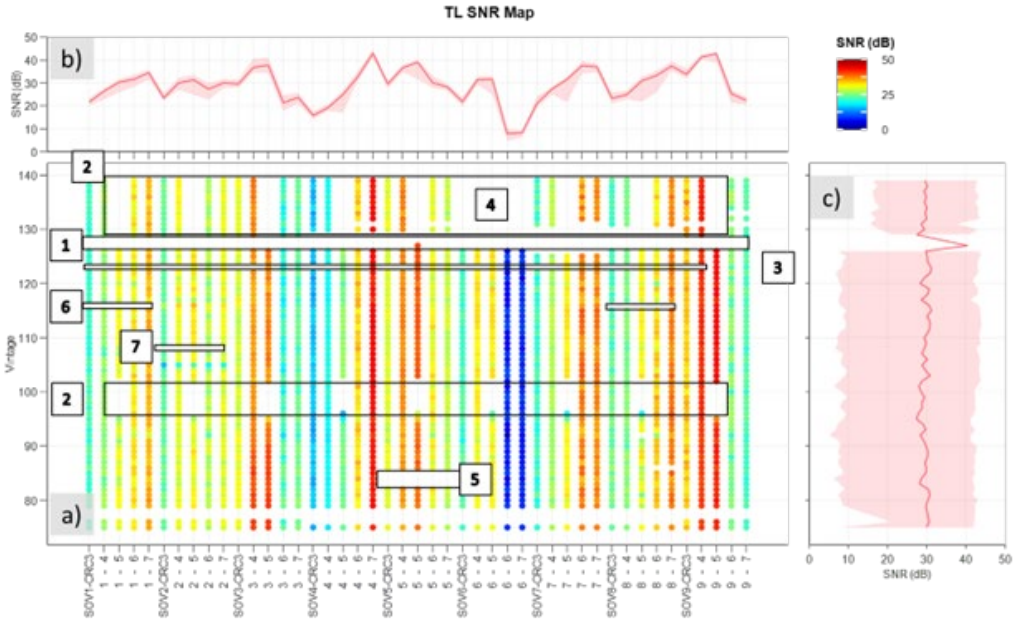

Figure 7 TL SNR distribution after designature for each Well-SOV pair, CW rotation. Colour of each dot on the map (a) represents SNR for a given vintage number and Well-SOV pair. The graphs (b and c) represent median SNR (red line) and 95% confidence interval (transparent red area) grouped by pairs (b) and vintages (c). Numbers in boxes are events listed in Table 2. One vintage corresponds to the two-day interval. RMS of the noise is estimated in a 400 ms window above first breaks; RMS of the signal is estimated in 150 ms window around first breaks in 900-1300 m depth interval.

5.2 REPEATABILITY

When a monitoring array operates normally the non-repeatability of the seismograms is due to the following main reasons:

- Source: weather effect on SOV and/or the geophone recording of the sweep signal; SOV mechanical deterioration;
- Receivers: borehole condition, injection noise, temperature effects on DAS;
- Variability of coherent noise – each wavefield component other than PP reflections - caused by the variations of the near-surface conditions.

Sweep deconvolution compensates for variability in the SOV parameters. Unfortunately, both SOV and sweep recording geophone are affected by near-surface conditions. This leads to variation in the wavelet shape: Figure 8a, c and e show the estimated wavelet and its power spectrum for the CRC7-SOV4 pair over about 130 days of acquisition. Although the wavelet shape remains similar, the

change of the amplitude level is significant: it decreases by a factor ~3.5 first and then gradually returns to the initial level. Since SNR is stable for all records, the source energy should be similar for all vintages, and hence the variations are likely due to coupling of the SOV geophone to the ground (Figure 7).

Such source fluctuations could compromise the data repeatability. However, the source signature can also be estimated from the direct wave arrival (average along the first breaks). Thus, the near-surface effect on the source signature or its recording by the geophone is compensated by the designature processing step. Figure 8 shows drastic improvement in the repeatability after the designature.

Next, we access the repeatability of wavelets for all well-SOV pairs. We perform repeatability analysis by comparing baseline with one of the monitor vintages at a time. To quantify the repeatability of the wavelets we use normalised root mean square metric NRMS (Kragh and Christie, 2002):

$$NRMS = 2\frac{RMS\ (BS - VT)}{RMS(BS) + RMS(VT)} \quad (1)$$

where BS is the baseline signal, VT the vintage wavelet, and RMS is the root mean square of a time series.

The wavelet NRMS can be estimated before and after designature. If two wavelets are exactly the same NRMS equals 0, if both wavelets are random noise then NRMS equals ~ 1.4. The NRMS is sensitive to both amplitude variations and time shifts. Typical good repeatability NRMS is 0.1 – 0.3 (Johnston, 2013). In the Stage 2C of the Otway project, the CO_2 plume of as little as 5 ktonnes in the same Paaratte formation was detected with 4D seismic with NRMS with an average NRMS of about 0.15 (Pevzner et al., 2017b). The data after sweep deconvolution has a clear trend towards the increase of NRMS (Figure 9a). NRMS after designature (Figure 9b) becomes significantly lower with 0.02 NRMS for SOV2 and 0.2 NRMS SOV6 while average wavelet NRMS is about 0.1-0.15 NRMS. Such repeatability is only possible because of the availability of direct waves in the offset VSP seismograms.

When grouped by boreholes (Figure 9c, d) we see that data have similar mean NRMS values: 0.4 NRMS before designature and 0.1 NRMS thereafter. This means that the main source of non-repeatability is SOV whereas the downhole DAS measurements are stable. However, the failure of a DAS is still the highest risk for monitoring. Another possible source of non-repeatability is a noise caused by the CO_2 injection itself and related site operations.

Figure 10 gives the overall picture of the survey repeatability. Unlike previous figures, here NRMS is estimated as an average value for traces at 900-1300 m depth interval. This means that non-repeatable noise may not be cancelled out so effectively by averaging. Most of the pairs have stable NRMS of about 0.1 (see Figure 7).

At last, dense time sampling of the vintages gives us a new way to analyse the data. We can plot vintages next to each other to get TL shot gather for each pair (Figure 8 (a, b)). A time slice may help to indicate changes in a specific wavefield component. As the primary P wavefield variations are compensated via designature, we can visually detect variations in non-primary P and S wave arrivals. Such an analysis helps trace sources of non-repeatability. Furthermore, having many vintages can improve repeatability even farther with predictive filtering.

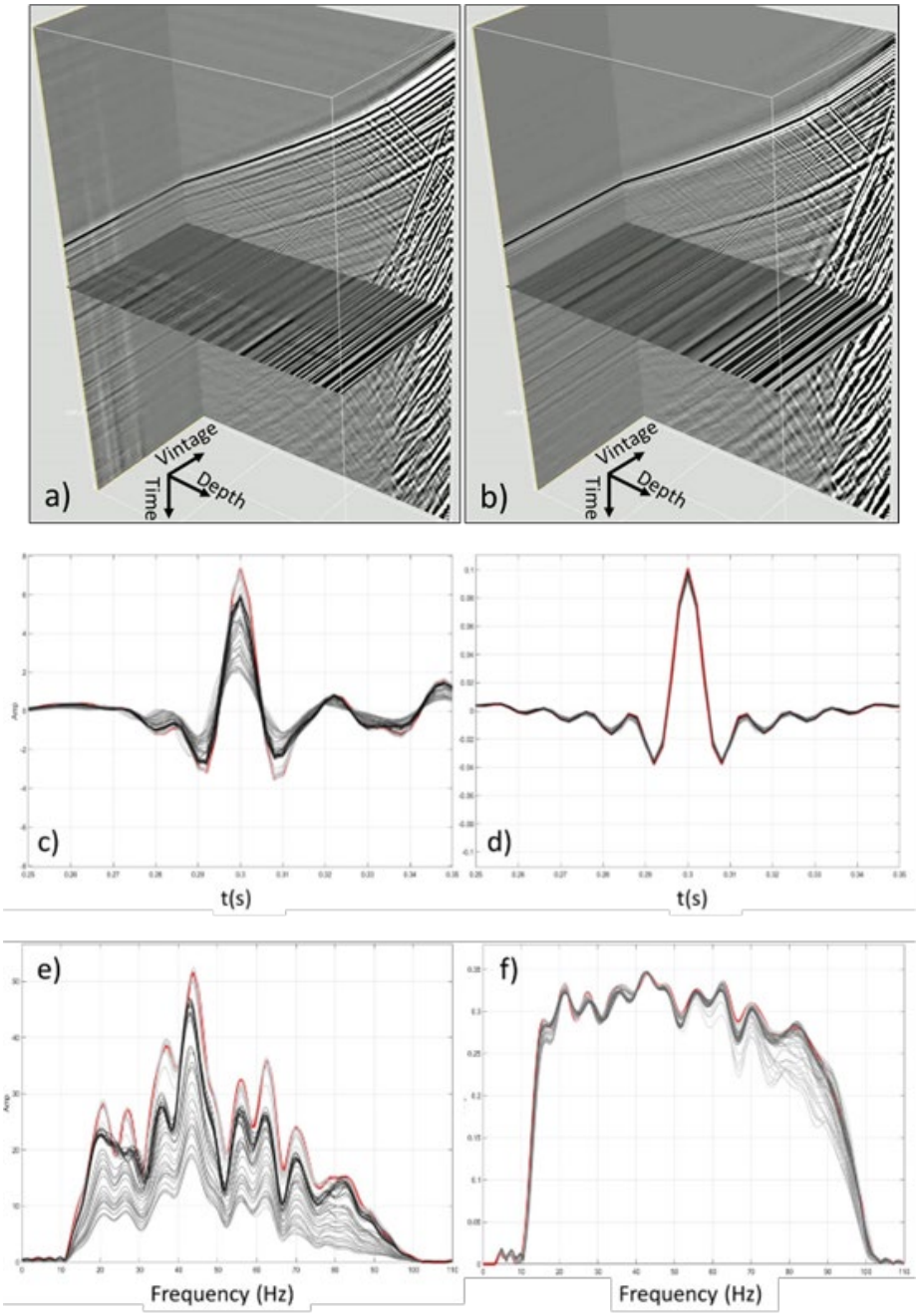

Figure 8 Time-lapse data after sweep deconvolution (a, c, e) and designature (b, d, f) for CRC7-SOV4 pair: TL shot gathers (a, b) in time-depth-vintage coordinates; extracted wavelet (c, d) and its spectra (e, f). Red lines correspond to the first vintage while gradation of grey represents vintage number – the lighter the colour the older the vintage.

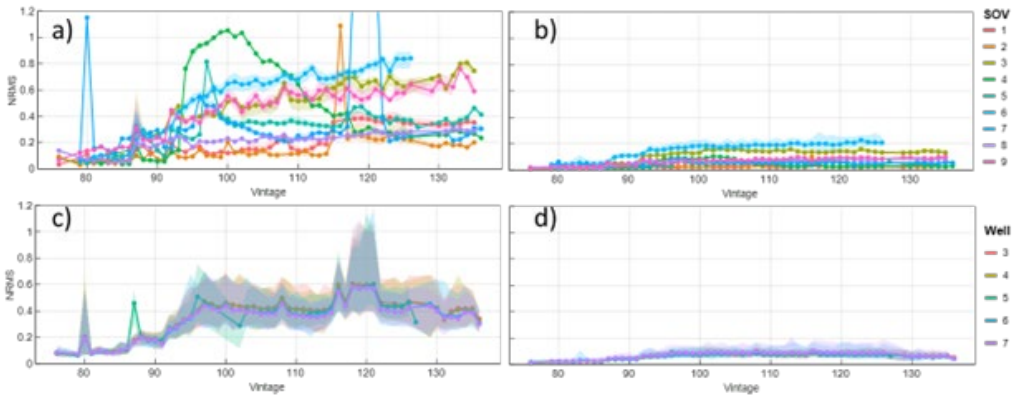

Figure 9 NRMS of the estimated wavelets after sweep deconvolution (a, c) and designature (b, d). Data is grouped by SOVs (a, b) and by wells (c, d). Solid lines – mean NRMS, transparent area – standard error of the mean, colour code – SOV/Well number. The vintage number is a halved number of days from 1st January 2020. Note, that before designature non-repeatability grows steadily for most of the SOVs while NRMS for SOV4 is peaked from 0.15 to about 1 in only a few days. After designature, we still observe an increase in non-repeatability while the rate is quite small.

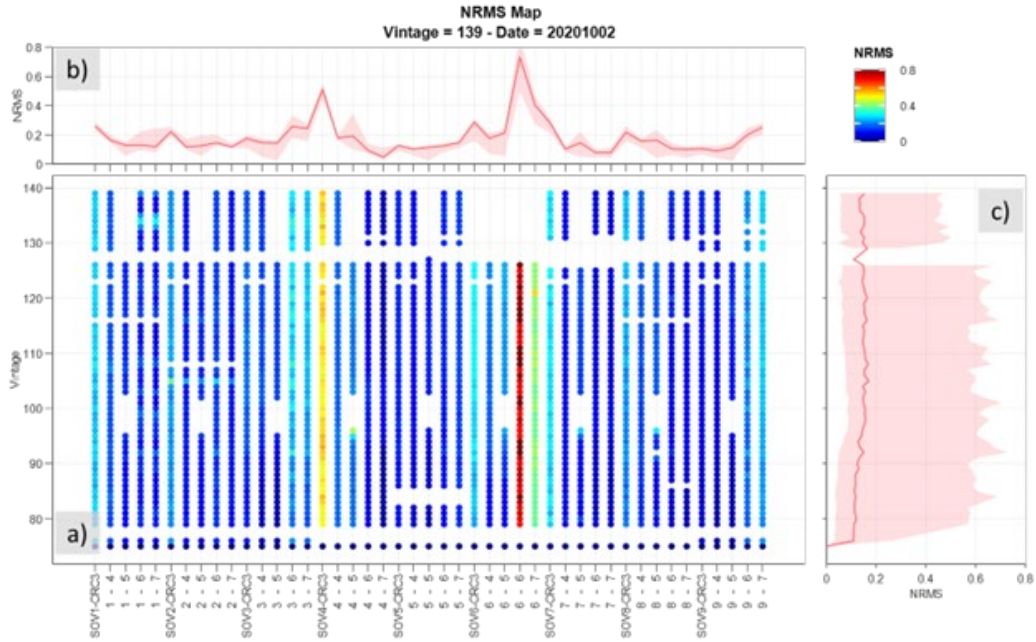

Figure 10 Same as Figure 7 but for NRMS instead of SNR. Note poor repeatability for SOV4-CRC3 and SOV6-CRC6,7. This is mainly due to large source-receiver offset. The average repeatability is about 0.1-0.15.

6 DISCUSSION

First 130 days of the recording provided encouraging results in terms of the data quality and operability of the data management system. However, the Stage 3 array provides only 45 offset VSP transects that cover ~0.7 km^2 area. Compared to SeisMovie®, our monitoring design has relatively sparse spatial coverage and different VSP transects usually have different amplitudes for the same reflection points, which complicates the quantitative interpretation of the data.

The key to excellent repeatability is the availability of the source signature from the direct wave in VSP seismograms: designature reduces NRMS down to about 0.1-0.15. The recorded data show significant variations in SOV signal amplitudes (e.g. SOV4). It is unclear if the cause was a deterioration of SOV performance or a change of their coupling due to weather changes, as the shot gathers depend both on the signal emitted by SOVs and on the medium where the pilot geophone is located. This could be further studied by analysing the effect of precipitation on DAS signals. This work is ongoing and beyond the scope of the present paper. To avoid weather effect on the geophone coupling it is preferable to deploy the pilot geophone below the water table (if possible).

In the trial period, the most significant contributor to the TL noise was malfunctioning of the instrumentation. To avoid possible data loss due to unit failure during injection and post-injection period, having a spare DAS unit on site is required. Another source of non-repeatability is near-surface variations. Even after compensation, these variations may affect surface-related multiples and S wave patterns which may interfere with primary P wave reflections. These effects will be analysed in a future study.

Our data quality analysis has focused on the direct wave. At the same time, the plume image will be formed by reflected waves, which have at least an order of magnitude lower intensity than the direct arrivals. Hence, the estimated high values of SNR levels and repeatability reported earlier is likely to be optimistic. Yet the repeatability can be improved substantially by stacking several sequential vintages. Indeed, our analysis so far has mainly focused on the comparison of the same signals in two vintages at a time. Yet we have the entire history of the monitoring at our disposal and can implement a batch-processing of the sequential data (many vintages at once), such as Kalman filtering (Evensen, 2009). This approach would

reduce the probability of the false detection of the plume arrival and increase the confidence of the plume images. From that point of view, the pairwise-type of estimates of the repeatability may be underestimated.

Furthermore, the current workflow uses primary P-wave reflections only and ignores all other wavefields. Primary S-waves, converted waves and multiples have a high potential of improving coverage and, thus, detectability, and can be utilised by employing PS wave migration, full waveform inversion and seismic interferometry, which may help extract more value from the data.

We acquired the data for CW and CCW SOV rotation and processed them separately. Stacking and subtracting these two rotations have the potential to separate source generated P and S wavefields. This will help reduce the interference of wavefields and allow the use of S waves to improve the coverage.

7 CONCLUSIONS

The Proposed monitoring system allows acquisition of seismic vintages every two days in an automated manner. The permanent installation requires no human effort on-site and thus drastically reduces the monitoring cost. Such a system can coexist within industrial or farm area as it produces a tolerable level of noise and operates only within the allowed time schedule (in the daytime).

The survey design is based on previous studies at Otway, especially, Stage 2C. The choice of VSP geometry has three advantages over surface seismic: VSP does not interfere with the infrastructure, the receivers are not affected by the weather conditions and the source wavelet can be directly estimated from VSP data.

The permanent installation of equipment (DAS in wells and SOVs on the surface) allows setting a single processing flow for all vintages, which can be run autonomously without manual input. Results of QC and processing reports may be sent daily to the operator in the office.

Unlike DAS receivers installed in boreholes, SOVs are cemented at the surface and thus the source signature is affected by local near-surface variations. Such variations can alter not only the SOV signature but also 3C geophone employed to record sweep. Such signature variations may affect the repeatability of TL survey. Yet, borehole measurements make it possible to estimate SOV signature and remove variations from the data via deconvolution. Deconvolution corrects not only the wave

shape but also amplitudes and time shifts. The average repeatability of processed data for the 130 days period is about 0.1-0.15 NRMS measured around the direct wave.

The short turnaround (2 days) monitor survey gives an opportunity to acquire about 180 vintages per year. Thus, each DAS-SOV dataset may be represented as a 3D volume in three coordinates: receiver location, travel time, vintage date. Thus, we can analyse seismic dataset as a time series and apply some advanced data assimilations techniques. Having seismic monitoring data almost daily may inform reservoir management decisions leading to a better understanding of the reservoir history and more effective CO_2 storage.

8 ACKNOWLEDGEMENTS

The Otway Project received CO2CRC funding through its industry members and research partners, the Australian Government under the CCS Flagships Programme, the Victorian State Government and the Global CCS Institute. The authors wish to acknowledge the financial assistance provided through Australian National Low Emissions Coal Research and Development (ANLEC R&D). ANLEC R&D is supported by COAL21 Ltd and the Australian Government through the Clean Energy Initiative.

9 REFERENCES

- ALKHALIFAH, T.A., TSVANKIN, I., 1995. VELOCITY ANALYSIS FOR TRANSVERSELY ISOTROPIC MEDIA. GEOPHYSICS 60, 1550-1566.
- ARTS, R., EIKEN, O., CHADWICK, A., ZWEIGEL, P., VAN DER MEER, L., ZINSZNER, B., 2003. MONITORING OF CO2 INJECTED AT SLEIPNER USING TIME LAPSE SEISMIC DATA, GREENHOUSE GAS CONTROL TECHNOLOGIES-6TH INTERNATIONAL CONFERENCE. ELSEVIER, PP. 347-352.
- BAGHERI, M., PEVZNER, R., JENKINS, C., RAAB, M., BARRACLOUGH, P., WATSON, M., DANCE, T., 2020. TECHNICAL DE-RISKING OF A DEMONSTRATION CCUS PROJECT FOR FINAL INVESTMENT DECISION IN AUSTRALIA. THE APPEA JOURNAL 60, 282-295.
- BAKKU, S.K., 2015. FRACTURE CHARACTERIZATION FROM SEISMIC MEASUREMENTS IN A BOREHOLE. MASSACHUSETTS INSTITUTE OF TECHNOLOGY.

- Bauer, R.A., Will, R., E. Greenberg, S., Whittaker, S.G., 2019. Illinois Basin–Decatur Project, in: Wilson, M., Landrø, M., Davis, T.L. (Eds.), Geophysics and Geosequestration. Cambridge University Press, Cambridge, pp. 339-370.
- Benson, S., Hoversten, M., Gasperikova, E., 2004. Overview of monitoring techniques and protocols for geologic storage projects. IEA Greenhouse Gas R & D Programme.
- Bona, A., Dean, T., Correa, J., Pevzner, R., Tertyshnikov, K., Van Zaanen, L., 2017. Amplitude and Phase Response of DAS Receivers, 79th EAGE Conference and Exhibition 2017. EAGE, Paris, France.
- Caspari, E., Pevzner, R., Gurevich, B., Dance, T., Ennis-King, J., Cinar, Y., Lebedev, M., 2015. Feasibility of CO2 plume detection using 4D seismic: CO2CRC Otway Project case study — Part 1: Rock-physics modeling. GEOPHYSICS 80, B95-B104.
- CGG, G.d.F., Institut Francais de Petrole, 2002. SeisMovie aims to be a blockbuster for 4D seismic reservoir monitoring. First Break 20.
- Chadwick, R.A., Noy, D., Arts, R., Eiken, O., 2009. Latest time-lapse seismic data from Sleipner yield new insights into CO2 plume development. Energy Procedia 1, 2103-2110.
- Cook, P., 2014. Geologically Storing Carbon: Learning from the Otway Project Experience. CSIRO PUBLISHING.
- Correa, J., Egorov, A., Tertyshnikov, K., Bona, A., Pevzner, R., Dean, T., Freifeld, B., Marshall, S., 2017. Analysis of signal to noise and directivity characteristics of DAS VSP at near and far offsets — A CO2CRC Otway Project data example. The Leading Edge 36, 994a991-994a997.
- Correa, J., Tertyshnikov, K., Wood, T., Yavuz, S., Freifeld, B., Pevzner, R., 2018. Time-lapse VSP with permanent seismic sources and distributed acoustic sensors: CO2CRC Stage 3 equipment trials, 14th Greenhouse Gas Control Technologies Conference Melbourne, pp. 21-26.
- Couëslan, M.L., Ali, S., Campbell, A., Nutt, W.L., Leaney, W.S., Finley, R.J., Greenberg, S.E., 2013. Monitoring CO 2 injection for carbon capture and storage using time-lapse 3D VSPs. 32, 1268-1276.

- Daley, T.M., Cox, D., 2001. Orbital vibrator seismic source for simultaneous P-and S-wave crosswell acquisition. Geophysics 66, 1471-1480.
- Dance, T., 2013. Assessment and geological characterisation of the CO2CRC Otway Project CO2 storage demonstration site: From prefeasibility to injection. Marine and Petroleum Geology 46, 251-269.
- Dance, T., LaForce, T., Glubokovskikh, S., Ennis-King, J., Pevzner, R., 2019. Illuminating the geology: Post-injection reservoir characterisation of the CO2CRC Otway site. International Journal of Greenhouse Gas Control 86, 146-157.
- Davis, T., Landrø, M., Wilson, M., 2019. Geophysics and Geosequestration. Cambridge University Press, Cambridge.
- Dillon, P.B., 1990. A comparison between Kirchoff and GRT migration on VSP data. Geophysical Prospecting 38, 757-777.
- Dou, S., Ajo-Franklin, J., Daley, T., Robertson, M., Wood, T., Freifeld, B., Pevzner, R., Correa, J., Tertyshnikov, K., Urosevic, M., 2016. Surface orbital vibrator (SOV) and fiber-optic DAS: Field demonstration of economical, continuous-land seismic time-lapse monitoring from the Australian CO2CRC Otway site, SEG Technical Program Expanded Abstracts 2016. Society of Exploration Geophysicists, pp. 5552-5556.
- Dou, S., Wood, T., Ajo-Franklin, J., Robertson, M., Daley, T., Freifeld, B., Pevzner, R., Gurevich, B., 2017. Surface orbital vibrator for permanent seismic monitoring: A signal contents and repeatability appraisal, 2017 SEG International Exposition and Annual Meeting. Society of Exploration Geophysicists, Houston, Texas, p. 5.
- Egorov, A., Correa, J., Bóna, A., Pevzner, R., Tertyshnikov, K., Glubokovskikh, S., Puzyrev, V., Gurevich, B., 2018. Elastic full-waveform inversion of vertical seismic profile data acquired with distributed acoustic sensors. GEOPHYSICS 83, R273-R281.
- Egorov, A., Pevzner, R., Bóna, A., Glubokovskikh, S., Puzyrev, V., Tertyshnikov, K., Gurevich, B., 2017. Time-lapse full waveform inversion of vertical seismic profile data: Workflow and application to the CO2CRC Otway project. Geophysical Research Letters 44, 7211-7218.

- Evensen, G., 2009. Data assimilation: the ensemble Kalman filter. Springer Science & Business Media.
- Freifeld, B.M., Pevzner, R., Dou, S., Correa, J., Daley, T.M., Robertson, M., Tertyshnikov, K., Wood, T., Ajo-Franklin, J., Urosevic, M., Gurevich, B., 2016. The CO2CRC Otway Project deployment of a Distributed Acoustic Sensing Network Coupled with Permanent Rotary Sources. 2016, 1-5.
- Glubokovskikh, S., Pevzner, R., Dance, T., Caspari, E., Popik, D., Shulakova, V., Gurevich, B., 2016. Seismic monitoring of CO2 geosequestration: CO2CRC Otway case study using full 4D FDTD approach. International Journal of Greenhouse Gas Control 49, 201-216.
- Glubokovskikh, S., Pevzner, R., Gunning, J., Dance, T., Shulakova, V., Popik, D., Popik, S., Bagheri, M., Gurevich, B., 2020. How well can time-lapse seismic characterize a small CO2 leakage into a saline aquifer: CO2CRC Otway 2C experiment (Victoria, Australia). International Journal of Greenhouse Gas Control 92, 102854.
- Hannis, S., 2013. Monitoring the geological storage of CO2, Geological Storage of Carbon Dioxide (CO2). Elsevier, pp. 68-96.
- Hartog, A.H., 2017. An Introduction to Distributed Optical Fibre Sensors. CRC Press (Taylor and Francis).
- Jenkins, C., 2020. The State of the Art in Monitoring and Verification: an update five years on. International Journal of Greenhouse Gas Control 100, 103118.
- Jenkins, C., Bagheri, M., Barraclough, P., Dance, T., Ennis-King, J., Freifeld, B., Glubokovskikh, S., Gunning, J., LaForce, T., Marshall, S., 2018. Fit for purpose monitoring-a progress report on the CO2CRC Otway Stage 3 project, 14th Greenhouse Gas Control Technologies Conference Melbourne, pp. 21-26.
- Jenkins, C., Marshall, S., Dance, T., Ennis-King, J., Glubokovskikh, S., Gurevich, B., La Force, T., Paterson, L., Pevzner, R., Tenthorey, E., Watson, M., 2017. Validating Subsurface Monitoring as an Alternative Option to Surface M&V - The CO2CRC's Otway Stage 3 Injection. Energy

Procedia 114, 3374-3384.Johnston, D.H., 2013. Practical applications of time-lapse seismic data. Society of Exploration Geophysicists.

- Kragh, E., Christie, P., 2002. Seismic repeatability, normalized rms, and predictability. The Leading Edge 21, 640-647.
- Kuvshinov, B.N., 2016. Interaction of helically wound fibre-optic cables with plane seismic waves: Interaction of fibre-optic cables. Geophysical Prospecting 64, 671-688.
- Lopez, J., Wills, P., La Follett, J., Hornman, J., Potters, J., van Lokven, M., Perkins, C., Trefanenko, C., 2015. Permanent seismic reservoir monitoring for real-time surveillance of thermal EOR at Peace River, Third EAGE Workshop on Permanent Reservoir Monitoring 2015. European Association of Geoscientists & Engineers, pp. 1-5.
- Lüth, S., Bergmann, P., Huang, F., Ivandic, M., Ivanova, A., Juhlin, C., Kempka, T., 2017. 4D seismic monitoring of CO2 storage during injection and post-closure at the Ketzin pilot site. Energy Procedia 114, 5761-5767.
- Nakatsukasa, M., Ban, H., Takanashi, M., Kato, A., Worth, K., White, D., 2017. Repeatability of a rotary seismic source at the Aquistore CCS site, SEG Technical Program Expanded Abstracts 2017. Society of Exploration Geophysicists, pp. 5911-5916.
- Oldenburg, C.M., 2018. Are we all in concordance with the meaning of the word conformance, and is our definition in conformity with standard definitions? Greenhouse Gases: Science and Technology 8, 210-214.
- Parker, T., Shatalin, S., Farhadiroushan, M., 2014. Distributed Acoustic Sensing-A New Tool for Seismic Applications. First Break 32, 61-69.
- Pevzner, R., Bona, A., Correa, J., Tertyshnikov, K., Palmer, G., Valishin, O., 2018. Optimising DAS VSP data acquisition parameters: theory and experiments at Curtin training well facility.
- Pevzner, R., Tertyshnikov, K., Sidenko, E., Ricard, L., 2020a. Monitoring Drilling and Completion Operations Using Distributed Acoustic Sensing: CO2CRC Stage 3 Project Case Study, First EAGE Workshop on Fibre Optic Sensing. European Association of Geoscientists & Engineers, pp. 1-5.

- Pevzner, R., Urosevic, M., Popik, D., Shulakova, V., Tertyshnikov, K., Caspari, E., Correa, J., Dance, T., Kepic, A., Glubokovskikh, S., Ziramov, S., Gurevich, B., Singh, R., Raab, M., Watson, M., Daley, T., Robertson, M., Freifeld, B., 2017a. 4D surface seismic tracks small supercritical CO2 injection into the subsurface: CO2CRC Otway Project. International Journal of Greenhouse Gas Control 63, 150-157.
- Pevzner, R., Urosevic, M., Tertyshnikov, K., ALNasser, H., Caspari, E., Correa, J., Daley, T., Dance, T., Freifeld, B., Glubokovskikh, S., Greenwood, A., Kepic, A., Popik, D., Popik, S., Raab, M., Robertson, M., Shulakova, V., Singh, R., Watson, M., Yavuz, S., Ziramov, S., Gurevich, B., 2020b. Chapter 6.1 - Active surface and borehole seismic monitoring of a small supercritical CO2 injection into the subsurface: experience from the CO2CRC Otway Project, in: Kasahara, J., Zhdanov, M.S., Mikada, H. (Eds.), Active Geophysical Monitoring (Second Edition). Elsevier, pp. 497-522.
- Pevzner, R., Urosevic, M., Tertyshnikov, K., Gurevich, B., Shulakova, V., Glubokovskikh, S., Popik, D., Correa, J., Kepic, A., Freifeld, B., Robertson, M., Wood, T., Daley, T., Singh, R., 2017b. Stage 2C of the CO2CRC Otway Project: Seismic Monitoring Operations and Preliminary Results. Energy Procedia 114, 3997-4007.
- Popik, S., Pevzner, R., Tertyshnikov, K., Popik, D., Urosevic, M., Shulakova, V., Glubokovskikh, S., Gurevich, B., 2020. 4D surface seismic monitoring the evolution of a small CO2 plume during and after injection: CO2CRC Otway Project study. Exploration Geophysics, 1-11.
- Roach, L.A., White, D., 2018. Evolution of a deep CO2 plume from time-lapse seismic imaging at the Aquistore storage site, Saskatchewan, Canada. International Journal of Greenhouse Gas Control 74, 79-86.
- Shatalin S.V., P.T., Farhadiroushan M. , In press 2020. High definition seismic and micro-seismic data acquisition using distributed and engineered fiber optic acoustic sensors. In: Distributed Acoustic Sensing; In Geophysics: Methods and Applications; AGU books.
- White, D., 2019. Integrated Geophysical Characterization and Monitoring at the Aquistore CO2 Storage Site, in: Wilson, M., Landrø, M., Davis, T.L.

(EDS.), GEOPHYSICS AND GEOSEQUESTRATION. CAMBRIDGE UNIVERSITY PRESS, CAMBRIDGE, PP. 257-279.

- WILDENBORG, T., DE BRUIN, G., KRONIMUS, A., NEELE, F., WOLLENWEBER, J., CHADWICK, A., 2014. TRANSFERRING RESPONSIBILITY OF CO2 STORAGE SITES TO THE COMPETENT AUTHORITY FOLLOWING SITE CLOSURE. ENERGY PROCEDIA 63, 6705-6716.
- YAVUZ, S., CORREA, J., PEVZNER, R., FREIFELD, B., WOOD, T., TERTYSHNIKOV, K., POPIK, S., ROBERTSON, M., 2019. ASSESSMENT OF THE PERMANENT SEISMIC SOURCES FOR BOREHOLE SEISMIC MONITORING APPLICATIONS: CO2CRC OTWAY PROJECT. ASEG EXTENDED ABSTRACTS 2019, 1-5.
- YAVUZ, S., ISAENKOV, R., PEVZNER, R., TERTYSHNIKOV, K., YURIKOV, A., CORREA, J., WOOD, T., FREIFELD, B., 2020. PROCESSING OF CONTINUOUS VERTICAL SEISMIC PROFILE DATA ACQUIRED WITH DISTRIBUTED ACOUSTIC SENSORS AND SURFACE ORBITAL VIBRATORS. 2020, 1-5.

Advanced time-lapse processing of continuous DAS VSP data for plume evolution monitoring: Stage 3 of the CO2CRC Otway project case study

Roman Isaenkov[1,2], Sinem Yavuz [1,2], Stanislav Glubokovskikh [5], Pavel Shashkin[1,2], Alexey Yurikov[1,2], Konstantin Tertyshnikov[1,2], Boris Gurevich[1,2], Julia Correa [3], Todd Wood [3], Barry Freifeld[4], Paul Barraclough[2] and Roman Pevzner [1,2]

The published version of the article is accessible by the following link:

https://doi.org/10.1016/j.ijggc.2022.103716

[1] Centre for Exploration Geophysics, Curtin University, GPO Box U1987, Perth 6845, WA, Australia

[2] CO2CRC, 11 – 15 Argyle Place South, Carlton, VIC, 3053, Australia

[3] Lawrence Berkeley National Laboratory, 1 Cyclotron Road, MS 74R-316C, Berkeley, CA, USA, 94720

[4] Class VI Solutions, Inc., 711 Jean St., Oakland, CA, USA, 94610

[5] Lawrence Berkeley National Laboratory, formerly at Curtin University

Corresponding author:

Roman Isaenkov

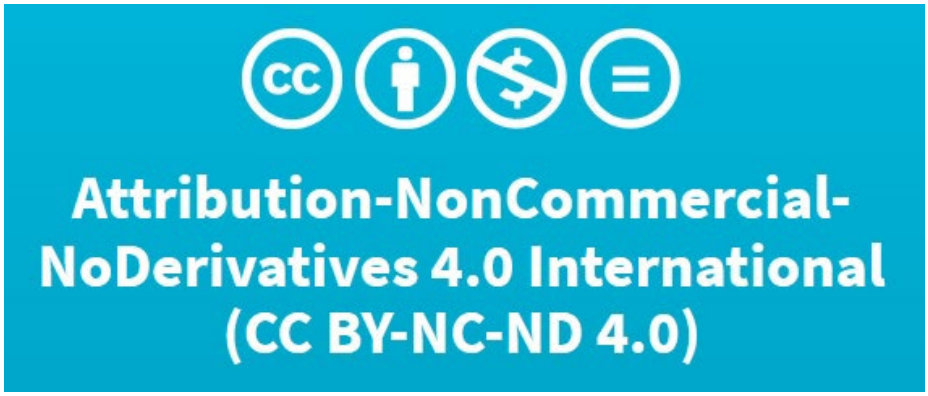

Keywords:

- Continuous automated reservoir monitoring
- Time-lapse seismic processing
- Seasonal variation of repeatability
- Seismic orbital vibrators
- Distributed acoustic sensors

ABSTRACT

Active time-lapse seismic monitoring technology is essential for carbon storage projects due to its ability to track the CO_2 plume in space and time. A particularly attractive implementation of this technology is permanent seismic reservoir monitoring (PRM) using permanent sources and receivers, which can track subsurface changes in near-real-time over decades. As the number of source points in such a setup is likely to be limited, repeatability and signal to noise ratio need to be improved by processing all the multiple vintages together rather than separately.

We explore the advantages of this approach using a PRM dataset acquired to monitor injection of 15 kt of CO_2 into a saline aquifer at the Otway International Test Centre (Australia). The monitoring employs continuous acquisition of multi-well offset VSP using nine permanent sources (surface orbital vibrators) and fibre-optic distributed acoustic sensors installed in five monitoring wells producing a vintage every two days for eighteen months before, during and after the injection.

Since data reveals seasonal repeatability variations, mainly created by seasonal variations in precipitation levels, for each monitor, an optimal baseline is the one acquired in the same season. The signal-to-noise ratio is further improved by wavefield decomposition of P and S waves. The consistency of the source signature is improved using Wiener filtering. These algorithms improve the data repeatability from about 15-20% to 10-15% normalised root mean square. The results show the CO_2 plume signal on the second day of the injection and subsequent time-lapse changes of a stable CO_2 plume created at the same reservoir 650 m up-dip five years earlier as a part of the previous field experiment (Stage 2C) at the site.

1 INTRODUCTION

Monitoring and verification are necessary for CO_2 geosequestration and to manage storage performance and risks (Jenkins, 2020). Active seismic monitoring has successfully been applied in several industrial-scale geosequestration projects (Ajayi et al., 2019). Compared to other remote sensing methods, active seismic monitoring has better spatial coverage and resolution (Johnston, 2013). However, relatively high cost, land usage, infrequent surveys (from several months to several years) and possibly large (several months) delays between acquisition and interpretable results may limit its application for CO_2 storage monitoring.

Permanent seismic reservoir monitoring (PRM) seeks to address some of these issues. Despite high initial installation costs, PRM is more economic over a long run (Detomo Jr and Quadt, 2011). Once the infrastructure is in place, PRM allows much more frequent surveys, which benefit long-term reservoir management (Caldwell et al., 2015; Kjølhamar et al., 2021). Equipment for PRM is often buried into the ground, which minimises land access.

Just as any other active seismic survey, PRM requires receivers and sources. The survey design and surface conditions (Smith et al., 2018) define the level of repeatability that can be achieved – similarity between baseline and monitor seismic surveys. The better repeatability, the smaller reservoir changes can be detected. Onshore, receiver arrays can be buried several meters below the surface (Pevzner et al., 2015) or installed in wells (Correa et al., 2017). Sources such as orbital vibrators can be placed on the surface (Nakatsukasa et al. (2017), Wang et al., 2020, Dou et al. (2017)) or in shallow wells (Lopez et al., 2015). Borehole based equipment is the least affected by near-surface variations and has better repeatability compared to surface or mixed installation (Schisselé et al., 2009), but is usually more expensive.

PRM can operate automatically producing frequent vintages. At the same time, since the number of permanent sources is usually small, and since all of these are fixed in space, the number of shot locations is much smaller than conventional 4D seismic with mobile sources such as vibroseis. As such, PRM data usually would have a relatively low fold, and thus is likely to have a lower signal-to-noise ratio and poorer repeatability.

Unlike 3D time-lapse seismic with an annual turnaround, PRM has temporally dense spaced vintages, time-lapse signal is expected to be repeatable from one vintage to the next while time-lapse noise is not. This can be used to improve repeatability (Mateeva et al., 2020). However, to date, the number of PRM projects with frequent acquisition is rather small and thus processing tools for such data are yet to be developed.

In this study, we develop an approach to process a specific time-lapse PRM dataset acquired to monitor injection of 15 kt of CO_2 into a saline aquifer at the Otway International Test Centre in the Australian State of Victoria (the project is known as Otway Stage 3). Five ~1600 m deep monitoring wells (CRC3-CRC7) equipped with distributed acoustic sensors (DAS) have recorded seismic data continuously 24/7 while nine surface orbital vibrators (SOV1-SOV9) excite seismic signals daily, 2.5 hours each, with sweeps recorded by a geophone, buried 3 m below the source. It takes two days to acquire a full vintage comprising of forty-five 2D offset-VSP transects. The data is acquired and processed automatically on site with the results available two days after acquisition (Isaenkov et al., 2021).

The location of the wells and SOVs has been chosen to cover the simulated CO_2 plume migration area (red contour in Figure 1) and previous Stage 2C plume (yellow contour in Figure 1). Both plumes were injected at ~1500 m depth into the Paaratte formation, a Late Cretaceous complex that comprises of high-quality sandstones with excellent porosity (~25%) and permeability (~1-2 Darcy). The reservoir complex is about 100-m thick and includes extensive intra-formational seals consisting of heterolytic interbedded siltstone and mudstone units (Dance et al., 2019). During the Stage 2C, 15,000 tonnes of CO_2 were injected into Paarate formation from January to April 2016 via CRC2; more details about Stage 2C plume injection and monitoring are given in Pevzner et al. (2017). The Stage 3 plume was expected to migrate from the injection CRC3 well in the eastern direction towards the location of the Stage 2C plume (Bagheri et al., 2020). The outer contour of the Stage 2C plume was derived from the flow simulations history-matched with 4D seismic data(LaForce et al., 2018; Glubokovskikh et al., 2020). Note that the simulations for the Stage 2C injection were performed independently and, while the presence of the Stage 2C plume was included in the Stage 3 simulations, no interaction between the plumes was predicted or taken into account.

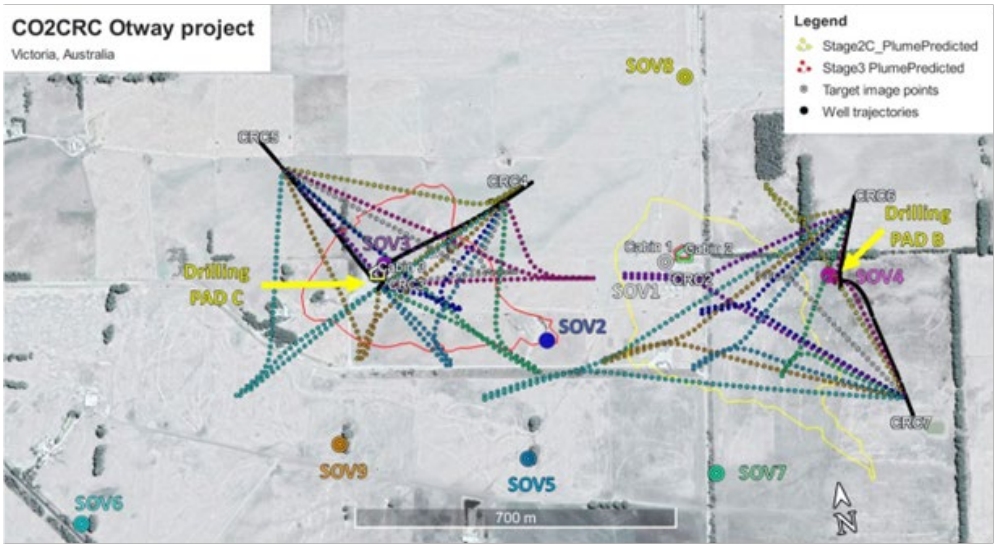

Figure 1 Location map of wells and SOVs. Dotted lines show the projection of specular reflection points at the target interval colour-coded by the corresponding SOV. Stage 2C (yellow) and Stage 3 plume (red) contours are predicted by flow simulation.

After SOVs were installed and tested, the continuous acquisition started in May 2020, six months before the start of the injection on 1 December 2020 (Table 1). The monitoring started well before the injection mainly to test the monitoring system performance, fix possible operational faults, establish a robust baseline, and develop the processing workflow. The injection finished on 17 April 2021 but the monitoring continued into 2022, producing 90 baseline and over 180 monitor vintages by the end of January 2022. There are several gaps in the continuous data due to on-site operations, power outages and some minor equipment faults (Isaenkov et al., 2021). Additional to continuous monitoring, one 4D VSP baseline and two monitor surveys with vibroseis sources, were acquired during that period.

Table 1 CO2CRC Otway Stage 3 continuous monitoring timeline

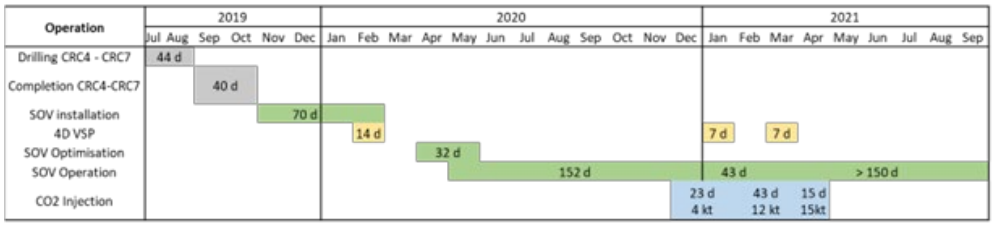

The initial processing was based on conventional offset-VSP processing workflows implemented in commercial software (RadExPro), adapted to address key challenges of the continuous DAS setup SOVs (Yavuz et al., 2021). The workflow was then implemented in Matlab as a stand-alone in-house software package for autonomous on-site processing. This processing sequence is currently used for on-site processing, and we refer to it as 'initial' processing.

The initial processing is applied to every vintage independently of each other. First, raw DAS data are deconvolved with SOV sweeps to produce the shot gathers. These shot gathers are stacked for each rotation direction to suppress random noise, increase the signal-to-noise ratio, and reduce the data size. Then, the second pass of deconvolution (designature) is applied using the wavelets estimated from the far-field first-break signatures. Designature improves the data resolution and repeatability. Next, several F-K filters are applied to isolate the upgoing reflected P waves from all other wavefield components. Subsurface images are then generated using VSP Kirchhoff time migration. Finally, time-lapse difference sections are calculated by subtracting the predefined initial baseline from a monitoring vintage (Isaenkov et al., 2021; Pevzner et al., 2021).

The predefined baseline was set as an average of the last ten vintages acquired before the start of the injection. This was based on known observations that repeatability is best when baseline and monitor are as close in time as possible (Bakulin et al., 2014). However, as many more baseline vintages are available, it is prudent to explore how a more optimal baseline vintage could be constructed.

This work aims to process all vintages together using information from the analysis of the entire dataset.

This analysis reveals:

- All vintages show strong seasonal variations, with vintages acquired in the same season showing the smallest differences. Thus, the repeatability can be improved if from each monitor, we subtract a baseline acquired in the same season.
- As S-waves are not corrected during the processing, their variations can mask the time-lapse signal. Wavefield decomposition based on stacking of clockwise (CW) and counterclockwise (CCW) SOV rotations can partially separate P and S wavefields, improve the signal-to-noise ratio and reduce time-lapse noise. CW and CCW SOV rotations have the same vertical but opposite horizontal motion polarities, resulting in the same P-wave and opposite S-wave polarities (Daley and Cox, 2001).
- Initial processing under-corrects the SOV signature resulting in up to 10% amplitude difference between baseline and monitor; this can be compensated for by Wiener filtering.

Application of these methods leads to improvement of repeatability from about 15-20% to 10-15% normalised root mean square (NRMS).

2 SMART PROCESSING OF CONTINUOUS DATA

A key objective of continuous time-lapse processing is to achieve the highest possible repeatability, which is necessary to detect small time-lapse signals. The repeatability is inevitably affected by many factors (ambient noise, source performance, coupling, near-surface, etc) which cannot be avoided. In on-shore permanent monitoring, the primary source of non-repeatability is the changes in the near-surface properties caused by seasonal variations of weather conditions, such as precipitation, which affects soil moisture and the water table. This, in turn, affects the source performance and all the wavefield propagating through the near-surface such as primaries and surface-related multiples, which increases time-lapse noise level when comparing vintages acquired in different seasons and different weather conditions. As such, the refined 'smart' processing is made to correct some of the issues: variations of primary P wavefield, variations of S wavefield and seasonal effect (Table 2).

As we mentioned above, some SOVs show up to 10% P wave amplitude variation. To correct it, we designed a Wiener matching filter that equalises the monitor to the baseline P wavelet.

Unlike primary P wavefield, S wave variations are not corrected which possibly can create a strong time-lapse noise. Moreover, S waves produce a converted SP field which interferes with the signal. To separate P

and S wavefields we modified the wavefield decomposition technique described by Daley and Cox (2001) based on the different polarisation of S wavefield on CW and CCW SOV rotations. We introduced a matching filter to equalise the P wavefield for both rotations which leads to better separation compared to simple CW + CCW stacking.

The variations of near-surface conditions are hard to measure independently, and, as such, it appears impossible to simulate and remove these effects from the data. However, if the variations are seasonal (repeat over a year interval), we can acquire several baseline vintages in different parts of the year and utilise them in time-lapse processing. Luckily, we have a 90-vintages baseline pool to select from. For each monitor, we can select one or several best-matching baselines from the pool for time-lapse differencing. We call that process 'smart baseline selection'. As we show later, such a process can reduce the seasonal variation effect and improve repeatability by about 30% compared to the initial 'fixed' baseline.

More details about these three procedures are described below. A brief comparison of initial and 'smart' processing is summarised in Table 2.

Table 2. Initial and smart processing flows

Initial processing	Smart processing	Parameters
Data decimation		Output data has channel spacing of 5 m and time sampling of 2 ms
Deterministic deconvolution with reference geophone data		Fourier domain, 0.1 white noise level
Vertical stacking		22 sweeps for each rotation direction
Geometry		Source and receiver geometry assigned; noisy channels removed
Deconvolution with an estimated wavelet and bandpass filtering (Designature)		Fourier domain, individual for each rotation, wavelet estimated by averaging downgoing P waves
Not Applied	Wavelet matching to baseline signature	Wavelets (CW, CCW) matched to baseline signature (ten-vintage average before injection start). Wiener matching filter length of 50 samples and the white noise level of 0.0015

Wavefield decomposition	Wavefield decomposition using rotation signature matching	CCW data matched to CW data and summed. Wiener matching filter computed to match CCW and CW wavelets, filter length is 50 samples, the white noise level is 0.0015
Wavefield separation		F-K filtering to isolate target PP reflections, bottom muting past source-generated S wave arrival
VSP Kirchhoff time migration		Kirchhoff migration: central dip = 0, dip range = 7 degrees, 1D isotropic velocity function from VSP in the CRC-3 well
The time-lapse difference with predefined baseline (average of the last ten pre-injection vintages)	The time-lapse difference with smart baseline selection from all pre-injection data	NRMS computation window: Non-migrated data: 60 ms Migrated data: 40 m

2.1 MATCHING MONITORS TO BASELINE SIGNATURE

While, in general, most SOVs show only minor temporal variations of source signature (<1% of maximum wavelet amplitude change over time), some SOVs show significant signal changes (>5 %) over time. For example, SOV3 shows the largest amplitude variation (about 10%) over the monitoring period. Conversely, SOV1 has the least amplitude variations (<1%). When comparing baseline and monitor seismograms, signature variations can mask time-lapse signal from the subsurface and, as such, should be corrected for. Some signature variations are inevitable because the surface source is affected by near-surface conditions. Here we describe a method that can correct these variations for the primary P wavefield.

Figure 2 shows a comparison of baseline (November 2020) and monitor (April 2021) wavelets acquired for SOV3. SOV3 was chosen as the one with the largest wavelet variations. The baseline wavelet is acquired for the initial baseline dataset and acts as a standard wavelet. The wavelets are estimated by averaging the first break signal above the injection interval, independently for CW and CCW SOV rotations. Figure 2 shows a stable CW signal over time, but the CCW signals have about a 10% amplitude difference. Such differences in amplitudes would create significant time-lapse noise and reduce data repeatability. To compensate for this, we design a Wiener matching filter for every well and SOV-rotation combination. First, the monitor wavelets are estimated from the data after designature by averaging the first break signals. The filters are then

calculated to match the monitor wavelet to the baseline wavelet using a $\pm$ 30 ms window around the central peak with a filter length of 50 samples (100 ms) and a white noise level of 0.15 %. These filters are then applied to seismic gathers.

The filter corrects only the primary P wave arrivals because it is based on the P wave signature. As such, variations of S wave arrivals will still be present in the data and appear as coherent time-lapse noise.

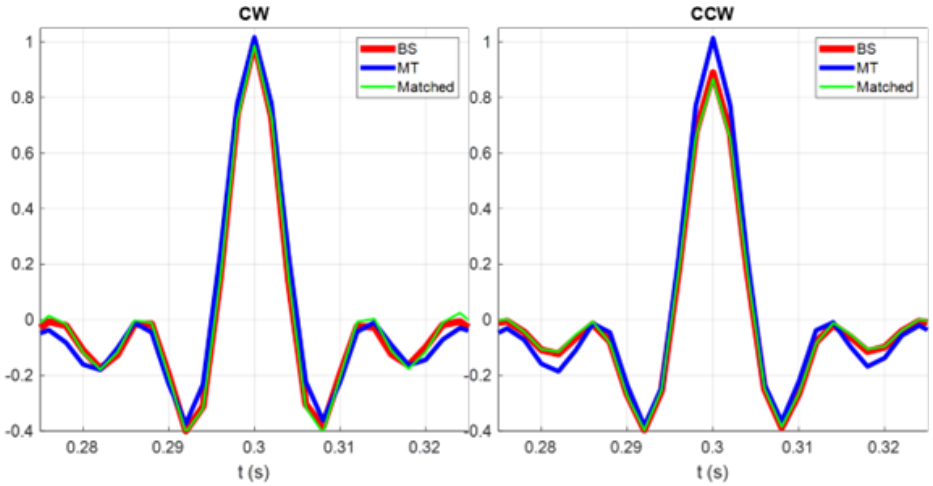

Figure 2. Matching monitor (MT) to baseline wavelets (BS) for CW and CCW rotations for CRC4-SOV3 and the result of the applied filter (matched). Wavelets are normalised by CW baseline maximum amplitude. Approximately 10% of amplitude difference is noticeable between BS and MT wavelets for CCW signals.

To quantitatively assess repeatability, we use a standard NRMS measure (Kragh and Christie, 2002). If two signals are identical, NRMS is 0%, and NRMS of two random noise realisations is about 140%. NRMS of 10-20% is considered as good repeatability, however, it naturally depends on many factors, including geological environment and acquisition equipment and geometry (Johnston, 2013).

The application of the filters to monitor seismic gathers leads to a noticeable time-lapse noise reduction (Figure 3). CRC4-SOV3 CCW time-lapse difference section (Figure 3a) demonstrates quite strong remnants of direct and primary reflected P energy (a green arrow in Figure 3a) before the filtering. The filter considerably attenuates these remnants (a green arrow in Figure 3b) and improves signal repeatability by about 5% NRMS above the target interval (Figure 3d).

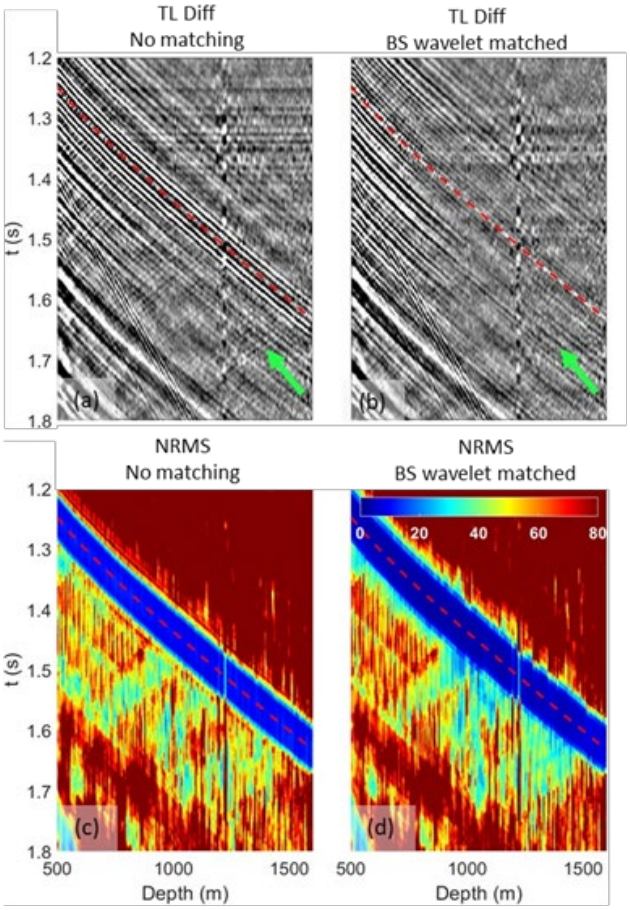

Figure 3. Time-lapse differences and NRMS before (a, c) and after (b, d) applying the matching filter for CRC4-SOV3 CCW. The first break peak is highlighted with a red dashed line. A relatively strong remnant of the reflected wave (green arrow) is noticeable around the target interval (1500 m depth) before applying a matching filter.

2.2 WAVEFIELD DECOMPOSITION

As mentioned earlier, another source of time-lapse noise is non-repeatable S waves. This effect obscures time-lapse signals and creates non-repeatable converted SP waves, which interfere with target reflections. In the initial processing, this effect was attenuated by several F-K filters to isolate P wave energy and attenuate S waves. However, such filtering cannot attenuate converted SP waves and is not very effective in

completely removing source-generated S waves on far offsets, where the difference in P and S wave apparent velocities is small.

The next step to improve data quality is to utilise CW and CCW rotation data in a way to enhance the P wave energy and attenuate the unwanted shear wave energy and related converted wavefield components. Each SOV generates a circularly polarised wavefield, thus exciting both P and S waves (Correa et al., 2018). The circular polarisation of SOVs can be decomposed into vertical and inline horizontal forces by adding and subtracting datasets acquired with CW and CCW rotations (Daley and Cox, 2001). The decomposition of circular polarisations into vertical and horizontal components can help to separate primary P and S wavefields. That is because for near-vertical angles of incidence horizontal force excites mainly S waves while a vertical force generates P energy.

CW and CCW rotations have the same polarity for the vertical force but an opposite polarity for the horizontal force. However, despite the apparent symmetry of the source, field data show an asymmetry between CW and CCW signals (perhaps due to lateral heterogeneity of the near-surface geology or source installation itself), which leads to some artefacts in the P and S wavefield decomposition (Figure 4) (Dou et al., 2016; Yavuz et al., 2021). To correct the difference, we introduce a Wiener filter to match the P wave signatures of CW and CCW data.

2.2.1 Matching rotation signatures

This matching Wiener filter is very similar to the filter described in the previous section. After the designature and baseline, signature-matching steps are completed (Figure 2a, b), we match CW and CCW wavelets to compensate for their signal asymmetry. We obtain CW and CCW wavelets by stacking P wave direct arrivals and designing Wiener filters to match these wavelets. In order not to distort the time-lapse signal, wavelets are estimated at about 750-1500 m depth above the reservoir. CW and CCW signatures have noticeable amplitude and phase differences. Figure 4 shows a CRC4-SOV3 CW and CCW signature-matching example. While the amplitudes of the original CW and CCW wavelets differ by about 10%, the matched CCW wavelet is almost identical to the CW signal (<1% amplitude difference).

Every SOV has a different level of asymmetry: while some require such correction, others do not. Installation procedures and orientation are the same for all the SOVs with SOV1-4 installed at the drill pads. However, soil composition and topographic elevation vary between SOVs, resulting in significant changes in the near-surface conditions. That is why we apply asymmetry correction to all the data to account for the possible SOV asymmetries that might occur over time.

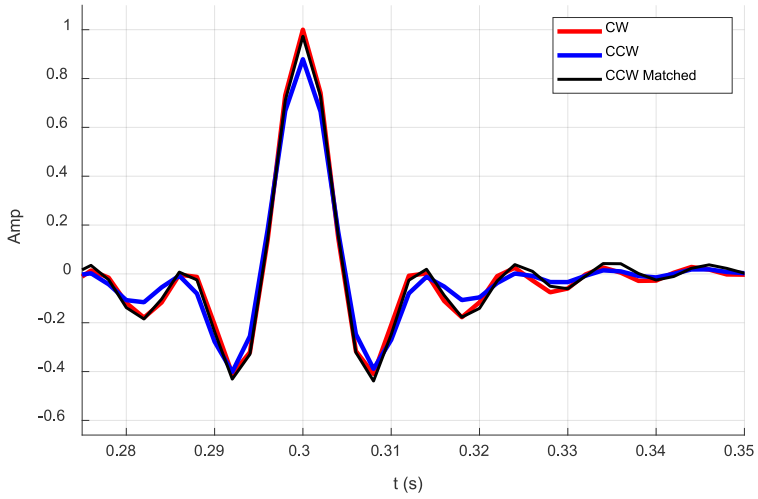

Figure 4. Estimated P wave wavelet from the first breaks after designature. Note the initial difference in CW and CCW response. The Wiener filter is designed to match CCW to CW signal.

To decompose the wavefield, first, we apply the designed filter to CCW seismic gather to ensure that the primary P wavefield matches that in the CW gather. Then, the vertical polarisation is obtained by subtraction of corrected CCW gather from CW gather (CW – CCW), the horizontal polarisation is the sum of these components (CW + CCW). We multiply the results by a factor of 0.5 to scale the amplitudes. Note, in this case, CW and CCW have vertical polarisation as the result of processing. SOV sweeps, recorded by the vertical component of a pilot geophone, are then deconvolved from raw records. This unifies the polarity of the vertical component for CW and CCW (Isaenkov et al, 2021).

The results of decomposition are presented in Figure 5 on a dataset with a well-to-SOV offset of ~350 m. Note that CW and CCW (Figure 5a, b) gathers have the same P wave polarity, but the polarity of S waves is reversed. The summation of CW and CCW gathers enhances P waves and attenuates the S waves (Figure 5c) while subtraction enhances S waves (Figure 5d). In Figure 5d, S and converted SP waves are dominant with almost no primary P energy present – an indicator of good P and S wavefields separation. In Figure 5c, the P wave energy is emphasised, and the S wavefield is suppressed. Some S wave energy is still present in Figure 5c due to the nature of the wavefield decomposition on vertical and horizontal forces. As the vertical force does also generate S waves, decomposition does not completely remove the S wavefield. Another reason for S wave remnants after decomposition is because we corrected asymmetry only for the P waves (vertical component) while S waves (horizontal component) are not corrected.

Similar results are observed when analysing the F-K spectra (Figure 6). While a similar amount of P and S wave energy is present in CW and CCW rotations, the rotation summation CW + CCW enhances the P wave energy and attenuates S waves. The P wavefield presence on the difference CW – CCW is most likely due to converted SP waves. Note, that CCW SOV rotation (Figure 6b) emits stronger S waves compared to CW rotation (Figure 6a). The cause of this difference is unclear and requires further research.

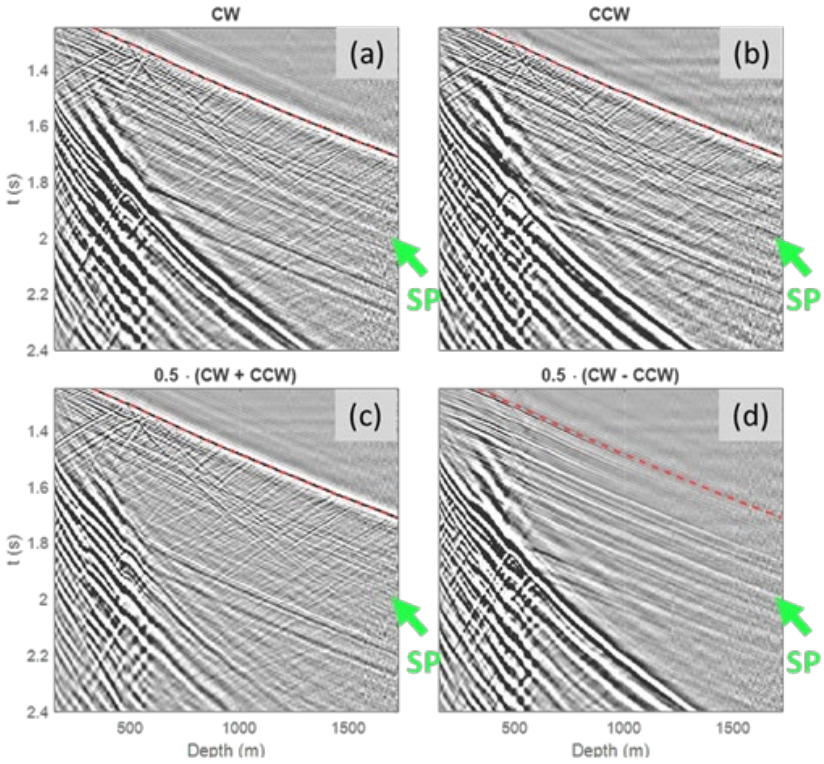

Figure 5. VSP shot gathers after designature: CW (a), CCW(b), 0.5 (CW + CCW) (c) and 0.5 (CW – CCW) (d). A factor of 0.5 is applied to scale amplitudes to the same level after decomposition. Notice different S wave polarity on CW and CCW gathers. Green arrows point to one of the converted SP waves – the amplitude is reduced after decomposition. Time and depth variable gains were applied for visualisation purposes.

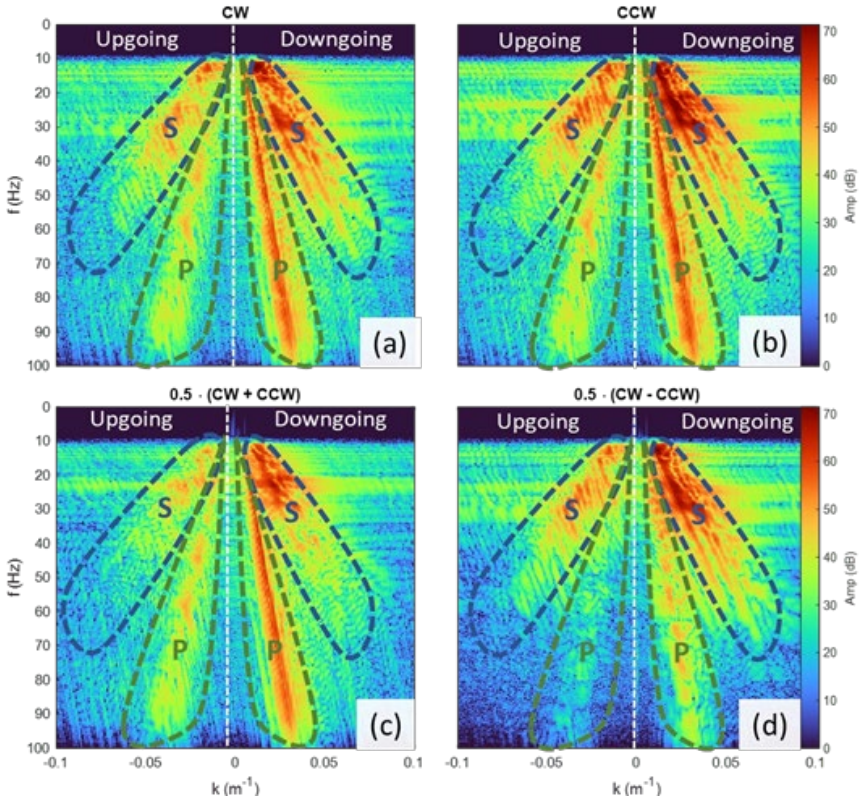

Figure 6. F-K spectra of the data from Figure 5. Notice the amount of P and S wavefield energy present for each dataset

2.2.2 Effect of wavefield decomposition on repeatability

Inspection of time-lapse data analysis reveals that the S wavefield changes quite drastically over three months and thus causes significant non-repeatability. Wavefield decomposition reduces this effect. Here we qualitatively assess how the proposed wavefield decomposition improves repeatability.

Figure 7 demonstrates the effect of wavefield decomposition on time-lapse data. Figure 7b suggests that the time-lapse noise is mainly caused by S waves. The reason for P and S wave variations is most likely due to near-surface variations such as soil moisture, groundwater level etc. These variations affect the source performance and the generated wavefield (e.g., short-term near-surface multiples). Time-lapse variations on primary P waves are minor as they are compensated by the designature and matching filters (see the previous section). After the application of wavefield decomposition (CW + CCW), S wave energy is attenuated. This step also reduces the time-lapse noise created by converted SP waves around the expected time-lapse signal (Figure 7d).

The current implementation of wavefield decomposition requires separate P wave source signature estimates for CW and CCW rotations from direct-wave arrivals and thus is only applicable to VSP data. SOV wavefield decomposition attenuates the S wavefield component and improves repeatability. Although it is not the focus of this paper, there is a potential for future studies on using separated S waves (CW - CCW) for imaging.

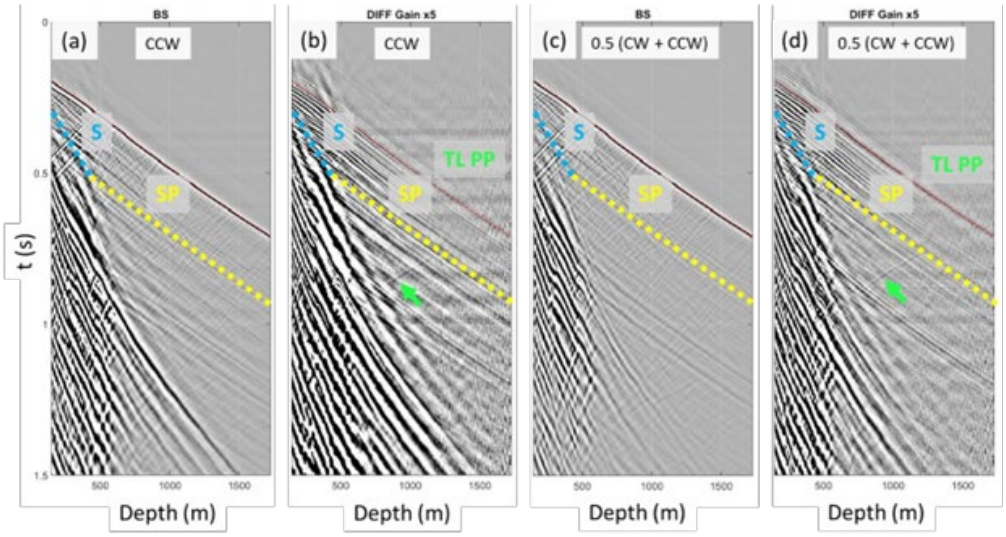

Figure 7 Baseline (BS) and time-lapse difference (DIFF) VSP gathers are given for a CCW rotation (a, b) and stacked rotations (c, d). Monitor survey was acquired three months after the baseline. Most time-lapse noise is formed by non-repeatable S (blue line) and converted SP (yellow line) waves, which mask the time-lapse response due to CO_2 injection (green arrow). The dashed red line shows the first breaks. Trace by trace and time-variant normalisation is applied for visual purposes; time-lapse differences are multiplied by a factor of 5. Data is shown for CRC4-SOV9

2.3 SMART BASELINE SELECTION

Conventional 4D seismic monitoring typically involves data acquisition every few months or years. Often, a single survey serves as the baseline. The DAS/SOV continuous monitoring system greatly benefits from the acquisition of 90 vintages of data over seven months before the injection. Each of these datasets could be used as a baseline. This poses the question, 'How do we select an optimal baseline?'. One approach could be using an average of all available baseline vintages to reduce the level of random noise. This would be the most appropriate approach if repeatability were controlled primarily by stationary random noise.

Previous research has shown that repeatability can deteriorate slowly over time, which is often attributed to variations in near-surface conditions due to seasonal changes or major weather events. Bakulin et al. (2014) noticed gradual decay of land 4D seismic repeatability with the increase of an interval between the baseline and monitor surveys. For the Otway site, Al Jabri (2011) analysed the effects of seasonal variations on soil moisture and groundwater level on the coupling of surface sources and receivers through a series of dedicated shallow seismic surveys and laboratory tests. More recently, Tertyshnikov et al. (2020) and Yavuz et al. (2019) analysed this effect on permanent DAS and geophone receiver arrays deployed in the shallow subsurface.

The borehole acquisition configuration gives an opportunity to study the wavefield structure and the relationship between different seismic waves in situ (Galperin, 1985). As such, by studying a year-long continuous VSP data, we can identify repeatable and non-repeatable components of downgoing and upgoing wavefields and design an approach for the selection of an optimal baseline.

2.3.1 Variation of repeatability

We can study variations of repeatability by comparing the time-lapse similarity between all combinations of pairs of vintages. To assess similarity in data after wavefield decomposition, we computed average NMRS values to measure within the time window from the first arrivals to 1.5 s and depth interval from 500 m to the bottom of the well (trace-by-trace) and then averaged. This time window contains primary PP and PS reflections, free-surface related multiples and source-generated S waves. The metric is sensitive to both amplitude and phase variations.

This procedure generates a repeatability matrix shown in Figure 8. Each row or column of the matrix represents NRMS between a particular vintage and all the other vintages. NRMS on the main diagonal line is zero by definition (a vintage compared to itself has NRMS = 0). When we move away from the diagonal, the time interval between baseline and monitor vintage increases and the repeatability decreases. The best repeatability between close vintages (i.e., vintages acquired within a several weeks interval) is observed for December-February and June-September 2021 (about 20-30%) while the data acquired in late May to early July 2020 is less repeatable.

The repeatability also shows seasonal variations. For a vintage acquired in early June 2020 (red arrow on Figure 8), repeatability with its nearest vintages is relatively high – about 45-50%. Then NRMS increases to nearly 70% in February 2021 and then decreases to approximately its initial value again at the end of March to early June 2021 (NRMS 50% about a year since June 2020) followed by the next rapid increase to 70% in the middle June 2021. The decrease in repeatability in June 2021 compared to June 2020 is very likely linked

to a significant increase in precipitation: 111 mm in June 2021 compared to 49 mm in June 2020 (http://www.bom.gov.au/, Station: Nullawarre).

20

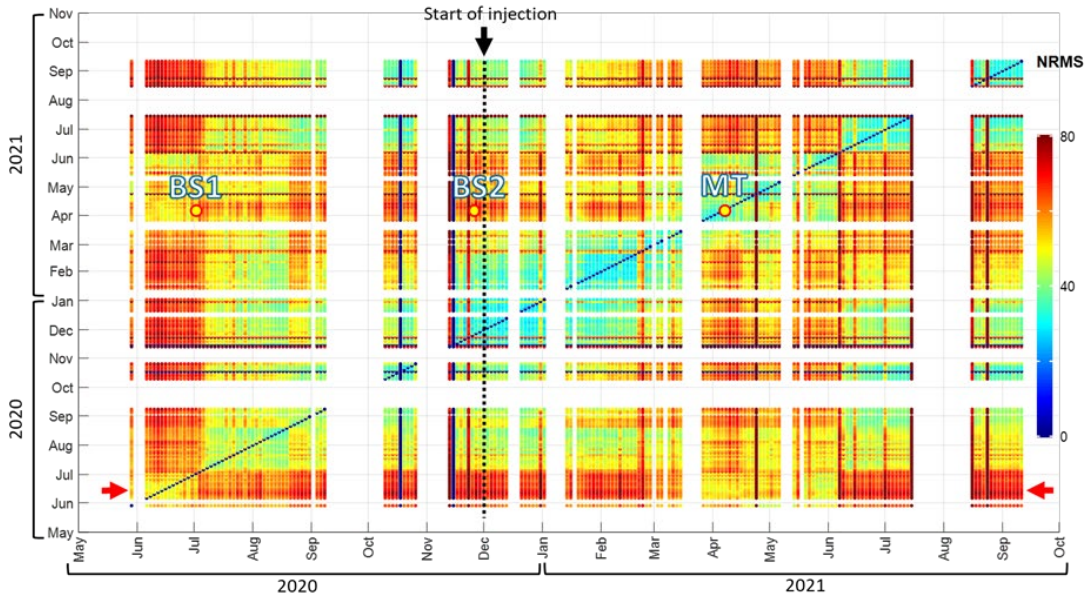

Figure 8. NRMS repeatability matrix. Red arrows are mentioned in the text. 'BS1', 'BS2' and 'MT' point to the location of the vintages used for Figure 9. The gaps in the matrix are mainly due to the faults of SOV6 or suspended operations during other seismic activities on the site (Isaenkov et al., 2021).

2.3.2 Sources of non-repeatability

To investigate how the choice of the baseline reference affects time-lapse noise, we selected two baselines: one at the end of November 2020 (BS2) just before the start of the injection and another at the end of June 2020 (BS1). The survey vintage acquired in April 2021 (MT) serves as a monitor (Figure 9). The June data was selected as it corresponds to the minimum NRMS value between all pre-injection surveys (see yellow dot 'BS1' in Figure 8).

For both cases, there is almost no primary PP wave energy on the time-lapse differences except for the time-lapse signal attributed to the injection. This means that in the processed data, the primary P waves are repeatable. However, there are two major contributors to the time-lapse noise. The first type of noise is surface-related P-wave multiples. On the gather, they appear parallel to the first breaks and are pronounced in the depth interval of 300-1000 m and time interval of 0.5-0.8 s. NRMS in that region increases from about 25-35% to 40-50% when switching between BS1 and BS2. The second type of coherent time-lapse noise is source-generated shear waves, which tend to have poor repeatability. NRMS in the area of their presence (red arrow on Figure 9) increases from about 40-50% (BS1) to about 80-100% (BS2). Note that the overall repeatability is 45% for BS1 and 60% for BS2.

Given that the DAS cables are installed in deep wells, we do not expect significant seasonal variation to impact DAS receivers. Thus, surface and near-surface rock/soil property variations impact the SOVs and lead to alterations in surface-related multiples. In particular, SOV performance can be affected by soil moisture, which can change its P- and S-wave signatures. While the primary P-wave signature is corrected in the processing, source-generated S waves are not. Furthermore, the soil moisture and groundwater level may alter the reflectivity of the free surface, resulting in non-repeatable surface-related multiples.

The use of BS1 provides better repeatability than BS2 and suppresses regular noise better. However, the level of ambient noise appears to be slightly higher for this vintage.

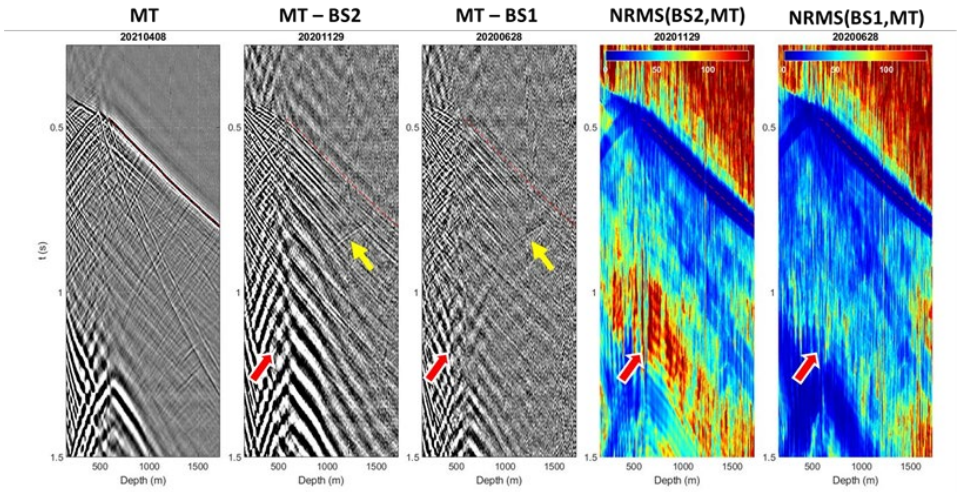

Figure 9. Time-lapse data plot. (MT) – monitor shot gather; (MT – BS2) and (MT – BS1) time-lapse differences between MT and BS2, BS1 respectively; NRMS (B2, MT) and NRMS (BS1, MT) are NRMS maps. The window to compute NRMS is 0.06 s. The Red dashed line is a first break pick. The yellow arrow highlights the time-lapse signal due to CO2 injection. Red arrows point to the area of strong time-lapse noise created by non-repeatable S waves. Time-lapse difference gain is increased five times compared to monitor gather.

2.3.3 Smart baseline selection

To improve the signal-to-noise ratio and create a better baseline, for every given monitor, we combine several vintages with the best repeatability based on the repeatability matrix. We call the process 'smart baseline selection' and it is as follows:

1) For each monitor, select a pre-injection vintage with the best repeatability and add it to the baseline list
2) Form baseline as an average of all vintages from the list
3) Compute time-lapse difference with this baseline and estimate repeatability
    a. If repeatability has improved, select a pre-injection vintage with the next best repeatability and repeat steps 2 and 3.
    b. If repeatability has decreased, remove the last vintage from the baseline list and form a final baseline

The comparison of the initial baseline (Figure 10 (c, d)) and single vintage smart baseline (Figure 10 (e, f)) shows a significant reduction of coherent time-lapse noise (mostly remnants of P wave multiples) and an overall decrease in NRMS from 36.9% to 31.9% even though the random noise level has increased. A combination of several good vintages for the baseline improves repeatability even further to 24% NRMS (Figure 10 (i, j)) which is 30% lower compared to the initial baseline.

SOV6-CRC4 VSP section has been chosen to demonstrate baseline selection for several reasons. SOV6 has one of the highest repeatability variations (Figure 12). This is two main causes. First, SOV6 has a relatively large offset compared to other SOVs and as such, a lower signal-to-noise ratio. As a result, stacking several baselines improves repeatability. Furthermore, SOV6 has significant seasonal repeatability variations. Also, the SOV6-CRC4 2D VSP transect crosses the CO_2 plume body (Figure1)

demonstrating signal improvement after baseline selection.

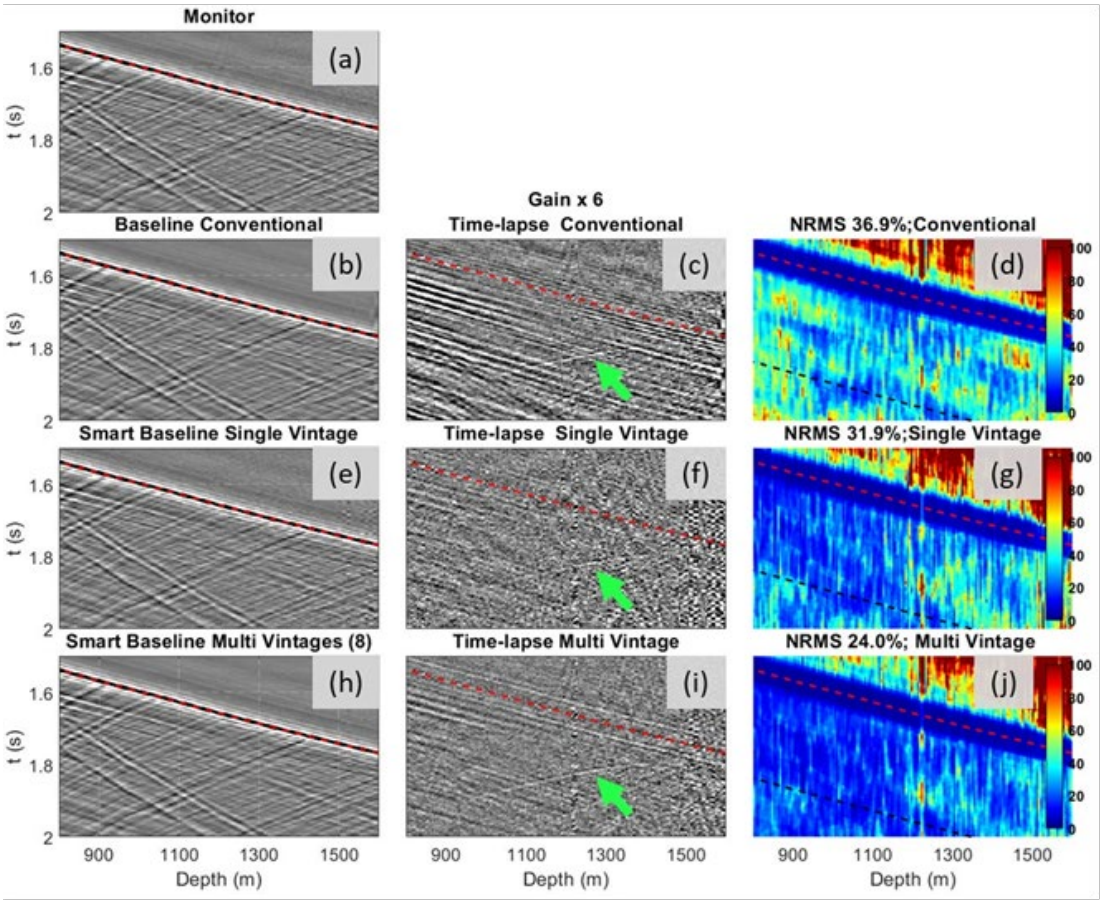

Figure 10. CRC4-SOV6 Comparison of time-lapse seismic gathers acquired with initial baseline, and single- and multi-vintage smart baseline selection. Time-lapse images were scaled by a factor of 6 compared to the baseline. The green arrow highlights the time-lapse signal due to the injection. For the current example, eight vintages were utilised for the multi-vintage baseline. The average NRMS value is computed in the interval from the red to the black dashed lines.

A similar outcome is observed in the processed images of the migrated 2D transects: the multi-vintage smart baseline selection improves repeatability by almost a third (Figure 11). The time-lapse signal due to the injection is located at about 1500 m depth, 200-400 m far from the well (a green arrow in Figure 11). All three types of time-lapse differencing can detect the CO_2 plume response. However, if the initial baseline is used, strongly correlated noise at about 700 m away from the well (Figure 11c, d) might be mistaken for a signal. This correlated noise is significantly reduced if a single vintage smart baseline is applied even if overall repeatability slightly decreased to 16.1% NRMS (Figure 11f, g). In Figure 11i, j, utilising eight vintages for a baseline improves repeatability to 11.6%

(by about a third) and reduces strong localised noise on the NRMS plot. For seismic migrated images, repeatability was measured in the interval from 800 to 1450 m.

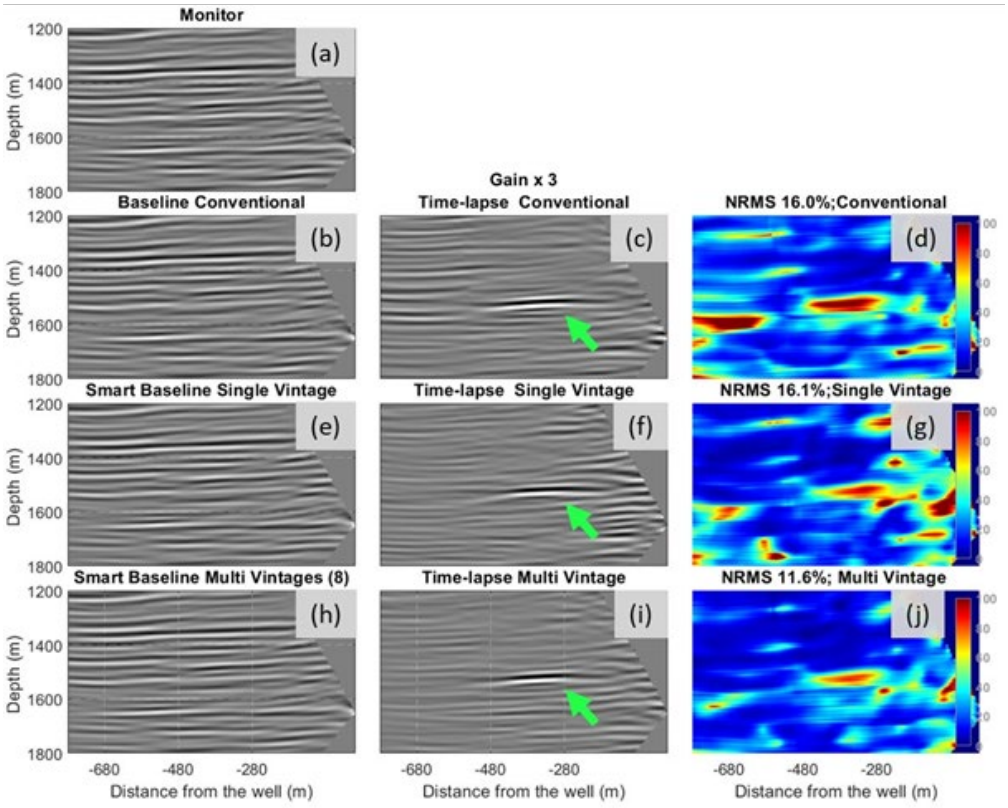

Figure 11. CRC4-SOV6 Comparison of time-lapse seismic images acquired with initial baseline, and single- and multi-vintage smart baseline selection. The green arrow highlights the time-lapse signal due to the injection. The average NRMS value is computed in the interval from 800 to 1450 m depth.

3 COMPARISON OF INITIAL AND SMART PROCESSING

To compare initial and smart processing (Table 2), we computed repeatability for all data. The repeatability measure is the same as for time-lapse images (Figure 11): an average NRMS in the interval from 800 to 1450 m for the images (above the reservoir level).

The comparison of initial and smart processing (Figure 12, Figure 13) shows that the repeatability from the injection start until 15th March 2021 (vintage 220) is very similar, probably, because the initial baseline is quite similar to the monitoring data, and hence, smart processing does not show significant improvement. However, from 15th March 2021 till at least the middle of July 2021 (vintage 280), the average NRMS improves by 3-5% NRMS (from 20-15% to 17-12%). Moreover, the

repeatability of SOV6 in that interval improves by about 10% NRMS from 30% to 20% and is below 20% for almost all SOVs.

As expected, a comparison of Figure 12a and Figure 12b suggests that the repeatability variations are linked to the SOVs – the difference in NRMS may reach up to 20% (see SOV6 and SOV2) – but not the wells. This, again, suggests that the variability is created by the near-surface conditions around SOVs but not at well locations (Figure 13).

The results suggest that having baselines acquired during different seasons can be beneficial for repeatability and more reliable time-lapse signal detection. It helps to reduce time-lapse noise created by non-repeatable surface-related multiples and S waves linked to near-surface seasonal variations. In our case, adaptive utilisation of the long baseline resulted in repeatability improvement by about 30% compared to the initial baseline. The smart processing can be improved even further by combining several neighbouring monitor vintages by the cost of the long-time resolution (e.g., moving window average along a vintage axis).

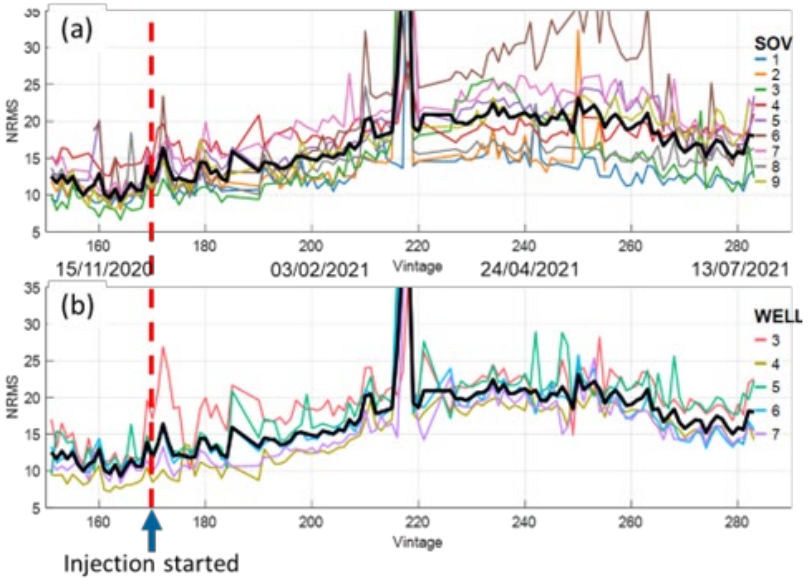

Figure 12. Average repeatability variation grouped by SOVs (a) and wells (b) for initial processing. The black solid line shows average repeatability. A vintage number is defined as a half number of days since 1 January 2020

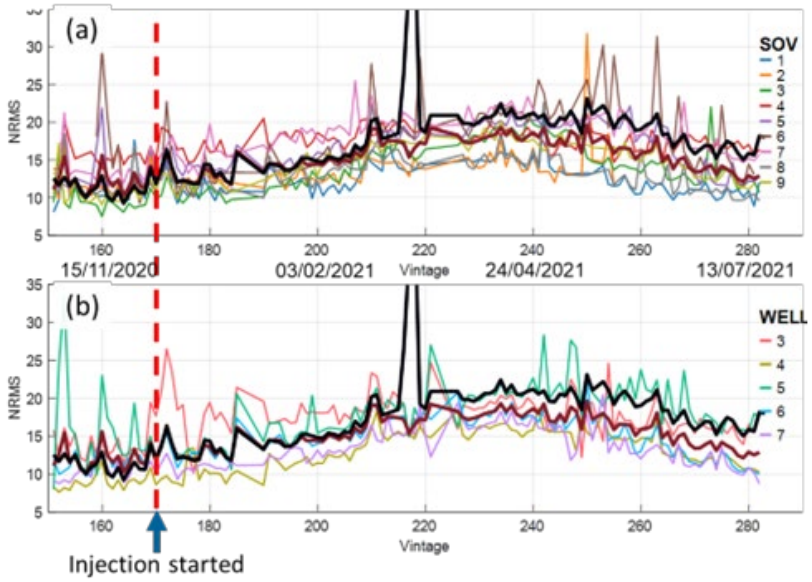

Figure 13. Average repeatability variation grouped by SOVs (a) and wells (b) for smart processing. The solid brown line shows smart processing average repeatability while the solid black line – initial processing average repeatability.

4 PLUME EVOLUTION FROM CONTINUOUS MONITORING

Having temporally dense measurements creates an opportunity to precisely trace the evolution of the CO_2 plume. While it is relatively straightforward to map strong anomalies around the injection well, the detection of the edges is difficult as the time-lapse signal becomes weaker. The detectability of small time-lapse signals can be improved by locating 'true' time-lapse events on several neighbour vintages, while 'false' events are not expected to be repeatable.

An example of small-scale signal detection confirmed by several monitoring vintages is shown in Figure 14. About a month after the end of injection, the difference section shows a small-time lapse reflector next to the CRC7 well (Figure 14e), which has increased over the next six months (Figure 14f). The fact that the time-lapse signal 'touches' the direct wave suggests that the CO_2 has reached the well.

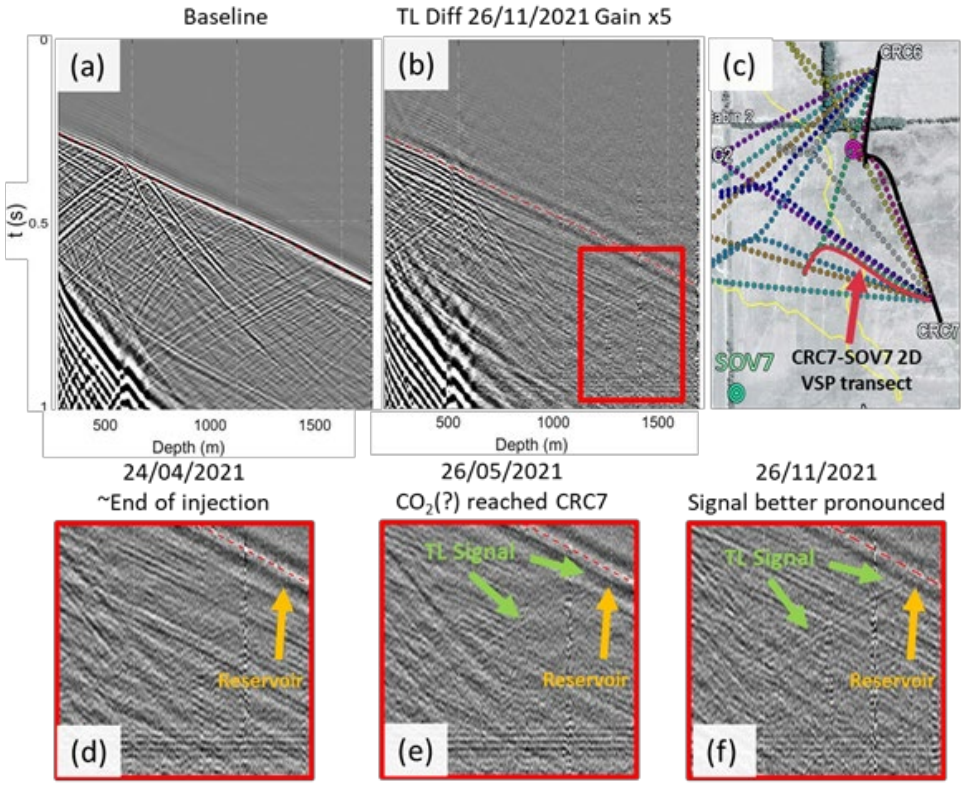

Figure 14 Detection of plume remobilisation for CRC7-SOV7. Baseline (a) and time-lapse difference (b) shot gather after wavefield decomposition. For the time-lapse difference, the gain was increased by a factor of 5 compared to the baseline. Location of CRC7-SOV7 VSP transect (refer to Figure 1). Zoomed time-lapse difference from the figure (b) before remobilisation detected (d), the first instance (e) and half a year after (f). Red-dashed line highlights direct wave arrivals.

An example of several time-lapse seismic transects is shown in Figure 15 for 24th August 2021. We observe a clear strong time-lapse anomaly around the injection interval at CRC3 with the time-lapse signal distinctly stretching in the eastern direction towards the CRC6 and CRC7 wells. We use these data to map the plume over the monitoring period.

To evaluate continuous monitoring plume mapping, we compare it with spatially dense 4D VSP. While well/SOV transects map the plume only along several 2D sections, 4D VSP data can delineate the CO_2 plume in map view. The same CRC3-CRC7 wells with DAS were utilised as a receiver array with a vibroseis source acquiring about 3000-4000 shot points per survey with source line spacing of ~100 m and shot interval of 15 m (Yurikov et al., 2021). 4D VSP monitoring baseline survey (M6) was acquired in March 2020 with the first monitoring survey (M7) acquired in January 2021 after injection of 5 kt and the second monitor survey (M8) in March-April 2021 after injection of 15 kt of

CO_2. The names of the baseline, first and second monitoring surveys of Stage 3: M6, M7 and M8 are inherited from the Otway project's previous stage (2C) (Pevzner et al., 2021).

Figure 16 shows how continuous monitoring captures the evolution of the CO_2 plume compared to plume contours acquired by 4D VSP M7 and M8 surveys. The normalised RMS amplitudes of the time-lapse signal detected on the well/SOV transects are displayed in Figure 16 after a week, two, three and six months after the injection. The corresponding amount of the injected gas is shown in each panel. Normalised RMS amplitudes of time-lapse difference highlight amplitude changes, where normalised RMS equals 0 if there is no time-lapse difference, and 1 for the maximum time-lapse signal during the period from December 2020 to April 2021. Continuous monitoring data shows that the plume's western, southern, and northern extents are quickly stabilised, and the gas started propagating towards the east where the previous Stage 2C plume is located. On 24th January 2021, just after the first monitor acquisition, the SOV data is juxtaposed with the spatial extents of the plume obtained from the 4D VSP. Similarly, the second Stage 3 monitoring survey M8 was acquired on 2nd April 2021 and displayed on the last panel in Figure 15d.

Both 4D VSP and continuous monitoring can image CO_2 plume(Pevzner et al., 2021). While the time-lapse signal is more smeared on the well/SOV 2D transects, it is more focused on the 4D images. However, the continuous DAS/SOV data has a higher signal-to-noise ratio, and hence we can distinguish smaller time-lapse signals. In particular, the time-lapse signal starts to appear at the eastern side of the Stage 2C plume close to CRC6 and CRC7 as early as the beginning of February 2021. At the end of February, as discussed earlier, the time-lapse anomaly in the area reaches the CRC7 well location. These observations suggest that at the beginning of February 2021, the Stage 3 plume reached the Stage 2C plume and caused those changes (see yellow contour in Figure 1). We hypnotize these changes to be associated with either change in thickness or saturation of the pre-existing plume. As the injection pressure is very low, the direct pressure effect is unlikely.

A key goal of the Stage 2C experiment was to demonstrate stabilisation of the plume over time expressed in the absence of noticeable changes in the plume configuration from fluid flow simulations calibrated by time-lapse seismic monitoring results. However, the timeframe of the experiment allowed seismic monitoring for just two years after the injection. Our analysis of the Stage 3 SOV data confirms the stabilisation of the Stage 2C plume through the absence of the detectable changes in the 6-9 months from the start of the monitoring in 2021 until the start of injection. It also revealsre-mobilisation of the legacy plume after the newly injected fluid reaches its boundary. The detection of plume re-mobilisation was achieved due to the high time-lapse repeatability of DAS/SOV data.

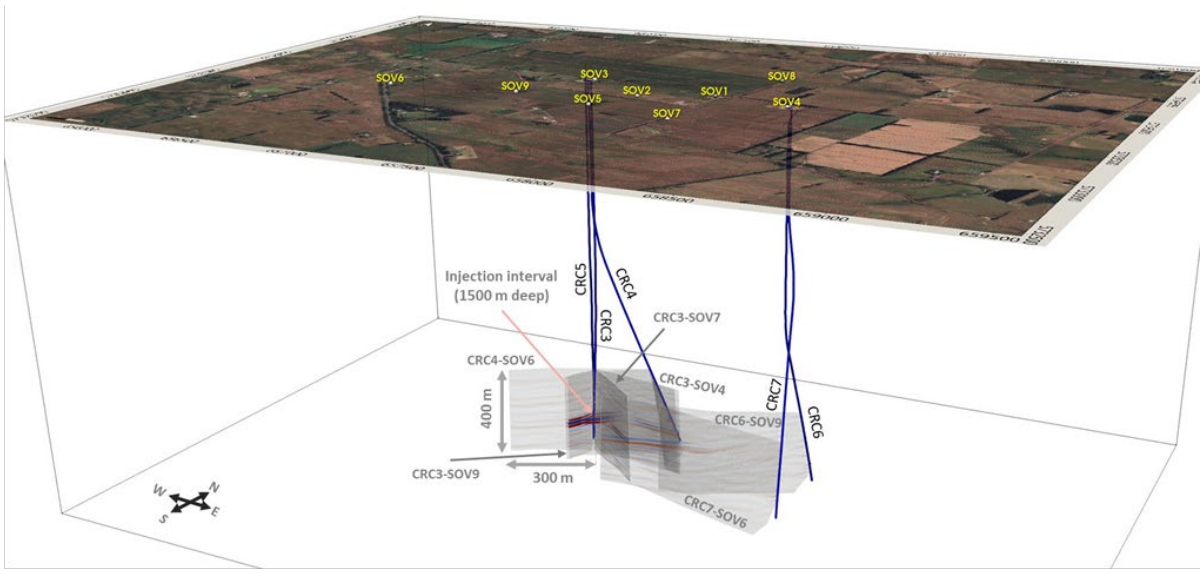

Figure 15 Several time-lapse seismic transects ten months after the injection started. Notice strong time-lapse signal near CRC3 injection interval and less strong anomaly stretching towards the east from CRC3 well.

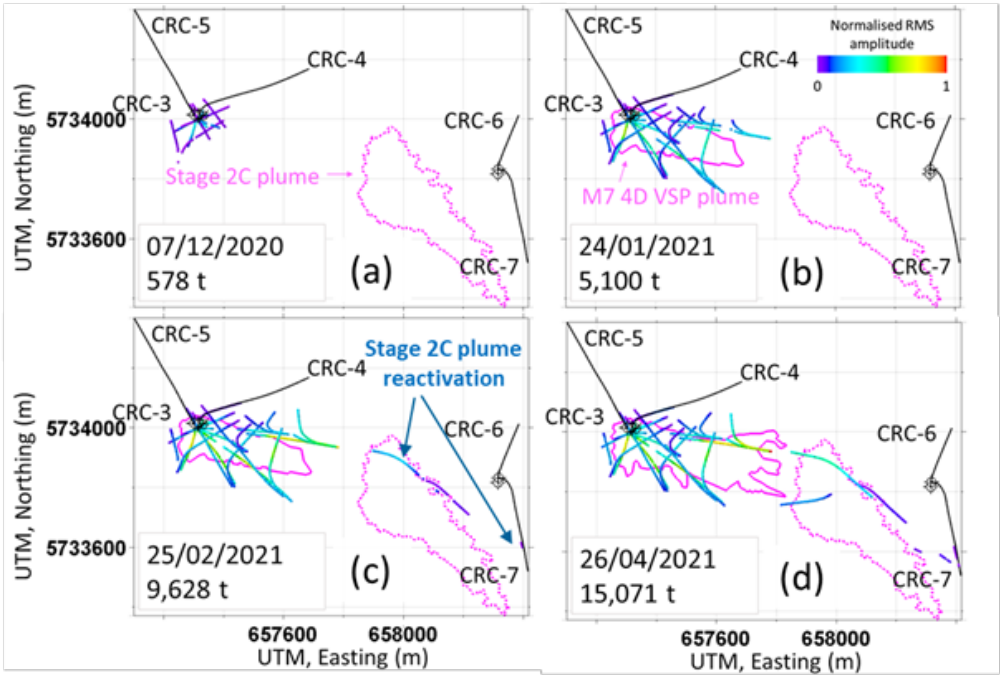

Figure 16: Evolution of the CO2 plume captured by the continuous offset VSP monitoring. The colour code shows the normalised RMS amplitude of the time-lapse signal at the well/SOV transects. The date and the amount of injected gas are displayed for each vintage. The dashed pink contour shows the spatial extents of the Stage 2C plume detected by the 4D surface seismic. The solid pink contours show the extent of the Stage 3 plume as detected by the multi-well 4D VSP. Note, that for each well/SOV transect, only the area with a time-lapse signal (as detected by an interpreter) is displayed.

5 DISCUSSION

Initial processing was set before the injection started. The main goal was to automate processing on-site, compress the data, send it to the office, and form daily QC reports. To illuminate the time-lapse signal and suppress random noise, the initial processing uses a fixed baseline formed by averaging the last ten vintages before the start of the injection. The resulting difference sections show the time-lapse response on the second day of injection (when as little as a few hundred tons of CO_2 had been injected)

However, over time, the time-lapse noise gradually increased, and for some April 2021 monitoring vintages and several DAS/SOV pairs exceeded the detectable level of the time-lapse signal. The main

sources of time-lapse noise are surface-related multiples and S waves. The primary P wave variability was corrected in the initial processing by designature. However, a pairwise comparison of all the vintages revealed the seasonal variation of repeatability and showed that a baseline vintage acquired in June 2020 matches the monitor vintage from April 2021 better than the nearest available baseline in November 2020. The time-lapse difference April 2021 – June 2020 significantly reduced the time-lapse noise present in April 2021 – November 2020 difference by decreasing non-repeatable S waves and surface multiples.

This observation led to the development of the smart baseline selection: a combination of several best-matching pre-injection vintages as the optimal baseline for a given monitor vintage to reduce time-lapse noise and boost repeatability. The smart baseline approach reduces the amplitude of coherent noise, which might be mistaken for a signal, and improves the repeatability by 30%. Such an approach is only possible due to several months of densely sampled pre-injection baseline data, which recorded different realisations of wavefield that cover slow seasonal variations of the near surface. Further studies are required to prove and quantify the link between the seasons, weather, near-surface variations, and repeatability.

Another considerable benefit of densely sampled monitor vintages is a new dimension for analysis - we can compare neighbour vintages. Unlike 'fast' seismic recording time, we call it 'slow time' on the order of days and weeks. For each monitor realisation, once a time-lapse signal appears the first time, it is expected to be present on all the subsequent vintages. On the second day of the injection, we observed a weak time-lapse signal that we could attribute to the injection only tentatively. However, the next few following days, as the injection progressed, the signal became stronger and thus was confidently identified as related to the CO_2 plume.

Each SOV/well pair forms an individual survey. Amplitude calibration between these surveys presents a challenge in the case of a combination of multiple deviated wells and SOVs. The main causes of this problem are directivity patterns, anelastic attenuation, source performance etc. These effects need to be compensated for before any quantitative amplitude analysis. If such normalisation is not possible, joined analysis of normalised attributes, such as NRMS, maybe a solution.

6 CONCLUSIONS

More than a year-long continuous seismic monitoring in Stage 3 of the Otway project generated a dataset of high temporal density. The data highlights the main source of non-repeatability - seasonal

changes in the near-surface, which affect both primary and secondary wavefields. To reduce seasonal effects and increase repeatability, we introduced several specific processing routines.

In particular, we use direct P wave measurements from VSP to correct for the variability of the primary P waves. The summation of SOV CW and CCW rotations considerably suppresses S wave energy by decomposing the wavefield into vertical polarisation. This technique requires measurements of the far-field P wave signature, which limits the application to VSP data. To correct seasonal repeatability variations, we designed an adaptive smart baseline selection approach. The extended baseline can properly represent the properties of time-lapse noise through the wet and dry periods. The optimal baseline for any monitor is composed of several of the most similar baseline vintages.

Despite low fold compared to 4D VSP data, DAS/SOV acquisition set up with adjusted processing flow demonstrates a high level of repeatability with CO_2 plume being detected on the second day of the injection. Furthermore, the data reveal a possible and re-mobilisation of the pre-existing Stage 2C plume. Potentially, such detectability can be employed for exploring the application of such a monitoring system to study CO_2 plume dissolution.

7 ACKNOWLEDGEMENTS

The Otway Project received CO2CRC Ltd funding through its industry members and research partners, the Australian Government under the CCS Flagships Programme, the Victorian State Government and the Global CCS Institute. The authors wish to acknowledge financial assistance provided through Australian National Low Emissions Coal Research and Development. ANLEC R&D is supported by Low Emission Technology Australia (LETA) and the Australian Government through the Department of Industry, Science, Energy and Resources. Funding for LBNL was provided through the Carbon Storage Program, U.S. DOE, Assistant Secretary for Fossil Energy, Office of Clean Coal and Carbon Management through the NETL, under contract No. DE-AC02-05CH11231. The authors thank Michael Mondanos and Stoyan Nikolov (Silixa inc.) for help with the fibre-optic equipment and Peter Dumesny (Upstream Production Solutions) for invaluable help with all aspects of field operations.

8 REFERENCES

Ajayi, T., Gomes, J.S., Bera, A., 2019. A review of CO 2 storage in geological formations emphasizing modeling, monitoring and capacity estimation approaches. Petroleum Science 16, 1028-1063, https://doi.org/10.1007/s12182-019-0340-8.

Al Jabri, Y., 2011. Land seismic repeatability prediction from near-surface investigations at Naylor Field, Otway, Faculty of Science and Engineering, Department of Exploration Geophysics. Curtin University, http://hdl.handle.net/20.500.11937/2372.

Bagheri, M., Pevzner, R., Jenkins, C., Raab, M., Barraclough, P., Watson, M., Dance, T., 2020. Technical de-risking of a demonstration CCUS project for final investment decision in Australia. The APPEA Journal 60, 282-295.

Bakulin, A., Smith, R., Jervis, M., Burnstad, R., 2014. Near surface changes and 4D seismic repeatability in desert environment: From days to years, SEG Technical Program Expanded Abstracts 2014, pp. 4843-4847.

Caldwell, J., Koudelka, E., Nesteroff, K., Price, R., Zhang, P., 2015. Seismic permanent reservoir monitoring (PRM)–A growing market. first break 33, https://doi.org/10.3997/1365-2397.33.11.83487

Correa, J.C., Freifeld, B.M., Robertson, M., Pevzner, R., Bona, A., Popik, D., 2017. Distributed Acoustic Sensing Applied to 4D Seismic: Preliminary Results From the CO2CRC Otway Site Field Trials. 2017, 1-5, https://doi.org/10.3997/2214-4609.201700811.

Correa, J., Tertyshnikov, K., Wood, T., Yavuz, S., Freifeld, B., Pevzner, R., 2018. Time-lapse VSP with permanent seismic sources and distributed acoustic sensors: CO2CRC Stage 3 equipment trials, 14th Greenhouse Gas Control Technologies Conference Melbourne, pp. 21-26, http://dx.doi.org/10.2139/ssrn.3365561

Correa, J., Wood, T., Freifeld, B., Mondanos, M., Nikolov, S., Barraclough, P., 2021. An automated system for continuous monitoring of CO2 geosequestration using multi-well offset VSP with permanent seismic sources and receivers: Stage 3 of the CO2CRC Otway Project. International Journal of Greenhouse Gas Control 108, 103317, https://doi.org/10.1016/j.ijggc.2021.103317.Daley, T.M., Cox, D., 2001. Orbital vibrator seismic source for simultaneous P-and S-wave crosswell acquisition. Geophysics 66, 1471-1480, https://doi.org/10.1190/1.1487092.

Dance, T., LaForce, T., Glubokovskikh, S., Ennis-King, J., Pevzner, R., 2019. Illuminating the geology: Post-injection reservoir characterisation of the CO2CRC Otway site. International Journal of Greenhouse Gas Control 86, 146-157.

Detomo Jr, R., Quadt, E., 2011. Life-cycle seismic for turbidite fields in deepwater Nigeria, SEG Technical Program Expanded Abstracts 2011. Society of Exploration Geophysicists, pp. 97-101.

Dou, S., Ajo-Franklin, J., Daley, T., Robertson, M., Wood, T., Freifeld, B., Pevzner, R., Correa, J., Tertyshnikov, K., Urosevic, M., 2016. Surface orbital vibrator (SOV) and fiber-optic DAS: Field demonstration of economical, continuous-land seismic time-lapse monitoring from the Australian CO2CRC Otway site, SEG Technical Program Expanded Abstracts 2016. Society of Exploration Geophysicists, pp. 5552-5556, https://doi.org/10.1190/segam2016-13974161.1.

Dou, S., Wood, T., Ajo-Franklin, J., Robertson, M., Daley, T., Freifeld, B., Pevzner, R., Gurevich, B., 2017. Surface orbital vibrator for permanent seismic monitoring: A signal contents and repeatability appraisal, 2017 SEG International Exposition and Annual Meeting. Society of Exploration Geophysicists, Houston, Texas, p. 5.

Galperin, E.I., 1985. Vertical seismic profiling and its exploration potential. Springer Netherlands.

Glubokovskikh, S., R Pevzner, J Gunning, T Dance, V Shulakova, D Popik, 2020, How well can time-lapse seismic characterize a small CO_2 leakage into a saline aquifer: CO2CRC Otway 2C experiment (Victoria, Australia), International Journal of Greenhouse Gas Control 92, 102854

Isaenkov, R., Pevzner, R., Glubokovskikh, S., Yavuz, S., Yurikov, A., Tertyshnikov, K., Gurevich, B.,

Jenkins, C., 2020. The State of the Art in Monitoring and Verification: an update five years on. International Journal of Greenhouse Gas Control 100, 103118, https://doi.org/10.1016/j.ijggc.2020.103118.

Johnston, D.H., 2013. Practical Applications of Time-lapse Seismic Data: 2013 Distinguished Instructor Short Course. Society of Exploration Geophysicists.

Kjølhamar, B., Planke, S., Bondeson, H., Langhammer, J., Bellwald, B., Waage, M., 2021. New approaches to CCS. First Break 39, 53-57, https://doi.org/10.3997/1365-2397.fb2021043.

Kragh, E., Christie, P., 2002. Seismic repeatability, normalized rms, and predictability. The Leading Edge 21, 640-647, http://dx.doi.org/10.1190/1.1497316.

LaForce, T., Dance, T., Ennis-King, J., Paterson, L., Cinar, Y., 2018. How good is good enough in CO2 storage modelling? Looking back over three generations of models for the Otway Stage 2C project, 14th Greenhouse Gas Control Technologies Conference Melbourne, pp. 21-26.

Lopez, J., Wills, P., La Follett, J., Hornman, J., Potters, J., van Lokven, M., Perkins, C., Trefanenko, C., 2015. Permanent seismic reservoir monitoring for real-time surveillance of thermal EOR at Peace River, Third EAGE Workshop on Permanent Reservoir Monitoring 2015. European

Association of Geoscientists & Engineers, pp. 1-5, https://doi.org/10.3997/2214-4609.201411961.

Mateeva, A., Kiyashchenko, D., Duan, Y., Chen, T., Wang, K., 2020. Considerations in planning, acquisition, processing and interpretation of 4D DAS VSP, SEG Technical Program Expanded Abstracts 2020. Society of Exploration Geophysicists, pp. 3729-3733.

Nakatsukasa, M., Ban, H., Takanashi, M., Kato, A., Worth, K., White, D., 2017. Repeatability of a rotary seismic source at the Aquistore CCS site, SEG Technical Program Expanded Abstracts 2017. Society of Exploration Geophysicists, pp. 5911-5916.

Pevzner, R., Isaenkov, R., Yavuz, S., Yurikov, A., Tertyshnikov, K., Shashkin, P., Gurevich, B., Correa, J., Glubokovskikh, S., Wood, T., 2021. Seismic monitoring of a small CO2 injection using a multi-well DAS array: Operations and initial results of Stage 3 of the CO2CRC Otway project. International Journal of Greenhouse Gas Control 110, 103437, https://doi.org/10.1016/j.ijggc.2021.103437.

Pevzner, R., Urosevic, M., Popik, D., Shulakova, V., Tertyshnikov, K., Caspari, E., Correa, J., Dance, T., Kepic, A., Glubokovskikh, S., Ziramov, S., Gurevich, B., Singh, R., Raab, M., Watson, M., Daley, T., Robertson, M., Freifeld, B., 2017. 4D surface seismic tracks small supercritical CO2 injection into the subsurface: CO2CRC Otway Project. International Journal of Greenhouse Gas Control 63, 150-157.

Pevzner, R., Tertyshnikov, K., Shulakova, V., Urosevic, M., Kepic, A., Gurevich, B., Singh, R., 2015. Design and deployment of a buried geophone array for CO2 geosequestration monitoring: CO2CRC Otway Project, Stage 2C, SEG Technical Program Expanded Abstracts 2015. Society of Exploration Geophysicists, pp. 266-270, doi:10.1190/segam2015-5902309.1.

Schisselé, E., Forgues, E., Echappé, J., Meunier, J., De Pellegars, O., Hubans, C., 2009. Seismic repeatability–Is there a Limit?, 71st EAGE Conference and Exhibition incorporating SPE EUROPEC 2009. European Association of Geoscientists & Engineers, pp. cp-127-00414, https://doi.org/10.3997/2214-4609.201400421.

Smith, R., Bakulin, A., Jervis, M., Hemyari, E., Alramadhan, A., Erickson, K., 2018. 4D Seismic Monitoring of a CO2-EOR Demonstration Project in a Desert Environment: Acquisition, Processing and Initial Results, SPE Kingdom of Saudi Arabia Annual Technical Symposium and Exhibition. OnePetro, https://doi.org/10.2118/192311-MS.

Tertyshnikov, K., Bergery, G., Freifeld, B., Pevzner, R., 2020. Seasonal Effects on DAS using Buried Helically Wound Cables, EAGE Workshop on Fiber Optic Sensing for Energy Applications in Asia Pacific. European Association of Geoscientists & Engineers, pp. 1-5, https://doi.org/10.3997/2214-4609.202070007.

Wang, X., Xue, B., Cui, R., Gu, G., Peng, C., Zheng, Y., Yang, J., 2020. A method of phase identification for seismic data acquired with the controlled accurate seismic source (CASS). Geophysical Journal International 222, 54-68.

Yavuz, S., Correa, J., Pevzner, R., Freifeld, B., Wood, T., Tertyshnikov, K., Popik, S., Robertson, M., 2019. Assessment of the permanent seismic sources for borehole seismic monitoring applications: CO2CRC Otway Project. ASEG Extended Abstracts 2019, 1-5, https://doi.org/10.1080/22020586.2019.12073157.

Yavuz, S., Isaenkov, R., Pevzner, R., Gurevich, B., Tertyshnikov, K., Yurikov, A., Correa, J., Wood, T., Freifeld, B., 2021. Processing of multi-well offset vertical seismic profile data acquired with distributed acoustic sensors and surface orbital vibrators: Stage 3 of the CO2CRC Otway Project case study. Geophysical Prospecting, https://doi.org/10.1111/1365-2478.13141.

Yurikov, A., Tertyshnikov, K., Isaenkov, R., Sidenko, E., Yavuz, S., Glubokovskikh, S., Barraclough, P., Shashkin, P., Pevzner, R., 2021. Multiwell 3D distributed acoustic sensing vertical seismic profile imaging with engineered fibers: CO2CRC Otway Project case study. Geophysics 86, D241-D248, https://doi.org/10.1190/geo2020-0670.1.

EAGE

EAGE Workshop on Fiber Optic Sensing for Energy Applications in Asia Pacific: Session 2 - Advances in Fibre Optic Sensing - II

Effect of Rocks Stiffness on Observed DAS VSP Amplitudes

R. Isaenkov[1]*, S. Glubokovskikh[1], K. Tertyshnikov[1], R. Pevzner[1], A. Bona[1]

[1] Curtin University*

Summary

This paper examines a factor affecting amplitudes in downhole seismograms - dependence on rock stiffness and density at the receiver location. Unlike surface seismic scenario, in VSP there is usually a systematic change of receiver conditions as rocks naturally become stiffer with depth due to compaction. Thus, we expect a trend in the intensity of the seismic signals on both, geophones and DAS, more pronounced on the latter. Thus, amplitudes should be corrected for that effect prior to any quantitative amplitude analysis or migration of VSP data. We outline an analytical model relating the DAS measurements to rock stiffness and validate it using full-waveform elastic simulations. We illustrate the theory using zero-offset VSP data acquired at the CO2CRC Otway Project site (Victoria, Australia).

Introduction

Borehole seismic is one of the key techniques which can be used for subsurface characterization and monitoring. Distributed acoustic sensing (DAS) is one of the technologies that facilitated rapid development of the borehole seismic in recent years as it provides a relatively cheap means for permanent deployment along the borehole. Compared to conventional geophones, a well-known disadvantage of DAS is limited offset between the borehole and source points due to strong directivity pattern of the sensor (Correa et al., 2017). Such selective sensitivity has to do with the fact that DAS measures only axial strain of the fiber (or strain rate) while downhole tools with 3-component geophones are believed to provide the full vector of displacement velocity.

This paper examines another factor affecting amplitudes in downhole seismograms - dependence on rock stiffness and density at the receiver location. Unlike surface seismic scenario, in VSP there is usually a systematic change of receiver conditions as rocks naturally become stiffer with depth due to compaction. Thus, we expect a trend in the intensity of the seismic signals on both, geophones and DAS, more pronounced on the latter. Thus, amplitudes should be corrected for that effect prior to any quantitative amplitude analysis or migration of VSP data. We outline an analytical model relating the DAS measurements to rock stiffness and validate it using full-waveform elastic simulations. We illustrate the theory using zero-offset VSP data acquired at the CO2CRC Otway Project site (Victoria, Australia) (Correa et al., 2017).

Theory

The amplitude of the signal recorded by conventional geophones (we consider vertical orientation only) is believed be proportional to the vertical component of particle velocity v_z. DAS measures dynamic strain or strain rate (Parker et al., 2014). According to (Bakku, 2015) geophone and strain rate, measurements might be linked as followed:

$$\dot{\varepsilon}_{zz} = \frac{\partial v_z}{\partial z} = ik_z v_z = \frac{i\omega \cos(\theta)}{V_p} v_z \quad (1)$$

Where z – receiver depth, v_z – particle velocity, $\dot{\varepsilon}_{zz}$ – strain rate, k_z – the vertical component of wavenumber, ω – angular frequency, θ – the angle of incidence $const$ - constant multiplier, and V_p – P-wave velocity. Thus, for a constant angle, we expect $\frac{v_z}{\dot{\varepsilon}_{zz}} \sim const \cdot V_p$, to some extent, it should be true for zero-offset VSP.

A more sophisticated transform from geophones to DAS was proposed by (Bona et al., 2017). It considers the DAS gauge length *G* and laser pulse length *L*. The spatial spectrum of the filter is given by the formula below:

$$F(k_z) = \frac{4 \sin\left(\frac{k_z L}{2}\right) sin\left(\frac{k_z G}{2}\right)}{ik_z} = -ik_z LG \; sinc\left(\frac{k_z L}{2}\right) sinc\left(\frac{k_z G}{2}\right), \quad (2)$$

The formula by itself is two spatial averaging filters (specific of DAS measurement) and spatial derivative (ik_z term).

Recorded amplitudes of plane P-wave travelling along borehole is also proportional to $A_{DAS} \sim \left(\rho V_p^3\right)^{-1/2}$ for DAS (strain rate) and $A_{GEO} \sim \left(\rho V_p\right)^{-1/2}$ for geophones (vertical particle velocity) due to conservation of energy-flux density for low contrast media, where ρ – rock density at the receiver location. Hence, rock compaction with depth causes a gradual decrease of amplitudes on both DAS and

geophones, where the ratio of the amplitudes obeys $A_{GEO}/A_{DAS}{\sim}V_p$. For oblique incidence at the angle θ, the ratio equals to the apparent velocity $V_p/sin\Theta$.

Direct wave analysis using field VSP data

To compare DAS and geophone amplitudes we used field near-offset VSP data acquired during Stage 3 of Otway project (Australia, Victoria) where a ~1700 m deep nearly vertical well CRC-3 is instrumented with DAS cables cemented behind the casing. A VSP survey using both DAS and geophones was conducted in 2017. Zero-offset data was acquired using conventional 26,000 lbs vibroseis truck positioned 50 m away from the well. Geophone data acquired at 15 m receiver interval while DAS data had 1 m channel spacing. Two different DAS interrogators (Silixa iDAS v2 and iDAS v3) we used for the survey.

Figure 1a shows the RMS amplitude (10 ms window) of the direct wave for DAS and vertical geophones. Amplitudes were normalized to be equal 0 dB at minimum depth. Geophone amplitudes were interpolated to the DAS receiver spacing. DAS data shows almost extra 7 dB amplitude decrease compared to geophones at 1600 m depth. If we assume that attenuation losses for DAS and geophones are the same, this amplitude decrease should be related to rock stiffness effect. To verify this hypothesis, we calculated geophone to DAS amplitude ratio and scaled it to match with the velocity at depth of 1200 m to compensate for constant multiplier (Figure 1b). It shows good correlation with interval velocity except for the shallow part of the borehole. This part lacks sonic log and thus the velocity is estimated from first arrivals, and hence might be inaccurate.

Effect of rock stiffness on reflected waves

Next step is to show the effect of rock stiffness on DAS and geophone sensitivity for reflected wave. For that purpose, we compute synthetic VSP data for ~1 km offset shot point.

To simulate synthetic data we used CRC-3 velocity profile obtained from DAS (top ~ 1 km section) and sonic log data to build a horizontally layered model for 1.5D elastic modelling in OASES software (Schmidt and Tango, 1986). Modelling parameters were chosen to simulate the field experiment. Receivers are placed into the vertical well from 200m up to 1700 m depth with 1 m depth interval. Time sampling is 1 ms. We use 50 Hz Ricker wavelet for the modelling.

The main problem to get reflected wave amplitudes is interference between the upgoing and downgoing waves. We applied the FK filter to remove downgoing PP and PS waves and upgoing PS waves. Also, we applied a correction for geometrical spreading.

We transformed synthetic particle velocity data to DAS response using filter described in formula (2). To simulate field experiment, we have chosen gauge length 10 m and pulse length 5 m. Conversion spectra from particle velocity to DAS and strain rate (Figure 1c) are similar only in wavenumber interval from 0 to ~0.03 m^{-1} while field DAS data k-spectrum exceeds this range. It means, that DAS proportional to strain rate only for low wavenumbers (for the chosen pulse and gauge length) and differ otherwise. Thus, DAS response differs from strain rate.

We focus on the target reflection at a depth of 1545 m (marked with the red line in Figure 2). RMS amplitudes are computed in centered 20 ms window along the picked travel time curve and normalized by the value at depth of 1525 m. The final curves for DAS and geophones are shown as the top of Figure 2. The effect of rock stiffness causes almost doubles the amplitude difference between the top and bottom of the borehole. If ignored, this effect would drastically overestimate the AVO effect for reflection angles ranging from 20° to 35°, which is expected to be only ~15%. Different geophone and DAS directivity pattern may account only for 5-15% amplitude difference and, thus, also cannot explain 2x times amplitude difference.

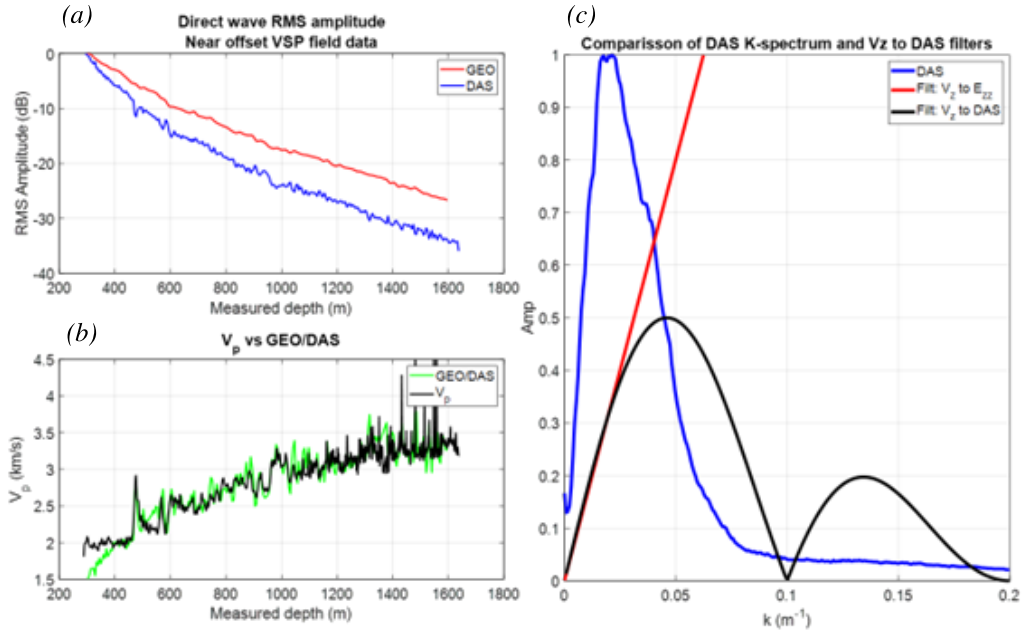

Figure 1 *(a) Direct wave scaled RMS amplitudes for near-offset VSP field data for DAS and vertical geophone (GEO) receivers. (b) Comparison of scaled GEO/DAS ratio with the Vp velocity profile for the field data. Synthetic RMS amplitudes are smoothed with 11m -long moving average filter. GEO/DAS ratio is scaled to match the velocity at depth = 1200m. (c) k-spectrum of zero-offset VSP iDASv2 data and absolute conversion filters spectra: particle velocity to strain rate (red line) and particle velocity to DAS (black line). Spectra normalized for display purpose.*

Conclusions

Receiver conditions systematically change with depth due to variation (often, systematic) of the rock stiffness and density causing a change in any seismic receiver sensitivity. As such, this variation must be taken into account in imaging or amplitude analysis. Typically, DAS data covers entire borehole and ignoring this could lead to misleading results. Moreover, rock stiffness effect on DAS sensitivity even higher than geophones. Field experiment data example suggest almost 7 dB (2.2x times) maximum difference of DAS and geophone amplitudes over 1300 m interval. This effect should be considered while processing and interpreting DAS amplitudes to avoid significant errors.

Analysis of conversion filter from particle velocity to DAS shows that DAS is not exactly a strain rate. It behaves as a strain rate for low wavenumbers and low gauge and pulse lengths and differs otherwise. There are several views in the literature explaining what DAS measures however the question is still not very clear (e.g. due to internal interrogator processing). To design a proper filter for rock stiffness effect compensation we must understand what is output units of DAS, thus, further studies on what DAS recorded units are required.

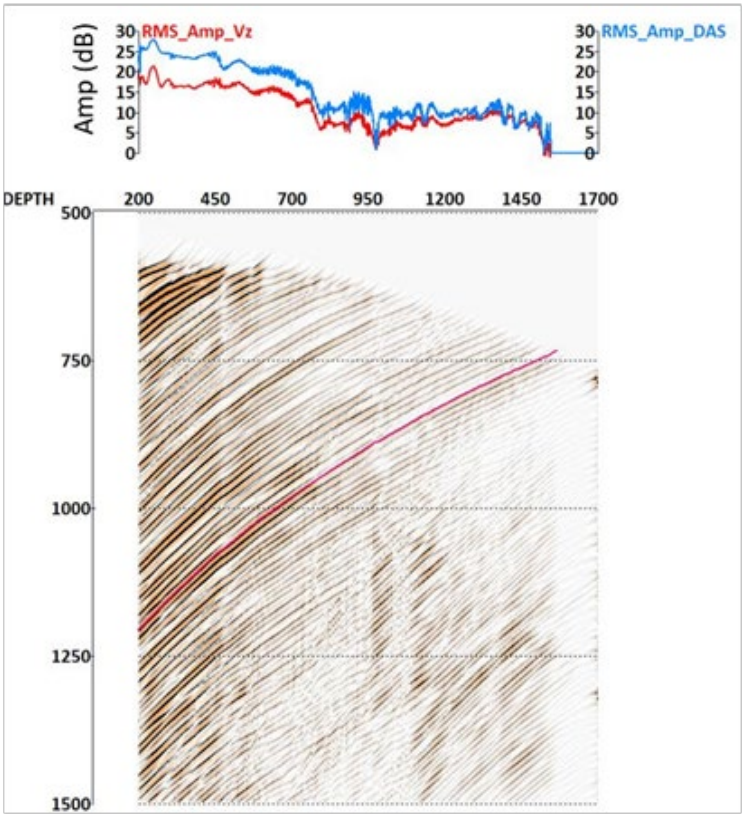

Figure 2 *Processed far-offset synthetic DAS VSP shot gather. Graphs on the top show scaled RMS reflection amplitude for vertical geophone (red) and DAS (blue). Red line on the shot gather shows the reflection travel times.*

Acknowledgements

This Project received CO2CRC funding through its industry members and research partners, the Australian Government under the CCS Flagships Program, the Victorian State Government and the Global CCS Institute. The authors wish to acknowledge the financial assistance provided through the Australian National Low Emissions Coal Research and Development (ANLEC R&D). ANLEC R&D is supported by COAL21 Ltd and the Australian Government through the Clean Energy Initiative. We are also grateful to support from sponsors of Curtin Reservoir Geophysical Consortium.

References

Bakku, S. K., 2015, Fracture Characterization from Seismic Measurements in a Borehole, Massachusetts Institute of Technology.

Bona, A., T. Dean, J. Correa, R. Pevzner, K. V. Tertyshnikov, and L. Van Zaanen, 2017, Amplitude and Phase Response of DAS Receivers: 79th EAGE Conference and Exhibition 2017, 2017, 1 - 5

Correa, J., A. Egorov, K. Tertyshnikov, A. Bona, R. Pevzner, T. Dean, B. Freifeld, and S. Marshall, 2017, Analysis of signal to noise and directivity characteristics of DAS VSP at near and far offsets — A CO2CRC Otway Project data example: The Leading Edge, **36**, no. 12, 994a991-994a997. http://dx.doi.org/10.1190/tle36120994a1.1.

Parker, T., S. Shatalin, and M. Farhadiroushan, 2014, Distributed Acoustic Sensing – a new tool for seismic applications: First Break, **32**, no. 2, 61 - 69 http://dx.doi.org/10.3997/1365-2397.2013034.

Schmidt, H., and G. Tango, 1986, Efficient global matrix approach to the computation of synthetic seismograms: Geophysical Journal of the Royal Astronomical Society, **84**, 331-359. http://dx.doi.org/10.1111/j.1365-246X.1986.tb04359.x.

sensors

Article

Effect of Source Mispositioning on the Repeatability of 4D Vertical Seismic Profiling Acquired with Distributed Acoustic Sensors

Roman Isaenkov, Konstantin Tertyshnikov, Alexey Yurikov, Pavel Shashkin and Roman Pevzner *

Centre for Exploration Geophysics, Curtin University, GPO Box U1987, Perth, WA 6845, Australia
* Correspondence: r.pevzner@curtin.edu.au

Abstract: Vertical seismic profiling (VSP) with distributed acoustic sensing (DAS) is an increasingly popular evolving technique for reservoir monitoring. DAS technology enables permanent fibre installations in wells and simultaneous seismic data recording along an entire borehole. Deploying the receivers closer to the reservoir allows for better detectability of smaller signals. A high level of repeatability is essential for the robust time-lapse monitoring of geological reservoirs. One of the prominent factors of repeatability degradation is a shift between source/receiver locations (mispositioning) during baseline and monitor surveys. While the mispositioning effect has been extensively studied for surface 4D seismic, the number of such studies for VSP is quite limited. To study the effects of source mispositioning on time-lapse data repeatability, we performed two VSP experiments at two on-shore sites with vibroseis. The first study was carried out at the Otway International Test Centre during Stage 3 of the Otway project and showed that the effect of source mispositioning on repeatability is negligible in comparison with the effect of temporal variations of the near-surface conditions. To avoid these limitations, we conducted a same-day controlled experiment at the Curtin University site. This second experiment showed that the effect of source mispositioning on repeatability is controlled by the degree of lateral variations of the near-surface conditions. Unlike in marine seismic measurements, lateral variations of near-surface properties can be strong and rapid and can degrade the repeatability for shifts of the source of a few meters. The greater the mispositioning, the higher the chance of such significant variations. When the near-surface conditions are laterally homogeneous, the effect of typical source mispositioning is small, and in all practical monitoring applications its contribution to non-repeatability is negligible.

Keywords: DAS; time-lapse seismic; VSP; repeatability; mispositioning

Citation: Isaenkov, R.; Tertyshnikov, K.; Yurikov, A.; Shashkin, P.; Pevzner, R. Effect of Source Mispositioning on the Repeatability of 4D Vertical Seismic Profiling Acquired with Distributed Acoustic Sensors. *Sensors* **2022**, 22, 9742. https://doi.org/10.3390/s22249742

Academic Editor: Iren E. Kuznetsova

Received: 21 November 2022
Accepted: 9 December 2022
Published: 12 December 2022

1. Introduction

Time-lapse seismic measurement is an important tool for monitoring underground processes such as oil/gas reservoir production or CO_2 geosequestration. This importance stems from the fact that the time-lapse seismic method has superior spatial resolution over other remote sensing methods [1,2]. Distributed acoustic sensing (DAS) technology has disruptive potential in seismic monitoring enabling the use of a fibre optic cable as an array of multiple seismic receivers [3]. A borehole equipped with fibre optic cable represents a dense and sensitive seismic receiver array. The introduction of optical sensors for borehole seismic measurement makes this technology the most effective for underground monitoring of the near-well medium.

Time-lapse DAS VSP has been applied for various geological tasks in industrial and research carbon dioxide geosequestration projects [4–7], water sweep monitoring in oil reservoirs, and in experiments on the shallow release of CO_2 [8]. Nevertheless, some projects have encountered several challenges, mainly related to non-optimal acquisition parameters, a weak time-lapse signal from the reservoir, and/or a high level of time-lapse noise. The level of time-lapse noise is an essential consideration for successful monitoring projects, and is affected by different factors. Some factors are determined by

nature (e.g., near-surface conditions), whereas others are influenced by acquisition design (e.g., equipment's noise level, accurate positioning of sensors and sources etc.). Some of the factors are listed below [1]:

1. Acquisition geometry differences
    a. Source, receiver mispositioning
    b. Source/receiver orientation
2. Near-surface conditions
    a. Near-surface variations
    b. Source/receiver coupling
3. Environment
    a. Soil moisture
    b. Groundwater level
    c. Vegetation
4. Noise
    a. Ambient noise
    b. Shot-generated noise
5. Geology
    a. Shallow gas
    b. Steep dips
    c. Fault shadows

In this paper, we focus on the effect of mispositioning—the spatial shift between sources/receivers' locations between the baseline and monitor surveys. Mispositioning is otherwise known as positioning difference [9]. In the case of VSP with permanently installed sensors (e.g., cemented behind the casing, deployed on tubing), the shift between receiver locations is not a concern as they are fixed in space. Still, the accurate placement of active sources in each vintage should be ensured.

Many researchers have studied the effect of acquisition parameters on repeatability for surface land [10–12] and offshore seismic measurements [13–15]. However, the number of such publications on time-lapse VSP data is limited. Landro [16] published the most detailed study of the mispositioning effect on marine VSP time-lapse data quality, where data were acquired with a string of geophones located at 2000 m depth with a relatively low frequency (up to 50 Hz) airgun seismic source. The study showed that a mispositioning of up to 5 to 10 m has a minor consequence on repeatability. However, these results cannot be directly extrapolated to the VSP data acquired on land, primarily due to strong spatial variation in near-surface conditions.

In our study, we used two research sites to assess the effect of mispositioning on repeatability. The first one was the Otway International Test Centre (Victoria, Australia). During Stage 3 of the Otway project, three 4D DAS VSP surveys were acquired. The surveys were separated by a few months, and several shot points had to be shifted to 0.5–3 m due to changes in land access. We assessed how these shifts affected seismic repeatability and observed the strong effect of seasonal variations on repeatability, which masks the misposition effect. Thus, we designed the second experiment to avoid the effect of seasonal variation. At the second site, the Curtin/NGL research facility, we designed a same-day dedicated survey to avoid weather/seasonal impact and simulated misposition of a vibroseis source in the range of ~0.5–20 m. While the effect of mispositioning on repeatability was detectable, spatial variations of near-surface conditions dominated in the resulting repeatability change.

2. Case Study 1: 4D DAS VSP for CO_2 Geosequestration Monitoring at the Otway International Test Centre

VSP experiments at the Otway International Test Centre have been an integral part of the CO2CRC Otway geosequestration project from its very start. Zero-offset VSP, offset VSP,

and 4D VSP surveys were carried out in 2007–2010 during Stage 1 of the Otway Project [17] in the CRC1 and Naylor-1 wells to monitor gas injected into Waare C formation at ~2 km depth with a standard geophone tool. The first effort to detect the injected substance was ineffective, as the supercritical mixture of CO_2-CH_4 was injected into the depleted reservoir with some residual saturation, resulting in a very small time-lapse signal. Further borehole seismic experiments conducted during Stage 2C (2015–2018) successfully detected as little as 5 kt of CO_2 using 4D VSP with geophones [18]. Stage 2C experiments also included a comparison of the sensitivity of DAS versus geophones [19,20] and experiments with permanent seismic sources [21]. These results were used to design the Stage 3 monitoring program, which comprises DAS VSP technology in combination with permanent surface sources [22,23] and conventional moving sources [6,24].

2.1. Experiment Design

The data for this study were acquired during baseline and monitor surveys for CO_2 geosequestration monitoring during the Stage 3 Otway Project [25]. The first baseline 4D VSP survey (M6) was acquired in March 2020, and the first monitor survey (M7) occurred in January 2021. In each survey, shot points were acquired using a vibroseis source (INOVA UniVib 26,000 lbs) and five ~1600 m deep wells (CRC3-CRC7) instrumented with an engineered single-mode optical fibre cemented behind the casing (Figures 1a and 2). Data were recorded using a Silixa iDAS v3 Carina unit with a 10 m gauge and 5 m pulse length. The vibroseis sweep parameters were a linear sweep, a frequency range 6-150 Hz, a sweep length of 24 s, cosine tapers of 0.5 s, and a listening time of 6 s. Data were recorded with a 1 ms temporal sampling rate and 1 m channel spacing along the well. The survey parameters are summarised in Table 1.

Figure 1. Photos of vibroseis truck at Otway (**a**), and close to NGL facility (**b**). Notice different soil conditions at the two sites. Sandy-clay soil at Otway is hard when dry and soft when wet, while sandy soil at NGL is less susceptible to moisture.

Due to the local farm activities during the first monitor M7, twelve shot points were shifted by ~1–2.5 m along the shot Line 13 (Figure 2). The mispositioning between most of the shots was below 0.25 m on Line 13 (Figure 2b). Shifts exceeding 0.5 m were included in this study to assess the deterioration of borehole seismic survey repeatability.

The actual shot location can differ from GPS measurement for up to 30 cm. That is because the vibroseis plate generally lands within 20–30 cm of the marked shot point location, and the differential GPS accuracy is within tens of cm. These errors increase uncertainty in measured mispositioning for up to 30 cm.

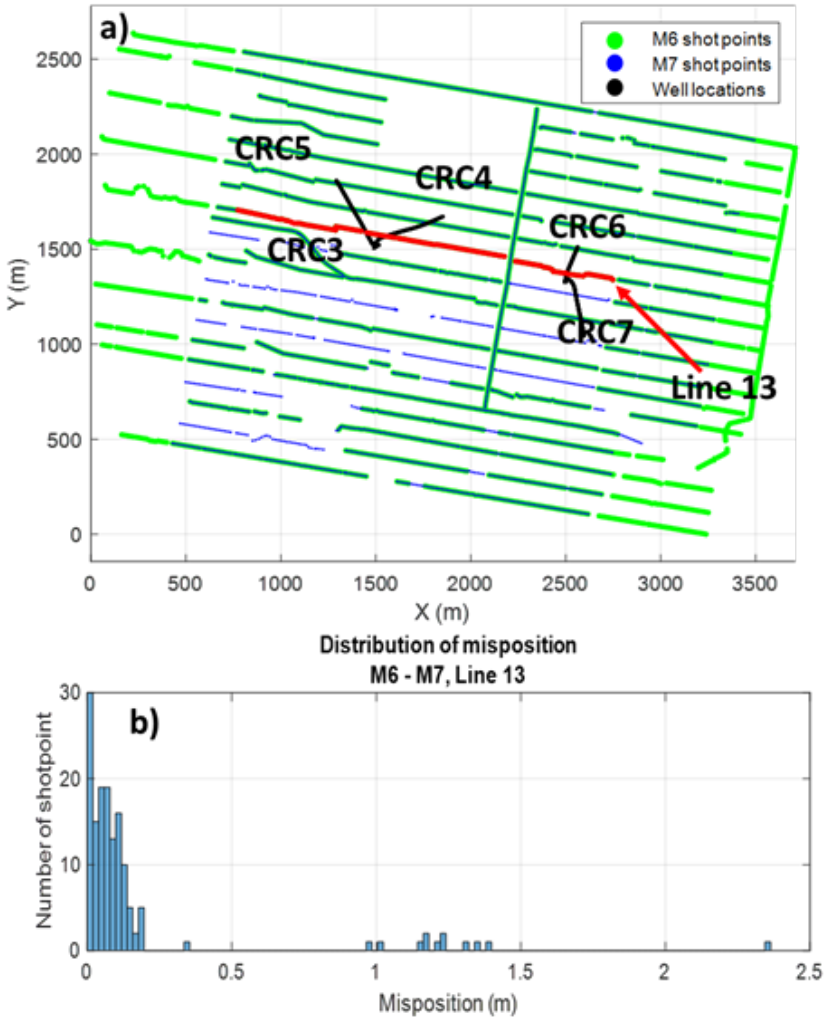

Figure 2. M6 and M7 acquisition map (**a**), and distribution of misposition of Line 13 (**b**). Green and blue dots indicate M6 and M7 survey shot points, respectively, and black lines are the horizontal location of CRC3–CRC7 monitoring wells. Red dots represent shifted Line 13.

Table 1. Survey parameters.

Parameter	Otway M6	Otway M7	NGL
Survey date	March 2020	January 2021	May 2021
Source	Vibroseis INOVA UniVib 26,000 lbs	Vibroseis INOVA UniVib 26,000 lbs	Vibroseis INOVA UniVib 26,000 lbs
Sweep	Linear 6–150 Hz	Linear 6–150 Hz	Linear 6–150 Hz
Number of Source Positions	4084	3085	76
Shot spacing (m)	15	15	0.5–5
Fiber optic cable installation	Cemented behind the casing	Cemented behind the casing	Cemented behind the casing
Type of fibre	Constellation	Constellation	Single mode
DAS interrogator	Silixa iDAS v3	Silixa iDAS v3	Silixa iDAS v2
Spacing between virtual receivers (m)	5	5	1
Well depth (m)	1600	1600	900

2.2. Effect of Mispositioning on Repeatability

To numerically evaluate the effect of mispositioning, we used normalised root mean square measure (NRMS), which for a pair of baseline and monitor traces is estimated as follows:

$$\mathrm{NRMS} = 200\% \cdot \frac{\mathrm{RMS}(\mathrm{BS} - \mathrm{MT})}{\mathrm{RMS}(\mathrm{BS}) + \mathrm{RMS}(\mathrm{MT})} \quad (1)$$

where BS and MT are baseline and monitor traces, and RMS is a root mean square operator [26].

For the repeatability analysis, we used data recorded in the CRC4 well. The recorded data had a good signal-to-noise ratio as the well is the closest to Line 13. Thus, random noise would not mask the mispositioning effect.

To study repeatability, we applied minimal processing prior to the data. Recorded data were decimated to a 2 ms sample rate and 5 m spatial channel sampling. The data were correlated with a single theoretical pilot vibroseis sweep. The temporal decimation should not degrade the data quality as the recorded frequencies were below 250 Hz, and the utilised engineered DAS fibre was designed for 5 m spacing. An example of initial data repeatability assessment is illustrated in Figure 3.

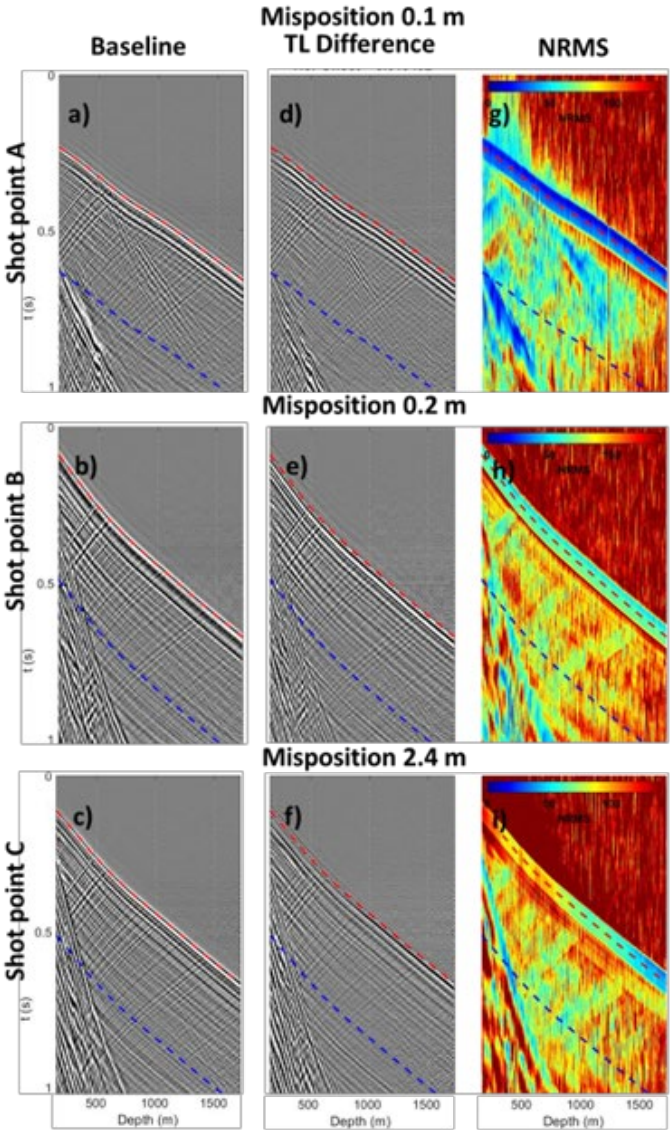

Figure 3. Comparison of shot points with relatively low and high misposition. Baseline shot points (**a–c**), time-lapse differences (**d–f**), and NRMS maps (**g–i**) are shown for shot points A, B and C with 0.1, 0.2 and 2.4 mispositioning, respectively. Time-lapse differences images have ×5 image gain for visual purpose.

Three baseline shot points (Figure 3a–c), their time-lapse differences (Figure 3d–f) and NRMS maps (Figure 3g–i) had mispositioning of 0.1, 0.2 and 2.4 m, denoted as A, B and C, respectively. NRMS plots were computed using a 60 ms running average window. In this example, shot point A (SP A) had the best repeatability with a misposition of 0.1 m, and NRMS level was primarily within 30–75% in a 400 ms window starting from direct wave (the region between red and blue dashed lines). SP B, with a low misposition of 0.2 m, and SP C, with a high 2.4 m mispositioning, had similar and relatively low repeatability within the 75–100% NRMS range. One can see that a pair of shots with significant misposition (>1 m) may have the same repeatability level as a pair with almost identical acquisition geometry (<0.3 m). In this case, the decrease in repeatability for SP B compared to SP A was likely to be caused by seasonal variation in near-surface conditions between baseline and monitor surveys.

To assess whether misposition has a major or minor effect on repeatability, we estimated average repeatability for every shot point on Line 13. Average repeatability was estimated within two windows: window A was a small 60 ms window around the direct P wave (±30 ms around the red dashed line Figure 3), and the larger 400 ms window B, which included primary, reflected, and multiple P wave reflections (400 ms down from the direct P wave, or the window between red and blue dashed lines Figure 3).

The average repeatability for both window A and window B strongly depended on the offset between a shot point and the well because the signal-to-noise ratio decreases with the distance. As the CRC4 well was deviated by 20° and had the lateral offset from the wellhead in the North-East direction of about 400 m, the shot points west from the well location (Figure 4, from −400 to 0 m) had a lower signal-to-noise ratio due to the distance and DAS directional sensitivity, resulting in poorer repeatability. This is because a straight DAS cable is not sensitive to P waves approaching the fibre at near-normal incidence [19] within the deviated part of the well. Conversely, shot points located above and east of the well had a higher signal-to-noise ratio and better repeatability. As such, for analysis, we chose offsets within the range of 0–400 m to minimise the effect of random noise on repeatability.

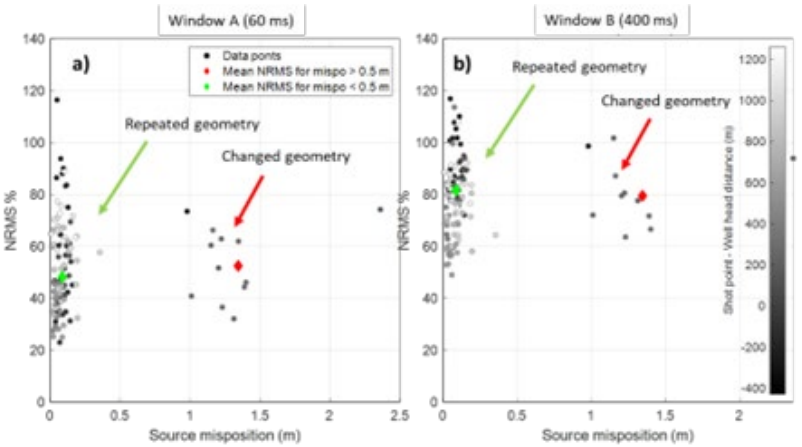

Figure 4. Distribution of repeatability for line 13 computed for a direct wave 60 ms window (**a**) and a P wavefield 400 ms window (**b**). Points are colour-coded by distance from the wellhead. A negative offset means the shot point is located east of the wellhead. Black and red diamonds are average misposition for 'normal' and mispositioned shot point groups.

The average repeatability for the changed geometry (mispositioning >0.5 m) and repeated geometry (mispositioning <0.5 m) was very similar (Figure 4). The average NRMS for window A was 48%, while shifted shots had an increase in NRMS of only 4%. The same observation was made for a larger window B: repeated shot points had 79.5% NRMS, while shifted shot points had 81.5% NRMS.

In this example, the datasets were acquired at different times of the year. It is evident that seasonal near-surface variations affected repeatability more significantly than positioning errors. The spread of NRMS for twelve consecutive shifted shots varied from about 60% to 100% NRMS, and for repeated shot points from 20 to 120%. In contrast, the difference in 2–4% NRMS created by mispositioning was negligible and statistically insignificant.

There are several considerations in this study that have to be noted. First, the study included a limited number of shot points: 110 shots in total, with 12 shots being mispositioned. The observed difference between repeated and shifted shot points was relatively small compared to the repeatability variance. Secondly, the major repeatability variations were likely to be linked to the seasonal effect of near-surface variations, as the data were acquired during different seasons [27]. Decoupling the mispositioning and seasonal variations effects was challenging. The main conclusion from this study for the Otway site is that the impact of mispositioning is negligible if shot points shifted for less than 1–2 m compared to the effects of seasonal near-surface variations.

3. Case Study 2: Controlled Experiment at Curtin Research Facility

To exclude the effect of seasonal near-surface variations, we conducted a controlled experiment at the Curtin/NGL research facility (Perth, Western Australia) (Figure 1b). We designed and acquired the DAS VSP survey using a vibroseis source (INOVA UniVib 26,000 lbs) and a fibre optic cable installed behind the casing in a 900 m deep well. Source points simulating the changes in acquisition geometry formed an eight-azimuth asterisk-shaped pattern (Figure 5). The central shot point was 130 m away from the wellhead. The length of each line was 10–15 m with 8–10 shot points per line starting from the centre. The central shot point was repeated eight times with different orientations of the vibroseis truck. The total number of shot points was 76. The distance between shot points was as small as 0.5 m (half the size of the vibroseis plate) near the centre of the asterisk and increased with the distance from the centre. The survey parameters are summarised in Table 1.

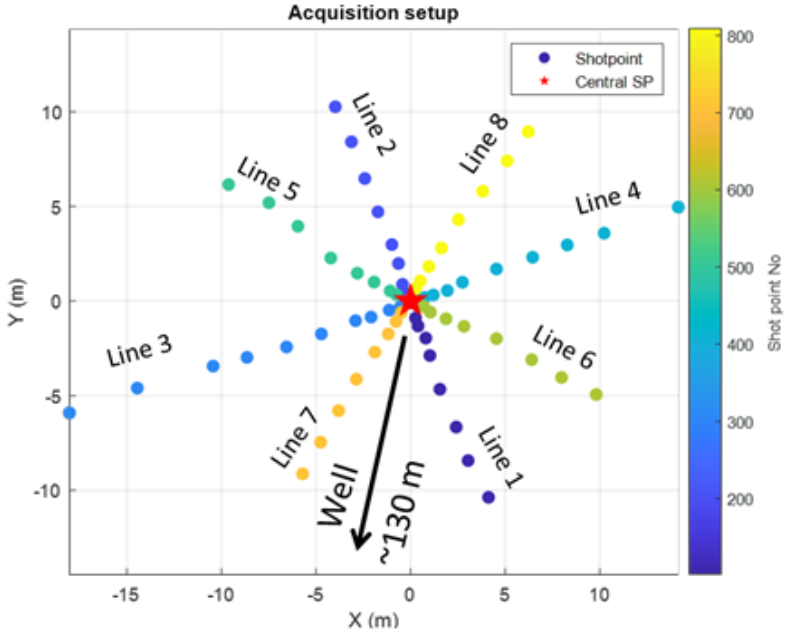

Figure 5. The acquisition map. Each line starts at the central shot point (red star). The well is 130 m to the south from the central shot point.

The vibroseis source generated linear sweeps of 24 s in duration and a 6–150 Hz frequency range. The DAS interrogator (Silixa iDAS v2, Hertfordshire, UK) was set to a

10 m gauge length and a 5 m pulse length with a spatial sampling interval of 1 m and temporal sampling of 1 ms. In such settings, random noise related to the recording hardware should be the main receiver-side factor affecting the repeatability, while mispositioning is the main source-side repeatability factor.

Raw data records were correlated with a synthetic sweep. To assess repeatability, we made a pairwise comparison of all 76 shot points. For a given pair of shots, we calculated the NRMS value in a 60 ms running window for every pair of traces (Figure 6d). Then, we estimated the average repeatability along the direct P wave (Window A, ±30 ms around the first breaks, the light blue window in Figure 6) and a larger window, B, starting from the first breaks 400 ms down (the red window in Figure 6), which includes the direct P wave, P wave reflections, and multiples.

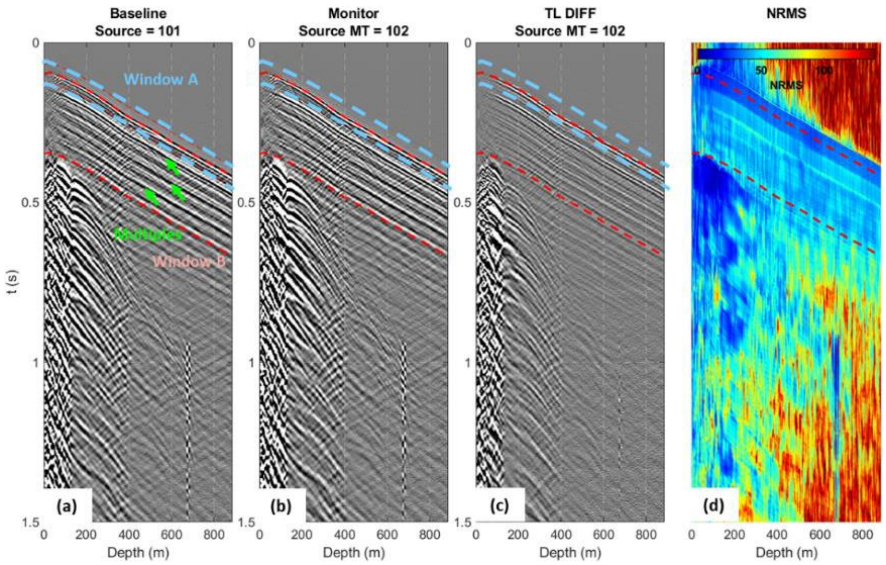

Figure 6. Two shot points located 0.93 m apart (**a**,**b**), their difference (**c**), and NRMS map (**d**). Computation windows for average NRMS are shown on (**a**): light blue window A includes direct P wave, and red window B includes direct P wave, reflected and multiple waves. Green arrows point to multiple waves.

Two shot points located about 1 m apart (Figure 6) showed quite good repeatability for window A (20–25% NRMS), but poorer for the larger window B—about 40–50% NRMS. It appears that the non-repeatable noise for the larger window was mainly created by surface-related multiples, which can be more sensitive to mispositioning.

Comparing the central shot point with all others revealed uneven spatial distribution in window A repeatability (Figure 7a). The near-central shot points (<1–2 m) were quite repeatable (NMRS ~20%), while distant shot points were not (NRMS > 40%). However, the repeatability dropped to an NRMS of 120–140% when moving 7 m to the west from the centre, while it remained in the range of 40–60% NRMS when moving the source to the east. This zonal distribution of the direct-wave repeatability was likely controlled by significant lateral variations in the near-surface conditions. The same pattern was observed for window B (Figure 7d) but was less pronounced. Other shot point comparisons (Figure 7b,c) also revealed the zonal distribution of repeatability. However, the east-west zonal distribution was still noticeable. In this case, the average repeatability level was worse mainly because short-term multiples and reflected waves were more sensitive to misposition, as can be seen by comparing the repeatability of shot points 6 and 18 m apart (Figure 8).

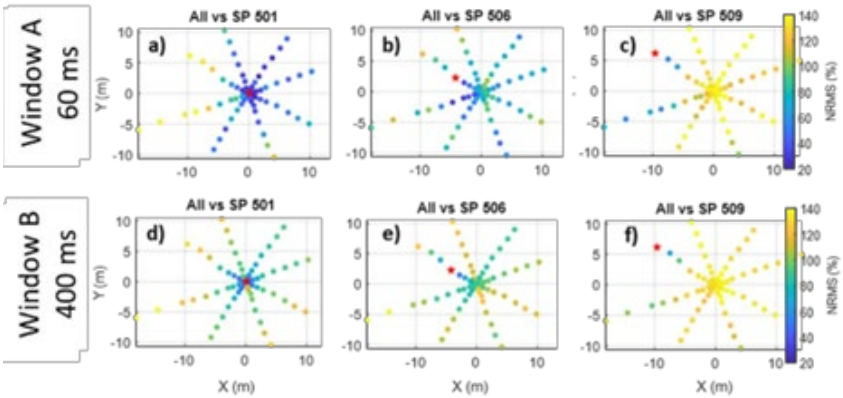

Figure 7. Comparison of one versus all shot points repeatability for central, middle, and far shot points of Line 5 for window A ((**a–c**) respectively, 60 ms window) and window B ((**d–f**) respectively 400 ms window). Shot points are colour-coded with NRMS value when comparing a red-star shot point with a given one. Notice a significant difference in repeatability between eastern and western regions.

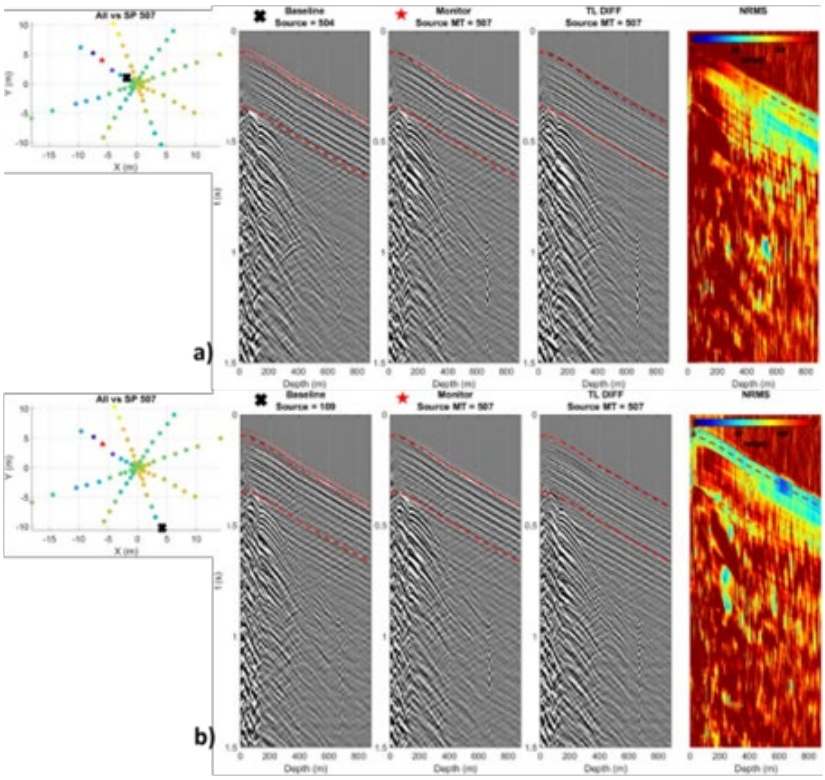

Figure 8. Selection of two shot points located 6 m (**a**) and 18 m (**b**) away. The shot points have similar repeatability levels and a significant difference in misposition.

A shot point from the western zone was compared to two shot points from the east zone located 6 m away and 18 m away from the west-like zone and had similar average repeatability. However, the closest shot points had an even distribution of repeatability along the well (Figure 8a). In contrast, the farthest shot point had poor repeatability at the top of the well, increasing with depth (Figure 8b). This is likely because shallow-depth

wavefield travel times are affected more by strong mispositioning than deeper wavefield travel times. This effect is more pronounced for near-offset shot points.

A pairwise comparison of all 76 shot points (Figure 9) revealed trends in repeatability versus mispositioning in the range from the first cm to about 30 m. Average window A repeatability (Figure 9a) was expectedly better (~45% NRMS) compared to window B repeatability (~95% NRMS) (Figure 9b) for the misposition range from 0.5 to 20 m. However, the direct wave was slightly less immediately affected by mispositioning (the red trend in Figure 9) but had a substantial spread because of near-surface variations. The latter created a spread in NRMS distribution, which increased significantly with the increase of misposition, starting from 20–60% NRMS at 1 m and reaching 20–160% NRMS at 10 m (Figure 9a). For window B, we observed a more pronounced trend in repeatability decrease with misposition starting from about 60–100% NRMS at 2 m and reaching 110% NRMS at 20 m, with the spread of ±30% NRMS likely attributable to spatial near-surface variations.

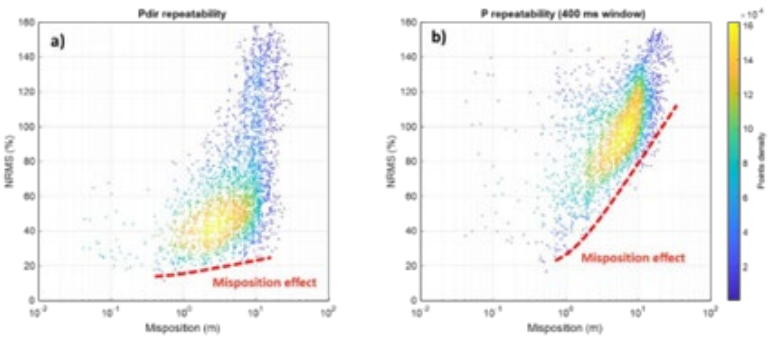

Figure 9. Distribution of repeatability (NRMS) vs. misposition for window A (**a**) and window B (**b**) for pairwise comparison of 76 shot points. Points are colour-coded by density distribution. The red dashed line highlights a possible misposition effect on repeatability. The spread is likely to be attributed to the spatial near-surface variations.

4. Discussion

While the primary focus of our study was the effect of mispositioning, repeatability can be affected by other factors. As shown in the Otway experiment, one such cause is temporal variations of near-surface conditions. Spatial near-surface variations can also strongly degrade repeatability, even for small source positioning variations. More generally, the way the survey is conducted can affect the data. For instance, the shape of the vibroseis plate has a particular directivity pattern, and thus changes in its azimuthal orientation, or up-hill/down-hill position, can degrade repeatability.

Our experiments are limited to only two geographical locations. The characteristic of spatial variations (homogeneous/heterogeneous, seasonal changes, among others) likely vary from site to site and depend on the local soil properties. The Otway site has sandy-clayey soil, while the Curtin site has a predominantly sandy surface. Systematic series of experiments on different types of surfaces are needed to study the effect on repeatability in more detail.

Our study was limited to vibroseis sources widely used in seismic on-shore exploration. The same factors, such as lateral variations of the near-surface, should affect the repeatability of other land sources, such as weight drop or explosives. However, there also may be source-specific effects. Lateral variations of soil conditions (wet/dry) can affect how a weight drop bounces off the landing plate. These soil conditions can also affect the directivity and strength of an explosion. These effects are source-specific and require additional studies.

Our study involved same-day experiment and different-day different-season experiments. However, it is important to understand what would happen if an experiment was conducted in different years in the same season. Jervis, Bakulin, Burnstad, Berron and Forgues [10] demonstrated same-day variations of repeatability reaching 1 ms and a 20%

amplitude change. Half a year of permanent source recordings showed seasonal repeatability variation, highlighting rapid repeatability decrease on rainy days [23]. Thus, even small-time intervals such as days or hours can lead to temporal variations of repeatability.

5. Conclusions

Two experiments were conducted to assess the effect of source mispositioning on 4D DAS VSP repeatability. The experiment at the Otway site demonstrates that the effect of source mispositioning on repeatability is negligible in comparison with the effect of temporal variations of the near-surface conditions. To avoid these limitations, we conducted a same-day controlled experiment at the Curtin University site. This second experiment showed that the effect of source mispositioning on repeatability was controlled by the degree of lateral variations of the near-surface conditions. Unlike in marine seismic measurements, spatial variations of near-surface properties can be laterally rapid and would degrade the repeatability for even a few meter shifts of the source. The greater the mispositioning, the higher the chance of such significant variations. When the near-surface conditions are laterally homogeneous, the effect of modest source mispositioning is small, and in all practical monitoring applications, its contribution to non-repeatability is negligible.

Author Contributions: Conceptualization, R.P. and K.T.; methodology, R.P. and K.T.; software, R.I.; validation, R.I., A.Y. and R.P.; formal analysis, R.I. and R.P.; investigation, R.P. and K.T.; resources, K.T.; data curation, R.I. and P.S.; writing—original draft preparation, R.I.; writing—review and editing, R.P. and K.T.; visualization, R.I.; supervision, R.P. and K.T.; project administration, K.T.; funding acquisition, K.T. All authors have read and agreed to the published version of the manuscript.

Funding: The Otway Project received CO2CRC Ltd. funding through its industry members and research partners, the Australian Government under the CCS Flagships Programme, the Victorian State Government and the Global CCS Institute. The authors wish to acknowledge the financial assistance provided through Australian National Low Emissions Coal Research and Development. ANLEC R&D is supported by Low Emission Technology Australia (LETA) and the Australian Government through the Department of Industry, Science, Energy and Resources. We also would like to acknowledge the support of the Curtin Reservoir Geophysics Consortium.

Institutional Review Board Statement: Not applicable.

Informed Consent Statement: Not applicable.

Data Availability Statement: Not applicable.

Acknowledgments: The authors thank Michael Mondanos and Stoyan Nikolov (Silixa Inc.) for help with the fibre-optic equipment and Peter Dumesny (Upstream Production Solutions) for invaluable help with all aspects of field operations. We would also like to thank Murray Hehir, Dominic Howman and Ruben Lopez Lema for conducting fieldworks. R.I. acknowledges CO2CRC for providing a PhD scholarship.

Conflicts of Interest: The authors declare no conflict of interest.

References

1. Johnston, D.H. *Practical Applications of Time-Lapse Seismic Data*; Society of Exploration Geophysicists: Houston, TX, USA, 2013. [CrossRef]
2. Lumley, D. 4D seismic monitoring of CO_2 sequestration. *Lead. Edge* **2010**, *29*, 150–155. [CrossRef]
3. Hartog, A.H. *An Introduction to Distributed Optical Fibre Sensors*; CRC Press (Taylor and Francis): Boca Raton, FL, USA, 2017; pp. 1–440. [CrossRef]
4. Harvey, S.; Hopkins, J.; Kuehl, H.; O'Brien, S.; Mateeva, A. Quest CCS facility: Time-lapse seismic campaigns. *Int. J. Greenh. Gas Control* **2022**, *117*, 103665. [CrossRef]
5. Götz, J.; Lüth, S.; Henninges, J.; Reinsch, T. Using a fibre optic cable as Distributed Acoustic Sensor for Vertical Seismic Profiling at the Ketzin CO_2 storage site. In Proceedings of the 77th EAGE Conference and Exhibition 2015, Madrid, Spain, 1–4 June 2015; European Association of Geoscientists & Engineers: Houten, The Netherlands, 2015; pp. 1–5. [CrossRef]
6. Pevzner, R.; Isaenkov, R.; Yavuz, S.; Yurikov, A.; Tertyshnikov, K.; Shashkin, P.; Gurevich, B.; Correa, J.; Glubokovskikh, S.; Wood, T. Seismic monitoring of a small CO_2 injection using a multi-well DAS array: Operations and initial results of Stage 3 of the CO2CRC Otway project. *Int. J. Greenh. Gas Control* **2021**, *110*, 103437. [CrossRef]

7. Bacci, V.O.; O'Brien, S.; Frank, J.; Anderson, M. Using a walk-away DAS time-lapse VSP for CO_2 plume monitoring at the Quest CCS Project. *CSEG Rec.* **2017**, *42*, 18–21. Available online: https://csegrecorder.com/articles/view/using-a-walk-away-das-time-lapse-vsp-for-co2-sub-plume-monitoring (accessed on 8 December 2022).
8. Tertyshnikov, K.; Pevzner, R.; Freifeld, B.; Ricard, L.; Avijegon, A. DAS VSP for Characterisation and Monitoring of the CO_2 Shallow Release Site: CSIRO In-Situ Laboratory Case Study. In Proceedings of the Fifth EAGE Workshop on Borehole Geophysics, The Hague, The Netherlands, 18–20 November 2019; European Association of Geoscientists & Engineers: Houten, The Netherlands, 2019; pp. 1–5. [CrossRef]
9. Morice, S.; Ronen, S.; Canter, P.; Welker, K.; Clark, D. The impact of positioning differences on 4D repeatability. In *SEG Technical Program Expanded Abstracts 2000*; Society of Exploration Geophysicists: Houston, TX, USA, 2000; pp. 1611–1614.
10. Jervis, M.; Bakulin, A.; Burnstad, R.; Berron, C.; Forgues, E. Suitability of vibrators for time-lapse monitoring in the Middle East. In *SEG Technical Program Expanded Abstracts 2012*; Society of Exploration Geophysicists: Houston, TX, USA, 2012; pp. 1–5. [CrossRef]
11. Bakulin, A.; Smith, R.; Jervis, M.; Burnstad, R. Use of early arrivals for 4D analysis and processing of buried receiver data on land. In *SEG Technical Program Expanded Abstracts 2015*; Society of Exploration Geophysicists: Houston, TX, USA, 2015; pp. 5493–5497. [CrossRef]
12. Smith, R.; Bakulin, A.; Jervis, M.; Hemyari, E.; Alramadhan, A.; Erickson, K. 4D Seismic Monitoring of a CO_2-EOR Demonstration Project in a Desert Environment: Acquisition, Processing and Initial Results. In Proceedings of the SPE Kingdom of Saudi Arabia Annual Technical Symposium and Exhibition, Dammam, Saudi Arabia, 23–26 April 2018; OnePetro: Richardson, TX, USA, 2018. [CrossRef]
13. Eiken, O.; Haugen, G.U.; Schonewille, M.; Duijndam, A. A proven method for acquiring highly repeatable towed streamer seismic data. *Geophysics* **2003**, *68*, 1303–1309. [CrossRef]
14. Smit, F.; Brain, J.; Watt, K. Repeatability monitoring during marine 4D streamer acquisition. In Proceedings of the 67th EAGE Conference & Exhibition, Madrid, Spain, 13–16 June 2005; European Association of Geoscientists & Engineers: Houten, The Netherlands, 2005; p. cp-1-00588. [CrossRef]
15. Brechet, E.; Sadeghi, E.; Giovannini, A.; Hubans, C. Seismic monitoring combining nodes and streamer data on Dalia Field. In Proceedings of the 73rd EAGE Conference and Exhibition incorporating SPE EUROPEC 2011, Vienna, Austria, 23–27 May 2011; European Association of Geoscientists & Engineers: Houten, The Netherlands, 2011; p. cp-238-00289. [CrossRef]
16. Landro, M. Repeatability issues of 3-D VSP data. *Geophysics* **1999**, *64*, 1673–1679. [CrossRef]
17. Pevzner, R.; Urosevic, M.; Nakanishi, S. Applicability of Zero-offset and Offset VSP for Time-lapse monitoring—CO2CRC Otway Project Case Study. In Proceedings of the 72nd EAGE Conference & Exhibition incorporating SPE EUROPEC 2010, Barcelona, Spain, 14–17 June 2010; EAGE: Barcelona, Spain, 2010; p. cp-161-00586. [CrossRef]
18. AlNasser, H.; Pevzner, R.; Tertyshnikov, K.V.; Popik, D.; Urosevic, M. Application of 4D VSP for Monitoring Of Small-Scale Supercritical CO2 Injection: Stage 2C of CO2CRC Otway Project Case Study. In Proceedings of the Fourth EAGE Borehole Geophysics Workshop, Abu Dhabi, United Arab Emirates, 19–22 November 2017. [CrossRef]
19. Correa, J.; Egorov, A.; Tertyshnikov, K.; Bona, A.; Pevzner, R.; Dean, T.; Freifeld, B.; Marshall, S. Analysis of signal to noise and directivity characteristics of DAS VSP at near and far offsets—A CO2CRC Otway Project data example. *Lead. Edge* **2017**, *36*, 994a1–994a7. [CrossRef]
20. Correa, J.; Pevzner, R.; Bona, A.; Tertyshnikov, K.; Freifeld, B.; Robertson, M.; Daley, T. 3D vertical seismic profile acquired with distributed acoustic sensing on tubing installation: A case study from the CO2CRC Otway Project. *Interpretation* **2019**, *7*, SA11–SA19. [CrossRef]
21. Dou, S.; Ajo-Franklin, J.; Daley, T.; Robertson, M.; Wood, T.; Freifeld, B.; Pevzner, R.; Correa, J.; Tertyshnikov, K.; Urosevic, M. Surface orbital vibrator (SOV) and fiber-optic DAS: Field demonstration of economical, continuous-land seismic time-lapse monitoring from the Australian CO2CRC Otway site. In *SEG Technical Program Expanded Abstracts 2016*; Society of Exploration Geophysicists: Houston, TX, USA, 2016; pp. 5552–5556. [CrossRef]
22. Yavuz, S.; Isaenkov, R.; Pevzner, R.; Gurevich, B.; Tertyshnikov, K.; Yurikov, A.; Correa, J.; Wood, T.; Freifeld, B. Processing of multi-well offset vertical seismic profile data acquired with distributed acoustic sensors and surface orbital vibrators: Stage 3 of the CO2CRC Otway Project case study. *Geophys. Prospect.* **2021**, *69*, 1664–1677. [CrossRef]
23. Isaenkov, R.; Pevzner, R.; Glubokovskikh, S.; Yavuz, S.; Yurikov, A.; Tertyshnikov, K.; Gurevich, B.; Correa, J.; Wood, T.; Freifeld, B.; et al. An automated system for continuous monitoring of CO_2 geosequestration using multi-well offset VSP with permanent seismic sources and receivers: Stage 3 of the CO2CRC Otway Project. *Int. J. Greenh. Gas Control* **2021**, *108*, 103317. [CrossRef]
24. Yurikov, A.; Tertyshnikov, K.; Isaenkov, R.; Sidenko, E.; Yavuz, S.; Glubokovskikh, S.; Barraclough, P.; Shashkin, P.; Pevzner, R. Multiwell 3D distributed acoustic sensing vertical seismic profile imaging with engineered fibers: CO2CRC Otway Project case study. *Geophysics* **2021**, *86*, D241–D248. [CrossRef]
25. Jenkins, C.; Bagheri, M.; Barraclough, P.; Dance, T.; Ennis-King, J.; Freifeld, B.; Glubokovskikh, S.; Gunning, J.; LaForce, T.; Marshall, S. Fit for purpose monitoring-a progress report on the CO2CRC Otway Stage 3 project. In Proceedings of the 14th Greenhouse Gas Control Technologies Conference Melbourne, Melbourne, VIC, Australia, 21–26 October 2018; pp. 21–26.

26. Kragh, E.; Christie, P. Seismic repeatability, normalized rms, and predictability. *Lead. Edge* **2002**, *21*, 640–647. [CrossRef]
27. Al Jabri, Y. Land Seismic Repeatability Prediction from Near-Surface Investigations at Naylor Field, Otway. Ph.D. Thesis, Curtin University, Bentley, Australia, 2011. Available online: http://hdl.handle.net/20.500.11937/2372 (accessed on 8 December 2022).

EAGE GEOTECH
THE SECOND EAGE GEOSCIENCE TECHNOLOGIES AND APPLICATIONS CONFERENCE AND EXHIBITION 2022

EAGE

11

Continuous DAS recording with permanent seismic sources reveals peculiar tube waves associated with the fluid flow

R. Isaenkov[1], A. Yurikov[1], K. Tertyshnikov[1], B. Gurevich[1], R. Pevzner[1]

[1] Curtin University

Summary

Tube waves are well known in vertical seismic profiling and generally considered as noise.
During the continuous seismic monitoring of CO2 injection at the Otway site, we observed an unusual tube wave in a buried horizontal pipeline. The tube wave is generated by a surface orbital vibrator located above the pipe and recorded with distributed acoustic sensing (DAS) helically wound surface cable. The cable is buried in the same trench as the pipe. The seismic acquisition is continuous covering the periods before, during and after the injection.

The tube wave is absent before but appears in the data upon the start of the CO2 injection. The event is also absent in the area where the CO2 pipeline is absent. The tube wave travel times, waveform and amplitudes vary during the injection and are likely related to the CO2 properties. Thus, the combination of DAS fibre installed along a pipeline and a permanent seismic source can be useful for pipeline flow monitoring.

Introduction

Tube waves in sonic logging and vertical seismic profiles are low-frequency pressure waves propagating along the borehole with a speed of sound in the mud. Usually, tube waves have a high amplitude and thus can mask useful signals (e.g. body waves) and are often considered as noise (Greenwood 2013). In some instances, the tube wave attributes (e.g. attenuation) can be used to detect fractures (Beydoun et al. 1985) or measure S-wave velocities and formation permeability (Wehner et al. 2017).

Stage 3 of the Otway project is mainly focused on the development of borehole-based monitoring (seismic and pressure tomography) of a small-scale 15 kt of CO_2 injection into a 1.5 km deep saline aquifer (Jenkins et al. 2021, Pevzner et al. 2021) at the Otway International Test Centre (Australia). As a part of the project's monitoring system, a helically wound cable (HWC) was buried 0.4 m above a 600 m-long gathering line buried at 1.2 m deep, which is transferring supercritical CO_2 from CRC2 facility to the injection well (CRC3) (Figure 1a). An extra 400 m of HWC is buried between CRC2 facility and CRC7 well pad. The HWC has an engineered Constellation (Silixa Ltd) fibre (with enhanced backscattering) wounded at a 30º pitch angle and it is connected to the Silixa iDAS v3 unit. HWC data is recorded continuously with 2 ms temporal and 5 m spatial sampling. The gauge length was set to 10 m and pulse length to 5 m.

Nine surface orbital vibrators (SOVs) (Freifeld et al. 2016) were utilised as permanent seismic sources for monitoring. SOV1 is installed near the CRC2 facility above the gathering line. The data from SOV1 was recorded by the HWC every two days starting six months prior to the injection (1/12/2020), four months during the injection (17/04/2021) and operated for another five months.

SOV1 operated every second day for 2.5 hours producing 22 clockwise and 22 counterclockwise sweeps, each 2.5 minutes long. The sweeps were recorded by a geophone buried 3 m below the SOV (Isaenkov et al. 2021). To create raw shot gathers, sweeps were deconvolved from records. The repeated sweeps are stacked together within each rotation group to enhance the signal-to-noise ratio. No additional processing was applied.

The data recorded by HWC shows a tube wave in the CO_2 filled gathering line created by SOV1 operations during the injection. We observe variations in travel times and amplitudes of the tube wave likely to be linked to the CO_2 flow characteristics.

Figure 1 *(a) Location of the buried HWC cable (yellow) and CO_2 pipeline (red) at Otway site. (b) A photo of HWC in the trench, the pipeline is buried 0.4 m below the cable.*

Results

Figure 2 displays two SOV1-HWC shots gathers before and after the start of the injection. After the injection, we observe a linear event starting about 250 m west from SOV1 at 200 ms and travelling

along the trench towards the CRC3 well. The event reaches the CRC3 pad at about 480 ms (Figure 2b, red arrow and magenta pick). Importantly, this wave does not appear in the interval between SOV1 and CRC7 as there is no CO_2-containing pipeline on this side. Thus, this arrival appears to be a tube wave generated by SOV1 in the gathering line.

The tube wave has several prominent features. First, it reflects in the middle (~250 m east from CRC3) and at the end of the trench (yellow arrows Figure 2b). It also has a ghost-like wave with a 100 ms delay (orange arrow Figure 2b). It has different apparent velocities throughout its course: near SOV1 and up to the middle of the trench, the velocity is 1.5 km/s, while closer to the end drops to 1.3 km/s (Figure 2b). Additionally, time shifts of up to 10 ms are observed over the injection period. These tube wave features are likely linked to CO_2 flow in the gathering line.

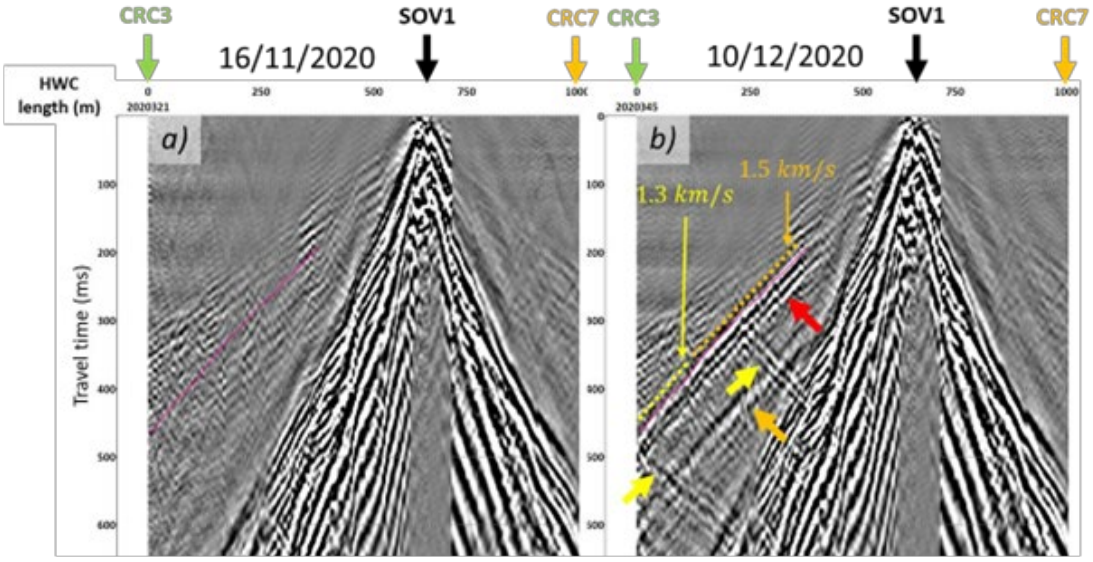

Figure 2 *(a) SOV1 – HWC shot gather before CO_2 injection (16/11/2020) and (b) after injection of ~1000 tons of CO_2 (10/12/2020). Notice the appearance of the tube wave between CRC3 and SOV1 after the injection (red arrows). Yellow arrows indicate reflected tube waves. Horizontal axis labels – distance along the cable in m, vertical axis – travel time in ms. Traces are normalised by their RMS amplitudes for visualisation purposes.*

Conclusions

A seismic source located close to a buried CO_2 pipeline excites a tube wave, which is recorded by a buried DAS cable. The tube wave is characterised by varying features (apparent velocity, travel times, amplitudes, etc.) throughout injection (4 months), which appear to be related to variations in the CO_2 flow. Thus, the combination of DAS fibre buried along the pipeline and a seismic source may be used for pipeline flow monitoring.

Acknowledgements

The Otway Project received CO2CRC Ltd funding through its industry members and research partners, the Australian Government under the CCS Flagships Programme, the Victorian State Government and the Global CCS Institute. The authors wish to acknowledge the financial assistance provided through Australian National Low Emissions Coal Research and Development. ANLEC R&D is supported by Low Emission Technology Australia (LETA) and the Australian Government through the Department of Industry, Science, Energy and Resources. Funding for LBNL was provided through the Carbon

Storage Program, U.S. DOE, Assistant Secretary for Fossil Energy, Office of Clean Coal and Carbon Management through the NETL, under contract No. DE-AC02- 05CH11231. The authors thank Michael Mondanos and Stoyan Nikolov (Silixa Ltd.) for help with the fibre-optic equipment and Peter Dumesny (Upstream Production Solutions) for invaluable help with all aspects of field operations.

References

Beydoun, W., Cheng, C. and Toksöz, M. [1985] Detection of open fractures with vertical seismic profiling. Journal of Geophysical Research: Solid Earth 90(B6), 4557-4566.

Freifeld, B. M., Pevzner, R., Dou, S., Correa, J., Daley, T. M., Robertson, M., Tertyshnikov, K., Wood, T., Ajo-Franklin, J., Urosevic, M. and Gurevich, B. [2016] The CO2CRC Otway Project deployment of a Distributed Acoustic Sensing Network Coupled with Permanent Rotary Sources. 2016(1), 1-5.

Greenwood, A. J. [2013] Application of vertical seismic profiling for the characterisation of hard rock. Department of Exploration Geophysics. Curtin University, Curtin University.

Isaenkov, R., Pevzner, R., Glubokovskikh, S., Yavuz, S., Yurikov, A., Tertyshnikov, K., Gurevich, B., Correa, J., Wood, T., Freifeld, B., Mondanos, M., Nikolov, S. and Barraclough, P. [2021] An automated system for continuous monitoring of CO2 geosequestration using multi-well offset VSP with permanent seismic sources and receivers: Stage 3 of the CO2CRC Otway Project. International Journal of Greenhouse Gas Control 108, 103317.

Jenkins, C., Barraclough, P., Bagheri, M., Correa, J., Dance, T., Ennis-King, J., Freifeld, B., Glubokovskikh, S., Green, C. and Gunning, J. [2021] Drilling an Array of Monitoring Wells for a CCS Experiment: Lessons From Otway Stage 3.

Pevzner, R., Isaenkov, R., Yavuz, S., Yurikov, A., Tertyshnikov, K., Shashkin, P., Gurevich, B., Correa, J., Glubokovskikh, S. and Wood, T. [2021] Seismic monitoring of a small CO2 injection using a multi-well DAS array: Operations and initial results of Stage 3 of the CO2CRC Otway project. International Journal of Greenhouse Gas Control 110, 103437.

Wehner, D., Liu, Y. and Landrø, M. [2017] Estimate the Shear Wave Velocity Close to Wells from Tube Waves–An Experimental Study. Fourth Sustainable Earth Sciences Conference, 1-5. European Association of Geoscientists & Engineers.

4 APPENDIX A: COPYRIGHT PERMISSION

The thesis utilises previously published material under the following papers published by Elsevier:

Isaenkov, R., Pevzner, R., Glubokovskikh, S., Yavuz, S., Shashkin, P., Yurikov, A., Tertyshnikov, K., Gurevich, B., Correa, J., Wood, T., 2022. Advanced time-lapse processing of continuous DAS VSP data for plume evolution monitoring: Stage 3 of the CO2CRC Otway project case study. International Journal of Greenhouse Gas Control 119, 103716, https://doi.org/10.1016/j.ijggc.2022.103716.

Isaenkov, R., Pevzner, R., Glubokovskikh, S., Yavuz, S., Yurikov, A., Tertyshnikov, K., Gurevich, B., Correa, J., Wood, T., Freifeld, B., Mondanos, M., Nikolov, S., Barraclough, P., 2021. An automated system for continuous monitoring of CO2 geosequestration using multi-well offset VSP with permanent seismic sources and receivers: Stage 3 of the CO2CRC Otway Project. International Journal of Greenhouse Gas Control 108, 103317, https://doi.org/10.1016/j.ijggc.2021.103317.

To this date (February 2023), as for Elsevier's copyright policy, the author has a right to re-use their material in new works without permission or payment (with full acknowledgement of the original article) to include an article in a subsequent compilation of their work. See an excerpt of the copyright policy from Elsevier's website below.

Table 1 Excerpt of Elsevier's copyright policy for authors (https://www.elsevier.com/about/policies/copyright)

Author rights in Elsevier's proprietary journals	Published open access	Published subscription
Retain patent and trademark rights	√	√
Retain the rights to use their research data freely without any restriction	√	√
Receive proper attribution and credit for their published work	√	√
Re-use their own material in new works without permission or payment (with full acknowledgement of the original article): 1. Extend an article to book length 2. Include an article in a subsequent compilation of their own work 3. Re-use portions, excerpts, and their own figures or tables in other works.	√	√

The thesis utilises published material by MDPI under the following paper:

Isaenkov, R.; Tertyshnikov, K.; Yurikov, A.; Shashkin, P.; Pevzner, R. Effect of Source Mispositioning on the Repeatability of 4D Vertical Seismic Profiling Acquired with Distributed Acoustic Sensors. *Sensors* 2022, *22*, 9742. https://doi.org/10.3390/s22249742

The journal allows to re-use published material and keeps authors' copyrights under Creative Commons Attribution License.

Authors and Readers Benefit from MDPI's Pledges to:

- **publish thoroughly peer-reviewed journals** of high scholarly impact
- **maintain quick publication** — manuscripts are published within 5-7 weeks of submission (provided no major revisions are required)
- **publish full open access journals** — readers can access all content published on this platform for free
- **publish citation-tracked journals** — MDPI continuously works towards quick coverage and citation-tracking of all of its journals in the top databases of Scopus, Web of Science, PMC, PubMed, and MEDLINE, along with various other databases

For Authors and Readers Open Access Means:

Read the full open access information here.

- **free availability** of the literature without any subscription or price barriers
- **immediate access** once an article is published (no embargo period)
- **authors retain all copyrights** - authors will not be forced to sign any copyright transfer agreements
- **permission of re-use** of the published material if proper accreditation is given (Creative Commons Attribution License)

Figure 1 Excerpt of MDPI's copyright policy for authors (https://www.mdpi.com/authors)

The thesis utilises published material by EAGE under the following papers:

Isaenkov, R., Glubokovskikh, S., Tertyshnikov, K., Pevzner, R., Bona, A., 2020. Effect of Rocks Stiffness on Observed DAS VSP Amplitudes, EAGE Workshop on Fiber Optic Sensing for Energy Applications in Asia Pacific. European Association of Geoscientists & Engineers, pp. 1-5, https://doi.org/10.3997/2214-4609.20224011.

Isaenkov, R., Yurikov, A., Tertyshnikov, K., Gurevich, B., Pevzner, R., 2022. Continuous Das Recording with Permanent Seismic Sources Reveals Peculiar Tube Waves Associated with the Fluid Flow, EAGE GeoTech 2022 Third EAGE Workshop on Distributed Fibre Optic Sensing. European Association of Geoscientists & Engineers, pp. 1-4. https://doi.org/10.3997/2214-4609.20224011.